Characterisation of the imidazoline site on monoamine oxidase type B

by

Glen Reid McDonald

A thesis submitted in partial fulfillment of the requirements for the degree of

Master of Science

Department of Pharmacology
University of Alberta

Abstract

Monoamine oxidase enzymes are largely involved in the catabolism of biogenic amines. Two forms of the enzyme are documented to exist, monoamine oxidase type A and B. The B form (MAO-B) of the enzyme has been noted to possess a high affinity site for some imidazoline ligands. This site (the I_2 site) appears to exist only on a small fraction of MAO-B enzymes but the function of the site is not known. The ligands that bind to this site with high affinity appear to inhibit catalytic activity at concentrations some 1000-fold higher than those required to bind to the I_2 site. The goal of the present work was to characterise the I_2 site on MAO-B through radio-ligand binding and kinetic assays. In doing so, phenylethylamine was found to create a high-affinty site for 2-BFI on MAO-B. The rate of site-formation is influenced by the presence of 2-BFI. This work represents a new understanding of MAO-B kinetics and opens the door for future research into the potential importance of the I_2 site on MAO-B.

To Mom, Dad, Brett and Anita. Your passion for science, discovery and debate lead me down my own path of enlightenment.

Thank-you for your endless support of all of my pursuits.

Acknowledgements

I wish to thank Drs. Andrew Holt and Alan Hudson for their support and guidance throughout my project. From patiently teaching me techniques to debating the merits of our own observations, they have taught me life-long skills that reach far beyond the doors of a laboratory.

I wish to also thank the members of my supervisory committee, which again include Drs. Hudson and Holt, as well as Dr. Glen Baker.

Finally, I must thank the Department of Pharmacology and the Faculty of Medicine and Dentistry at the University of Alberta for their financial support. This work was also supported by a Queen Elizabeth II Graduate Scholarship.

Table of Contents

List of Tables

List of Figures

List of Abbreviations

2-BFI: 2-(2-benzofuranyl)-2-imidazoline hydrochloride

DiHEMDA: di(2-hydroxyethyl)methyldodecylammonium

hMAO-B: purified human monoamine oxidase type B

MAO-B: monoamine oxidase type B

PEA: phenylethylamine

TCP: tranylcypromine

WT-MAO-B: membrane-bound human monoamine oxidase type B

1 Chapter 1: Introduction to monoamine oxidases

1.1 Historical data on amine oxidases

1.1.1 Discovery of Amine Oxidases

Research into the fate of amines in living organisms dates back to the late 19th century, when Oswald Schmiedeberg[1] administered benzylamine to dogs and determined it was metabolised to hippuric acid[2]. Interest in amine metabolism, however, increased markedly 20 years later after Dale and Dixon published that administration of tyramine by injection produces effects similar to adrenaline in cats, dogs and rabbits[3]. Tyramine had been isolated from foodstuffs such as cheese and putrid meats, from human tissue including the liver, pancreas, and placenta, and was also isolated from liquid extract of ergot[4]. Tyramine's relative ubiquity in the world, as well as its similarity in structure to tyrosine, adrenaline and thyroxine, made the fate of tyramine extremely interesting to medical researchers[4,5].

In 1910, Ewins and Laidlaw administered tyramine via tissue perfusion into cat liver as well as rabbit liver and uterus tissue[4]. They observed, particularly in the cases of liver perfusion, tyramine was metabolised almost entirely into *p*-hydroxyphenylacetic acid[4]. No such metabolism occurred when heart tissue was perfused with tyramine[4]. They later performed similar experiments examining the fate of tryptamine, discovering the product indoleacetic acid[6]. During this time of discovery, it was assumed that the

deamination process was hydrolytic with an intermediate carboxylic acid group. It was not until 1928, when Mary Hare described an enzyme that oxidises tyramine (*tyramine oxidase*) that this paradigm was overturned[5].

The widespread use of the Barcroft differential manometer in the 1920s allowed Hare to measure the consumption of oxygen by tissues in the presence of tyramine. Using liver homogenates, Hare adequately showed that an enzyme was responsible for the metabolism of tyramine[5]. Homogenates of kidney, lung, suprarenals, skeletal muscle and the heart were also tested, but with the exception of kidneys, no activity was observed. Beyond demonstrating the existence of an enzyme, Hare also showed that hydrogen peroxide is produced during the reaction, and that deamination occurs simultaneously with oxidation[5]. From this, the schematic basis of all amine oxidase reactions was formed:

$$R\text{-}CH_2\text{-}NR_1R_2 + O_2 + H_2O \rightarrow R\text{-}CHO + NH\text{-}R_1R_2 + H_2O_2$$

All previous work on the fate of tyramine indicated that mammalian liver is extremely rich in amine oxidase activity. However, other tissues have since been found to contain amine oxidases, including the blood vessels[7], male sex organs (testes)[8], the suprarenal gland[8,9], the thyroid gland[8], as well as the heart[8]. Within these tissues, the enzyme is always localised intracellularly, within the insoluble constituents of the cell[2]. The ubiquity of this enzyme throughout the mammalian physiology indicates a relative importance.

1.1.2 Classifying Monoamine Oxidase

By 1938, it was recognised that the broad class of enzymes termed Amine Oxidases could be broken into two distinguishable groups. The enzyme Hare had characterised as tyramine oxidase was renamed and classified as a monoamine oxidase (MAO) in 1938 by Zeller after numerous molecules containing different aliphatic chain lengths were identified as substrates [10-13]. Zeller also reclassified the enzyme histaminase, previously described by Best in 1929, to diamine oxidase (DAO)[10,14]. As the naming suggests, monoamine oxidase enzymes were defined by their ability to oxidise aliphatic monoamines, but not histamine or short-chain aliphatic diamines such as putrescine or cadaverine. MAO and DAO were also distinguished by their inhibitors in 1938, wherein DAO was known to be sensitive to inhibition by cyanide and semicarbazide, while MAO was not.

As work continued on MAO, it became apparent that the catalytic functionality stemmed from the presence of a flavin adenine dinucleotide (FAD) prosthetic group in the active site. It was observed by Erwin and Hellerman in 1967, in a relatively well-purified preparation from bovine kidney, that spectral absorption was maximal at 460 nm in the presence of benzylamine under anaerobic conditions [15]. They also observed a fluorescent peak at 520 nm when an activating wavelength of 450 nm was used [15]. Numerous other groups produced similar results from different MAO isolates [16]. These observations were highly consistent with the characteristics of a flavin group. The FAD group was later found to be attached at position 8 via a

thio-ether from a cysteine within the polypeptide chain of MAO[17]. The synthesis of a thio-ether cysteine linked FAD group, synthesized for the first time in 1971, provided evidence of similar characteristics to those seen with the FAD group in MAO[18].

1.1.3 Monoamine Oxidase Subtypes

For many years there was significant debate regarding the existence of two separate enzyme entities. Both enzymes are integral proteins found in the outer membrane of the mitochondria, making it relatively difficult to separate the two[19]. Both enzymes are widely distributed throughout the body, concentrating mostly in the liver, kidney, intestines and the brain[20,21].

In 1968, Johnston provided evidence that at least two monoamine subtypes existed in rat liver. These two subtypes were differentiable by their sensitivity to the inhibitor clorgyline[22], wherein the clorgyline-sensitive form was termed monoamine oxidase A (MAO-A) and the clorgyline-resistant form was termed monoamine oxidase B (MAO-B). Further experiments by Knoll and Magyar showed that MAO-B was more sensitive to inhibition by l-deprenyl than MAO-A[23].

From these observations, two hypotheses were proposed to explain the subtypes: 1) both MAO-A and –B are the same enzyme but present with different substrate/inhibitor specificities depending on the microenvironment[24], or 2) the subtypes are distinctly different enzymes with a different peptide sequence, although evolutionarily similar in structure[25].

The genetic studies of the 1980s, which showed that MAO-A and –B are encoded on separate genes and have an amino acid homology of approximately 70% (based on cDNA library comparisons from human liver), have since put the debate to rest[26].

1.1.4 Distribution of Monoamine Oxidases

1.1.4.1 Distribution of monoamine oxidase across species

Monoamine oxidase enzymes appear to exist in many, if not all, animals. Activity that mimics that of MAO has been found in amphibians (salamanders[27]), fish (carp[28,29], goldfish[30], and perch[31]) and birds (ring-dove[32]). In some of the studied species, MAO activity has varied depending on the stages of development, suggesting an ancient and essential regulatory role. In toad eggs, MAO-A and –B activities steadily decrease until the neural tube develops, at which point activities increase again to levels exceeding prior catabolism[33]. Similar observations have been made in sea urchin eggs and sperm. Such observations suggest an active role of MAO substrates in regulation of development. Recent studies indicate that MAO-A specifically plays a role in regulating apoptosis during embryonic development[34]. Loss of function mutations in MAO-A in humans leads to Brunner syndrome, a disease consisting of severe mental retardation, aggression, sleep and mood disturbances[35]. Loss of both MAO-A and –B in humans has been reported, resulting in short stature and features of autism[36,37].

Of particular note is that invertebrate organisms such as starfish and insects appear to lack amine oxidase activity, at least with any semblance of the vertebrate amine oxidases[38,39].

1.1.4.2 Distribution of monoamine oxidase within mammalian tissue

Monoamine oxidase activity appears to be present in all mammalian tissues, with the exception of erythrocytes[2]. Both MAO-A and –B are expressed in almost all tissues, although a few tissues appear to express only one isoform[2]. MAO-A is likely to be the only isoform present in human placenta[40], while human platelets appear to express only the B form of MAO[41-43]. Classically, bovine liver and kidney have been reliable sources of the enzyme for scientific research[44,45].

Modern techniques, including positron emission tomography, have allowed researchers to assess isozyme activity in human peripheral tissue. The results indicate that the liver, the duodenum (particularly the enterocytes and cryptocytes), the lungs, and the tubules of the nephrons are very high in MAO activity. This suggests an important role in the metabolism of exogenous monoamines, such as tyramine. The research also confirmed high levels of expression of MAO-A in the placenta (with non-existent expression of MAO-B) as well as exclusive expression of MAO-B on platelets[46]. The majority of the interest in MAO enzymes, however, comes from the role they play in neurotransmitter regulation in the brain.

1.1.4.3 Distribution of monoamine oxidase in the nervous system

The distribution of MAO in the brain and nervous system is not homogenous. It is thought that MAO-B is found in anywhere from 2 to 8 times the amount of MAO-A in the brain. MAO-B is expressed in histaminergic neurons as well as the cell bodies of serotonergic cells and astrocytes[47]. In the axon terminal of serotonergic cells in rat brain, MAO-B appears to be absent from its regular location on mitochondrial membranes[48]. Dopaminergic and noradrenergic neurons typically express MAO-A[49], although MAO-A mRNA has been found in the axons on serotonergic neurons in rats[50,51]. It appears odd that MAO-B, the isoform for which serotonin is considered less of a substrate than MAO-A, is localised in serotonergic cell bodies. Hypotheses around this occurrence include segregation of MAO-A from the cell body to the axons to facilitate serotonin catabolism near the synapse, as well as that expression of MAO-B in the cell body may provide a protective function[47].

Both enzyme isoforms can be found in high amounts in the thalamus, the gateway between the cortex and the midbrain of humans. MAO-A is found in greater amounts in the cortical areas of the brain, while MAO-B is found in greater quantity in subcortical areas[52]. MAO-B expression in the brain appears to increase consistently with age[52]. Interestingly, in persons with Alzheimer's dementia, MAO clusters are observed in the astrocytes of the amygdala, hippocampus and insular cortex[53]. The MAO clusters appear to possess mostly MAO-B activity[53].

1.1.5 Substrate Specificity of Monoamine Oxidases

The major biogenic amines found in humans are dopamine, serotonin, noradrenaline, adrenaline, tyramine, and phenylethylamine. Serotonin and noradrenaline are classical MAO-A substrates, while phenylethylamine and benzylamine (non-endogenous) are classical MAO-B substrates. Dopamine and kynuramine are typically considered substrates for both enzymes. Interestingly, MAO-A is the main dopamine degradation pathway in rodent brain, while in human and primate brains, MAO-B catabolises a larger proportion of dopamine[54-56]. Regardless of any interspecies differences, the two enzymes are best differentiated by their inhibitor selectivity: MAO-B is irreversibly inhibited by l-deprenyl and MAO-A[23] is inhibited by low concentrations of clorgyline[22].

1.1.6 Structure of Monoamine Oxidase Isozymes

As mentioned previously, the active site of MAOs contains an FAD prosthetic group linked to the enzyme via a cysteine residue. That the two pharmacologically different forms of the enzyme were different structurally was not clear until 1983, when Denney *et al.* isolated both MAO-A and –B from a single tissue using an immunoaffinity column directed towards the –B isoform[43]. Since then, purified enzyme from cDNA has enabled X-ray crystal structures to be determined for both MAO-A and –B[57].

Human MAO-A (Figure 1.1.6.1, left panel) is a protein made up of 527 amino acids with a mass of 59.8 kDa[57], while MAO-B (Figure 1.1.6.1, right

panel) consists of 520 amino acids and has a mass of approximately 58.8 kDa[57,58]. The environments in the site proximal to the FAD group in both enzymes are remarkably similar. This area of the active site is hydrophobic and possesses an aromatic cage, which appears to be important in catalysis[59]. Moving distally from the FAD group, the enzymes differ from each other significantly.

Human MAO-A crystallises monomerically and possess a monopartite active site approximately 550 $Å^3$ in volume[60]. This is in stark contrast to MAO-B, which crystallises in a dimeric fashion and possess a bipartite cavity (compared in Figure 1.1.6.1 and Figure 1.1.6.2), consisting of a substrate entrance cavity (290 $Å^3$) and a larger substrate-binding cavity (430 $Å^3$)[57,58,61,62]. An isoleucine (Ile199) gate separates the two cavities and, in conjunction with a tyrosine residue (Tyr326), determines substrate and inhibitor recognition[57]. The cavity distal to the flavin is referred to as the entrance cavity, while the proximal space is termed the active site[57].

Both enzymes appear to anchor to lipid membranes via an α-helix at the C-terminus[57,60]

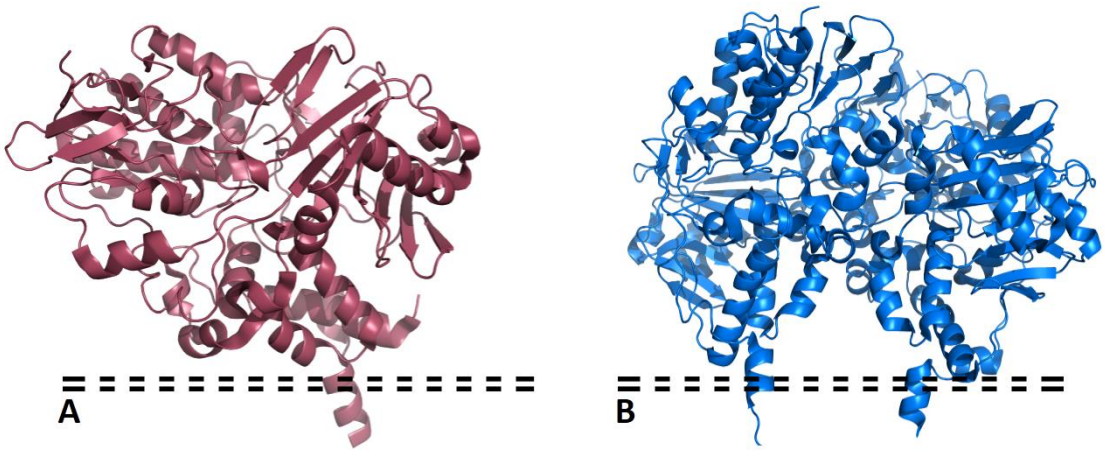

Figure 1.1.6.1 Protein structures of MAO-A and MAO-B
Crystal structures of MAO-A (left) and MAO-B (right). The dotted line represents the lipid bilayer. Note that MAO-B has crystallized in a dimeric fashion.

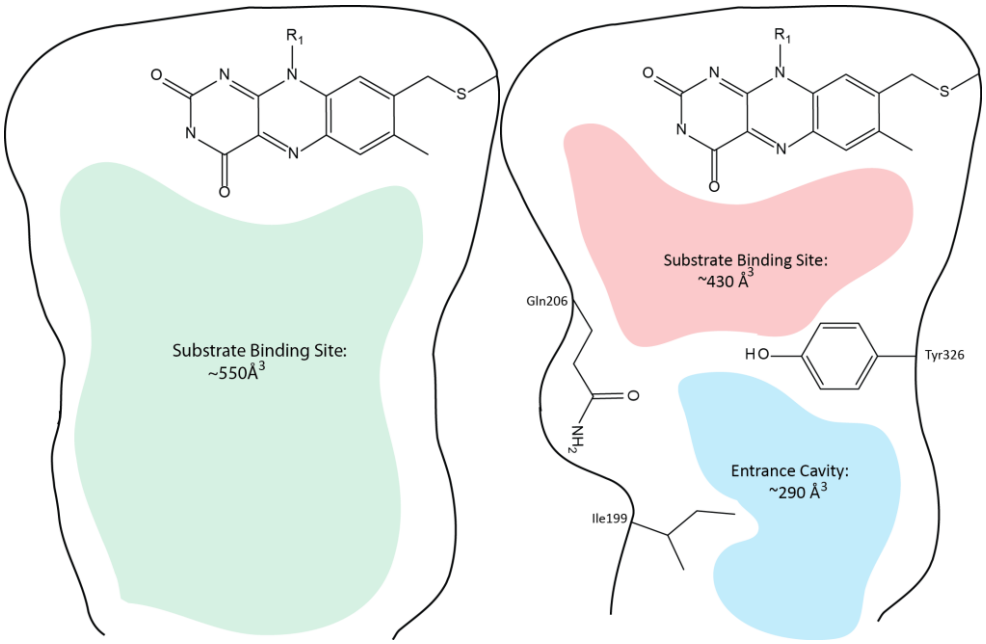

Figure 1.1.6.2 Comparison of MAO-A and MAO-B active sites
Cartoon drawings of MAO-A (left) and MAO-B (right) active sites based on crystal structures in the literature[57,62-64]. MAO-A exhibits a large, monopartite substrate-binding site, while MAO-B has a bipartite cavity made up of a substrate-binding site and an entrance cavity. These cavities are thought to be gated by isoleucine 199 (Ile199), shown in the open form above.

Figure 1.1.6.2 shows the important residues within MAO-B that may be involved in substrate and inhibitor specificity. Long chain inhibitors such as *trans,trans*-farnesol that bind in the substrate binding site have a long tail that

traverses both sites, preventing the Ile199 gate from being in a closed conformation (Figure 1.1.6.3, left)[61]. Smaller molecules that are entirely contained in the substrate-binding site allow the Ile199 to adopt the closed conformation (Figure 1.1.6.3, right)[61].

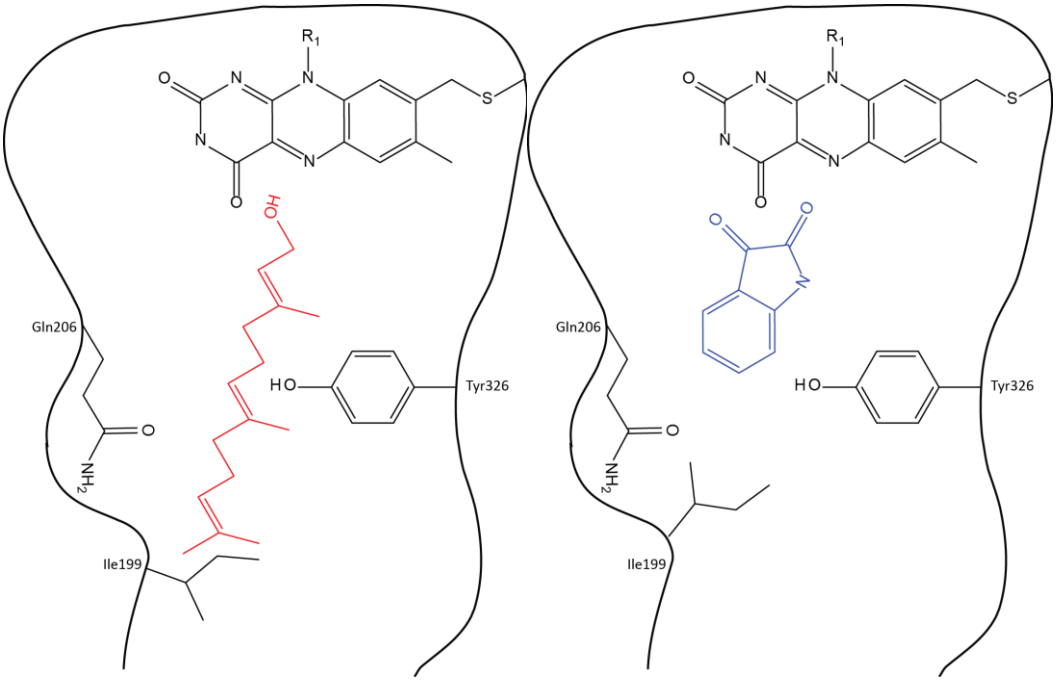

Figure 1.1.6.3 Opening and closing of isoleucine gate
Long inhibitors, such as *trans,trans*-farnesol, are capable of traversing both the substrate-binding site and the entrance cavity, forcing isoleucine 199 to be in an "open" conformation (left). Small molecules such as isatin allow the gate to close fully (right).

Based on the crystal structures that elucidated the bipartite nature of MAO-B, researchers created point mutations to replace the isoleucine with alanine or phenylalanine. Alanine contains a single methyl group side-chain, causing the gate to confer a permanently "open" position and resulted in minimal change in affinity of molecules for the enzyme[57]. Phenylalanine possesses a bulkier side chain and is thought to mimic the "closure" of the gate.

In Ile199Phe mutants, large molecules such as *trans,trans*-farnesol showed a decreased affinity, while isatin binding was not affected[61,65]. These observations suggest that the isoleucine gate is an important determinant of substrate and inhibitor specificity between MAO-A and –B.

1.1.7 Structures of substrates and inhibitors of MAO-B

The structural differences between MAO-A and –B, based on crystallographic data, suggest that many substrates and inhibitors will bind selectively. Included in Figure 1.1.7.1 and Figure 1.1.7.2 are select structures of substrates for MAO-A and –B as well as inhibitors of MAO-B that will be discussed in Sections 2.7 and 4.2.

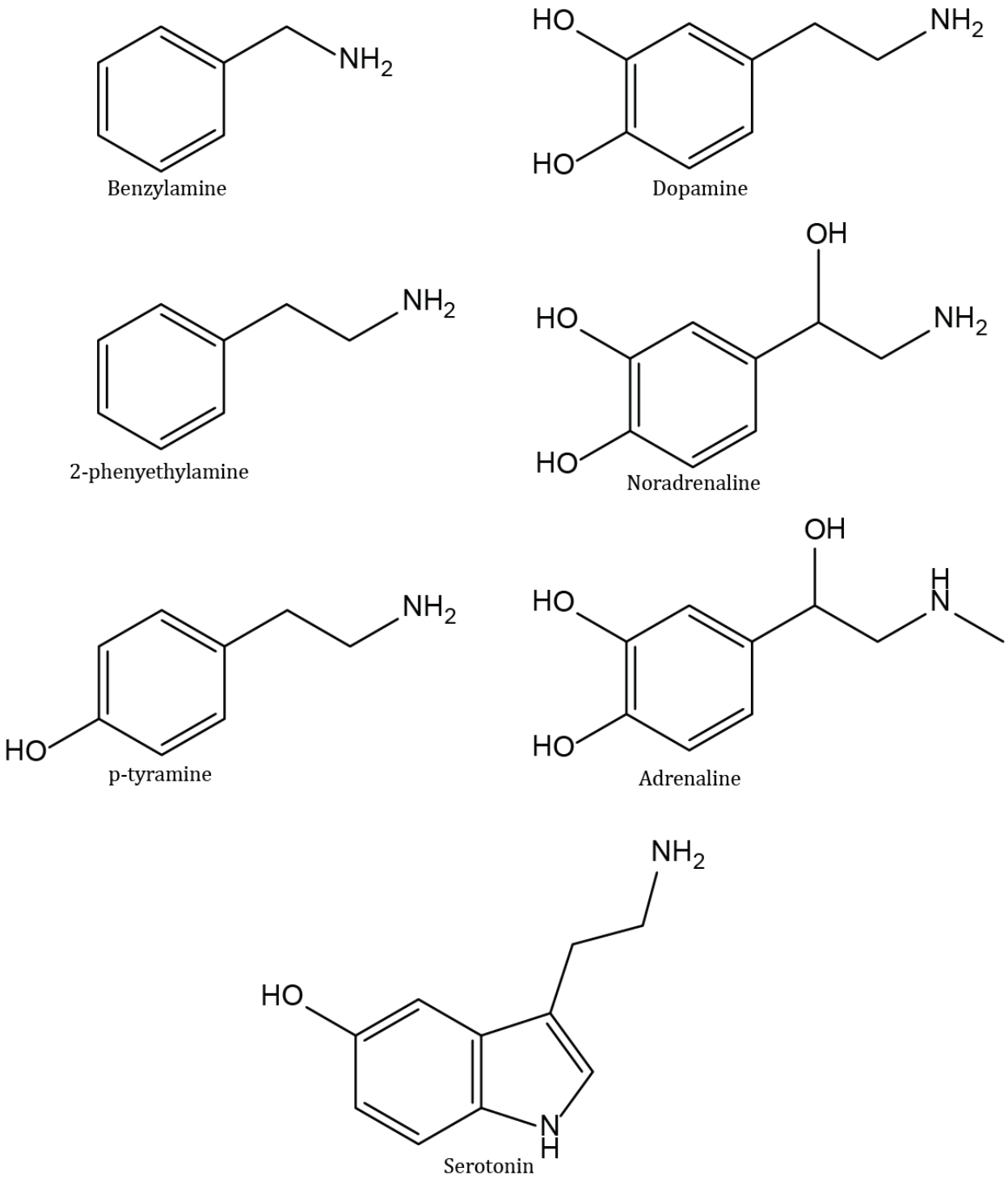

Figure 1.1.7.1 Structures of MAO-A and MAO-B Substrates

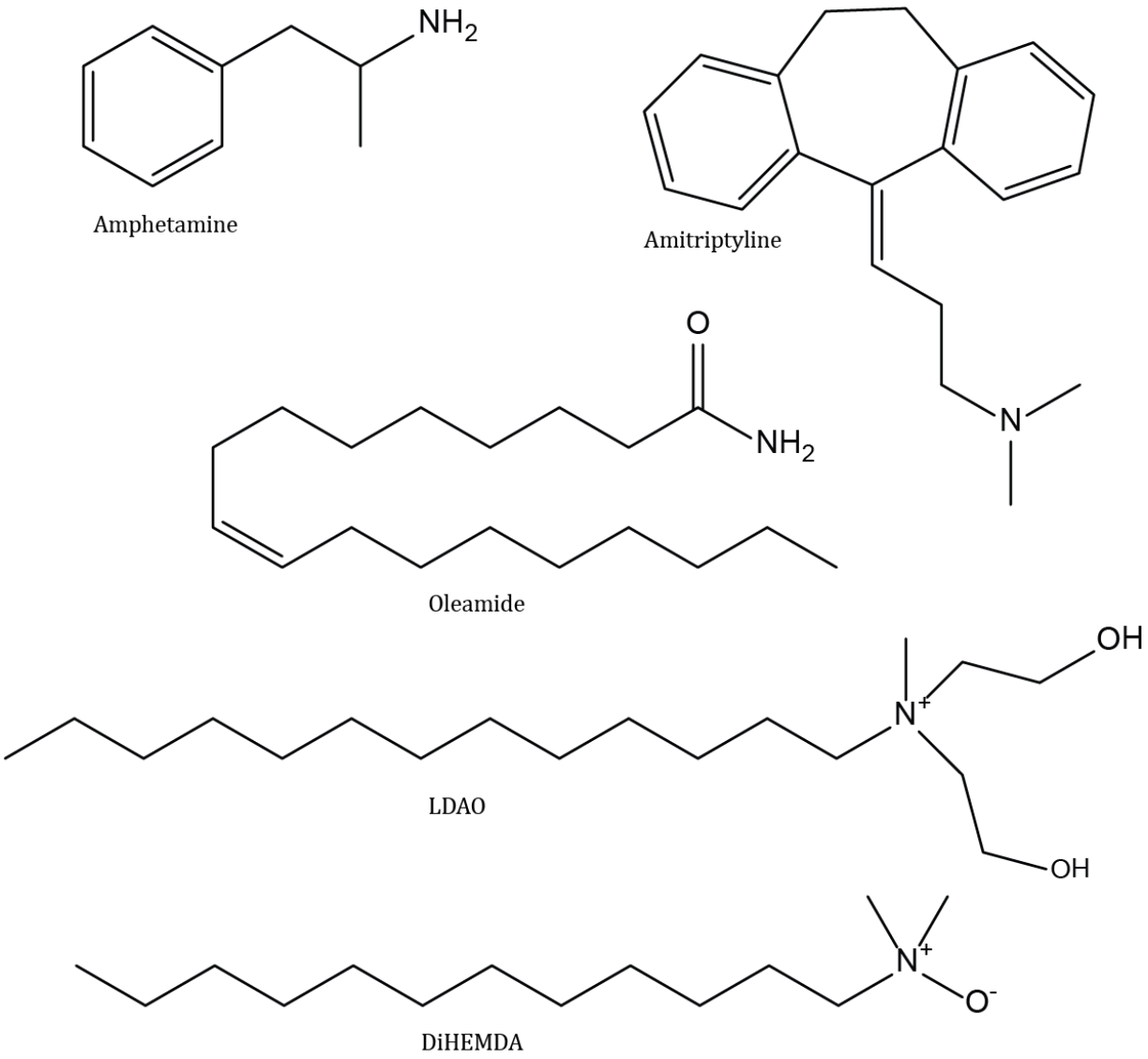

Figure 1.1.7.2 Structures of Reversible MAO-B Inhibitors

1.1.8 Therapeutic Importance of Monoamine Oxidases

Indication that monoamine oxidases were clinically relevant came when O'Connor observed an elevation in mood, appetite and weight gain in 27 tuberculosis patients treated with iproniazid[66]. Patients treated with isoniazid did not show similar changes in mood. Work previously done by Zeller

indicated that iproniazid was capable of inhibiting monoamine oxidase from liver preparations[67]. Treatment with isoniazid did not significantly inhibit monoamine oxidase activity. This led to the monoamine hypothesis of depression, wherein depression is caused by a decreased level of monoamines in the brain, including serotonin, dopamine, and noradrenaline [68].

The use of MAO inhibitors as antidepressants is limited by a perception of a high risk of dangerous side effects. As would be expected from the history presented herein, foodstuffs containing tyramine may be particularly dangerous, as the inhibition of MAO prevents the breakdown of ingested tyramine, leading to sympathetic stimulation and a hypertensive crisis, known as the "cheese effect"[69]. This side-effect was the reason for the development of l-deprenyl (a selective MAO-B irreversible inhibitor) and moclobemide (a reversible MAO-A inhibitor) as pharmaceutical agents for depression.

Therapeutically, drugs with safer side effect profiles in depression, such as serotonin-selective re-uptake inhibitors (SSRIs) and serotonin-noradrenaline re-uptake inhibitors (SNRIs), have largely replaced monoamine oxidase inhibitors because they lack the risk of a hypertensive crisis in patients. Drugs such as phenelzine and tranylcypromine (irreversible, non-selective inhibitors) remain a therapeutic option in cases of refractory, atypical depression[70].

l-Deprenyl, an irreversible inhibitor of MAO-B, was originally used in combination with L-DOPA for the treatment of Parkinsonism to prolong the duration of action of dopamine. l-Deprenyl has since fallen out of favour

clinically, being replaced by carbidopa which inhibits catabolism of dopamine in the periphery only. One of the difficulties in development of inhibitors for clinical use is the incomplete understanding of the kinetics of MAO-B. A more thorough understanding of exactly how MAO-B handles substrates could lead to insights into developing a selective, reversible inhibitor that could have important therapeutic implications.

Determining the precise role of MAO-B in the brain has been more difficult than MAO-A, however it appears to have a role in emotional regulation. MAO-B function has been associated with psychotic disorders, depression, addiction and neurodegenerative disease[49]. The thought that MAO-B activity may be associated with addiction has led to attempts to use MAO-B inhibitors for smoking cessation, although clinical trials have not shown promising results[71].

It is important to consider that there appears to be a large amount of therapeutic potential for modulating MAO-B activity, but many attempts have been unsuccessful. This does not mean that MAO-B should be abandoned as a potential target. The distribution of MAO-B is vast throughout the human body and the enzyme has numerous roles.

In a clinical setting, practitioners typically would prefer to inhibit a specific activity occurring in a specific area of the brain rather than inhibiting activity in the entire body. One of the ways to do this is to look very carefully at the kinetics of the enzyme and consider what conditions are being created within the enzymatic environment that could differ with distribution. An example of this would be the different distribution of substrates throughout

the human brain. If a clinician desired to inhibit oxidation of phenylethylamine but not dopamine turnover, would it be possible to create an inhibitor that selectively inhibits MAO-B in a manner dependent upon the presence of phenylethylamine? Extending this idea even further, could the activity of MAO-B be inhibited in a specific area of the brain based on the *combination* of substrates present? If this was possible, an extremely powerful clinical tool could be developed that would allow us to carefully select the precise MAO-B activity to be regulated. Unfortunately, our understanding of MAO-B and its handling of substrates does not yet allow us to know if this is even possible. A major reason for performing kinetic experiments and accurately describing the mechanism of MAO-B is to determine if any exploitable property exists that may be of clinical benefit in the future.

1.2 The Imidazoline Binding Site

The literature surrounding an imidazoline binding site can be overwhelming to an uninitiated investigator. Three general classes of sites appear to exist: The I_1 receptor (I_1R) has been the best studied imidazoline site and is thought to be involved centrally with lowering of blood pressure[112]. It is distributed throughout the brain and the brainstem. The I_2 binding site (I_2BS) has been associated with MAO, although its location on the enzyme and the role it plays has never been elucidated[112]. The I_3 binding site is the most recently-described site and is thought to have a role in insulin secretion[112]. The three sites have been largely discerned by their pharmacological properties, but in all cases the characterisation of these receptors/binding sites has been limited[72].

1.2.1 Discovery of the Imidazoline Binding Site

Investigating whether α_2-receptor stimulation in the nucleus reticularis lateralis (NRL) region of the brain results in hypotensive effects, Bousquet *et al.* examined the central hypotensive effects of agonists linked to the activation of α_2-adrenergic receptors[73]. Utilising anaesthetised cats, the group observed that catecholamine-based α_2 agonists such as α-methylnorepinephrine do not produce hypotensive effects, whereas imidazoline-based α_1-agonists, such as cirazoline, yield dose-dependent hypotensive effects[73]. Clonidine, an imidazoline-based α_2-receptor agonist, also yielded dose-dependent hypotensive effects. The authors went on to suggest that the NRL region might

1.2 The Imidazoline Binding Site

The literature surrounding an imidazoline binding site can be overwhelming to an uninitiated investigator. Three general classes of sites appear to exist: The I_1 receptor (I_1R) has been the best studied imidazoline site and is thought to be involved centrally with lowering of blood pressure. It is distributed throughout the brain and the brainstem. The I_2 binding site (I_2BS) has been associated with MAO, although its location on the enzyme and the role it plays has never been elucidated. The I_3 binding site is the most recently-described site and is thought to have a role in insulin secretion. The three sites have been largely discerned by their pharmacological properties, but in all cases the characterisation of these receptors/binding sites has been limited[72].

1.2.1 Discovery of the Imidazoline Binding Site

Investigating whether α_2-receptor stimulation in the nucleus reticularis lateralis (NRL) region of the brain results in hypotensive effects, Bousquet *et al.* examined the central hypotensive effects of agonists linked to the activation of α_2-adrenergic receptors[73]. Utilising anaesthetised cats, the group observed that catecholamine-based α_2 agonists such as α-methylnorepinephrine do not produce hypotensive effects, whereas imidazoline-based α_1-agonists, such as cirazoline, yield dose-dependent hypotensive effects[73]. Clonidine, an imidazoline-based α_2-receptor agonist, also yielded dose-dependent hypotensive effects. The authors went on to suggest that the NRL region might contain a specific subtype of receptor that is sensitive to imidazolines and not

contain a specific subtype of receptor that is sensitive to imidazolines and not catecholamines [73]. These observations spawned a great deal of interest in the anti-hypertensive imidazoline moiety and laid the groundwork for an entirely novel class of discrete receptors.

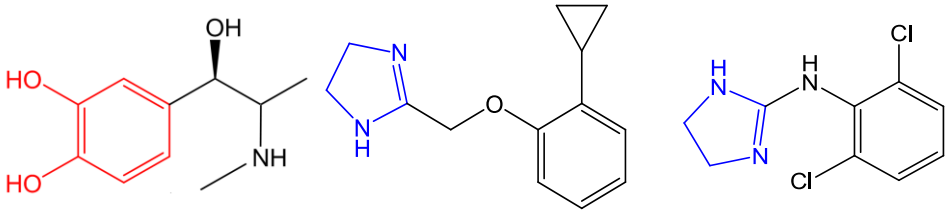

α-Methylepinephrine Cirazoline Clonidine

Figure 1.2.1.1 Structures of α-Methlyepineprine, Cirazoline and Clonidine
Structures of α-Methylepinephrine (α_2 agonist), cirazoline (α_1 agonist) and clonidine (a_2 agonist) with the catechol and imidazoline structures show in red and blue, respectively.

The structures of α-methylepinephrine, cirazoline and clonidine are shown in Figure 1.2.1.1 for comparison purposes. Both cirazoline and clonidine are α-agonists that produce hypotension in anaesthetised cats when given centrally, while α-methylepinephrine, an α2-agonist, produces no such effect[73]. Both cirazoline and clonidine possess an imidazoline ring (shown in blue), while α-methylepinephrine possesses the classical catechol group (red).

1.2.2 Evidence for a unique imidazoline receptor

Substantial evidence for an imidazoline receptor comes from radioligand binding assays. Using bovine brain membranes in 1987, Ernsberger *et al.* showed that noradrenaline only displaces 70% of the radioligand [^{3}H]*p*-aminoclonidine[74]. The imidazoline-containing structures of clonidine, phentolamine and naphazoline yielded biphasic displacement of [^{3}H]*p*-aminoclonidine with high affinity [74].

In following years, numerous groups reported the presence of an imidazoline-site insensitive to catecholamines in other tissues including rabbit, human brain and kidney[75-77]. The inability of catecholamine ligands to displace either [^{3}H]*p*-aminoclonidine or [^{3}H]idazoxan[75] (another imidazoline-based ligand) completely suggests the presence of a discrete imidazoline receptor.

1.2.3 Classification of imidazoline binding sites

Following a large number of binding assays with different radioactive imidazoline ligands and even more displacing ligands, two sub-classes of imidazoline sites were defined. I_1-sites were defined by binding *both* clonidine and idazoxan but were otherwise insensitive to catecholamines[78]. I_2 sites were defined as binding idazoxan but not clonidine. Poor correlation between pharmacological classification and physiological function, particularly with the role of pancreatic imidazoline receptors, led to further classification of receptors termed non-I_1, non-I_2 receptors[79]. These receptors, when associated with an ATP-sensitive potassium channel, were termed I_3 receptors in 1995[80].

1.3 The I_2 -site on MAO-B

Association of the idazoxan binding site with mitochondrial-membrane fractions obtained from liver led investigators to propose that MAO may possess the I_2-site[81]. In 1997, Raddatz *et al*. photoaffinity-labelled human and rat liver homogenates with [^{125}I]AZIPI (based on a cirazoline derivative). The covalent photoaffinity adduct was found to incorporate between amino acids lysine 149 and methionine 222 of MAO-B, which includes the residues of isoleucine 199 (Ile199) and glutamine 206 (Gln206). Ile199 and Gln206 both appear to exist at the interface between the substrate-binding site and the entrance cavity (shown in Figure 1.1.6.2 and Figure 1.1.6.3). Still, concerns about the association between MAO-B and an I_2-site exist.

Human liver MAO-B expressed in *Saccharomyces cerevisiae* shows a 10-50 fold lower affinity for [^{3}H]idazoxan than tissue-derived homogenates[82]. Homogenates typically show binding that corresponds to only 5-20% of MAO-B present in that sample, with the percentage varying depending on the source tissue[78,83]. Furthermore, while the I_2-site may be associated with amino acids lining the entrance cavity to the active site of MAO-B, inhibition of enzyme activity does not occur at the same concentrations seen in binding experiments. Kinetic inhibition assays suggest K_I values that are 100- to 1000-fold higher than K_D values determined from radioligand binding assays[84]. This discrepancy could be because I_2 ligands do not inhibit MAO-B through binding at their high affinity sites or because the kinetic values have been determined with the application of an incorrect model of inhibition.

Prior to the develpoment of a selective I_2 ligand 2-(2-Benzofuranyl)-2-imidazoline hydrochloride (referred to as 2-BFI hereafter)[113], the high affinity of idazoxan for α-adrenoceptors required adrenoceptors to be masked with saturating concentrations of rauwolscine in homogenate preparations[84]. 2-BFI is reported to have a greater affinity and I_2/α_2 selectivity ratio than idazoxan[85,114], potentially making it a better ligand to use than idazoxan in characterising the I_2-site on MAO-B[114].

In characterising the I_2-site on MAO-B, Wiest and Steinberg incubated MAO-B with tranylcypromine, an irreversible inhibitor of MAO-B, and observed that the high affinity [^{3}H]2-BFI binding was increased by 5-fold[83,86]. This peculiar observation suggested that tranylcypromine is capable of creating or exposing the high affinity site on MAO-B. To compare the tranylcypromine-induced site to the site found on 5-20% of MAO-B derived from human tissue, Wiest and Steinberg displaced [^{3}H]2-BFI from both platelet-derived tissue and tranylcypromine-treated tissue using numerous imidazoline ligands. The results of these experiments suggested the site yielded by tranylcypromine incubation is different from the site normally seen on MAO-B from *in vivo* homogenates[83,86,87]. Combined with the observation that some ligands show biphasic displacement (particularly with amiloride) of [^{3}H]2-BFI from *in vivo* homogenates, some investigators suggest that two subtypes of I_2 sites may exist (I_2A and I_2B)[83,86-88].

The high affinity I_2-site has a complicated history and the role and relationship to substrate turnover remains elusive. One of the goals during the

work leading to this thesis was to determine the mechanism through which 2-BFI affects MAO-B catalysis of substrates and how this fits with the role of the I_2 site.

1.3.1 Structures of I_2 ligands

Two I_2 ligands were used experimentally in preparation for this thesis. Idazoxan and 2-BFI are classical ligands described to have high affinity for the I_2 site.

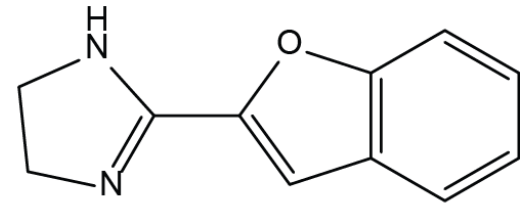

2-BFI

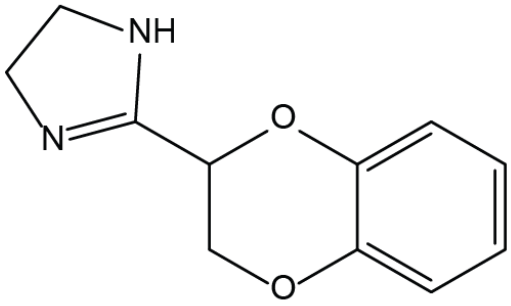

Idazoxan

Figure 1.3.1.1 Structures of I_2 ligands

1.4 Relevance and Outline

Monoamine oxidase (MAO) has been a clinically relevant target since the discovery that inhibition of the enzyme resulted in an elevation in mood[66,67]. A great deal of resources has been dedicated by industry and academia to investigate the role of MAO and to develop novel, selective inhibitors. With clinical implications in Parkinsonism, motivational control, and smoking cessation, specific MAO-B inhibition is desired clinically, yet no reversible, high affinity MAO-B-specific inhibitors are available[89].

The prospect of a high affinity site on MAO-B, but not MAO-A, as well as the difference in active site of the enzyme, provide exploitable differences between the two enzymes. Unfortunately, kinetic experiments show that imidazolines are poor inhibitors of MAO-B activity [84]. The inconsistent and often cryptic results involving the I_2-site have clarified neither the characteristics nor the role of the site on MAO-B.

Herein, the location and nature of the I_2-site on monoamine oxidase are predicted and characterised through the use of kinetic models and radioligand binding assays, and are latterly confirmed by crystal structure data[64]. MAO-B kinetics are examined and modelled to a novel mathematical equation. The equation, in modified form, is used to determine the inhibition mechanisms of classical and novel MAO-B inhibitors, including 2-BFI. Radioligand binding assays with [^{3}H]2-BFI reveal information about the formation and location of an I_2-site on MAO-B which, when analysed with the kinetic data, suggest novel physiological and regulatory roles for MAO-B.

2 Chapter 2: Kinetic modeling of MAO-B

2.1 Publications

Data and findings presented in this chapter have been published previously:

On the formation and nature of the imidazoline I2 binding site on human monoamine oxidase-B. **McDonald GR**, Olivieri A, Ramsay RR, Holt A. *Pharmacol Res*. 2010 Dec;62(6):475-88.

Potentiation of ligand binding through cooperative effects in monoamine oxidase B. Bonivento D, Milczek EM, **McDonald GR**, Binda C, Holt A, Edmondson DE, Mattevi A. *J Biol Chem*. 2010 Nov 19;285(47):36849-56

Bioactive contaminants leach from disposable laboratory plasticware. **McDonald GR**, Hudson AL, Dunn SM, You H, Baker GB, Whittal RM, Martin JW, Jha A, Edmondson DE, Holt A. *Science*. 2008 Nov 7;322(5903):917

2.2 Fundamentals of Enzyme Kinetics

Enzyme kinetics is an area of research that quantitatively investigates the rate of enzyme-catalysed reactions in the presence of different ligands. The systematic study of enzymes can yield information regarding the steps enzymes take to catalyse metabolism of substrates to yield a product.

The ubiquity of enzymes reflects their importance in regulating homeostasis, as well as their role in allowing systems to adapt to stressors. This characteristic makes enzymes a valuable target for drug design. Studying the kinetics of an enzyme can provide information on how substrates and inhibitors interact to affect the rate of catalysis. Designing an optimal

therapeutic agent based around an enzyme requires knowledge about the kinetics of the enzyme if the activity is to be modulated for clinical purposes.

2.2.1 Defining the Chemical Reaction and Activation Energy

A major aspect of a kinetic analysis is describing the interaction between ligands in a model which can be tested through experimentation. Mathematical equations representing hypothesised models are a valuable tool in assessing the ligand interactions. The first step in the derivation of a mathematical equation to represent a potential kinetic model requires a balanced chemical equation. A balanced equation shows, with correct stoichiometry, the reactants and the products involved:

$$A + B \leftrightharpoons C + D$$

The above schema represents a reversible process, wherein A and B could together yield products C and D. The process is also reversible wherein C and D could be the reactants yielding products A and B. The two-way arrows represent this in the above schema. The predominant direction of the reaction depends on which combination has the most favourable thermodynamic properties. Gibbs free energy change (ΔG) determines the direction of the reaction. The value for ΔG is calculated from the difference between products and reactants in their enthalpy and entropy at a given temperature. A negative

ΔG value indicates that the reaction is *spontaneous,* although nothing about the rate of the reaction can be determined from ΔG alone.

For a reaction to proceed and yield products, the reactants must first form a transient transition state complex. This transition complex is often represented with a double dagger(‡):

$$A + B \leftrightharpoons A\text{-}B^{\ddagger} \longrightarrow C + D$$

The formation of a transition complex is dependent on the standard free energy change (ΔG^{o}_{f}). ΔG^{o}_{f} represents the amount of energy required to overcome the barrier in formation of a transition complex. This barrier can also be referred to as activation energy, which is the amount of energy required to proceed with the reaction. ΔG^{o}_{f} can be determined in relationship to an equilibrium constant (K_{eq}) for the products and reactants:

$$\Delta G^{o}_{f} = -RT \ln (K_{eq})$$

Wherein R is the gas constant (8.31 J/mol^{o}K) and T is absolute temperature in degrees Kelvin. If the concentrations of products and reactants are at equilibrium, the K_{eq} for Equation 1 where C and D are products is:

$$K_{eq} = \frac{[C][D]}{[A][B]}$$

where the concentrations of the reactants and products are in mol/L.

ΔG^{o}_{f} represents the energy requirement for the formation of the transition molecule. As a barrier to the progression of a reaction, the requirement for activation energy limits *the rate* at which the reaction proceeds. There are two potential ways to increase the rate of the reaction. The first is increasing the temperature of the reaction so more transition complexes can form. The second includes the use of catalysts. Catalysts, exemplified here by enzymes are capable of lowering the activation energy, ΔG^{o}_{f} , by creating an environment in the active site that stabilises the transition state molecules. In this way, they are able to speed up, or catalyse, the rate of the reaction.

2.2.2 Development of the field of enzyme kinetics

The field of enzyme kinetics arguably began in 1892 when Adrian Brown, a British chemist, discovered that the rate of fermentation of sucrose by yeast was dependent on the concentrations of sucrose and oxygen[90]. It was not until 1902, however, that Henri first related catalytic rate to concentration mathematically[91]. Henri observed that an increase in substrate concentration produced a non-linear increase in rate of catalysis. He also observed that the (initial) rate of reaction was in proportion to the amount of enzyme present in a sample.

The schematic for the mathematical foundation of enzymatic catalysis was proposed by Henri:

$$E + S \leftrightharpoons ES \rightharpoonup E + P$$

Wherein E represents the enzyme, S represents the substrate, ES represents an enzyme-substrate complex, and P represents the product.

This simple model for enzyme catalysis is based upon numerous assumptions: the enzyme is a true catalyst and is not consumed in the process of the reaction; the substrate concentration is in great excess over enzyme concentration such that the binding of substrate to enzyme does not significantly change the concentration of substrate; the rate limiting step is the breakdown of ES to E + P; and rapid equilibrium exists. The rapid equilibrium assumption is that E, S and ES are all at equilibrium rapidly at the start of the reaction measurement.

This model also assumes that there is only one substrate involved in the process, although this was known not to be the case from as far back as the work by Adrian Brown who showed multiple substrates dictating the rate of yeast fermentation [90]. Nonetheless, the model has formed the backbone of many drug discoveries.

In 1913, Michaelis and Menten[92] confirmed the work of Henri and developed the Michaelis-Menten version of the model (presented in more detail in Section 2.2.3). Modifications and extrapolations of the Michaelis-Menten model allow for incorporation of data from substrates and inhibitors. These modifications are essential in analysing the steady-state kinetics of MAO-B.

2.2.3 Steady-state kinetics

In all of the kinetic experiments presented herein as original work, steady state kinetics are utilised. Most enzymes, including MAO-B, catabolise more than one substrate during catalysis. Studying the effect of a single substrate (amine) while maintaining the concentration of the second substrate (oxygen) creates a pseudo-first-order condition that allows for application of single substrate models.

The acquisition of data for steady-state kinetic analyses requires the measurement of the initial rate of the catalysed reaction. This initial rate provides the best estimate of enzyme activity in the specified environment before any significant contributions from products, denaturation of the enzyme, and changes in pH can occur. The initial rate (v) increases in relation to increases in substrate concentration [S], until the velocity reaches a maximum value (V_{max}). As described by Henri, the maximum rate increases in proportion to the amount of enzyme in the sample. Thus, the rate of product formation by a single enzyme molecule(k_p) multiplied by the total amount of enzyme ($[E]_t$) is equal to V_{MAX}. Plotting initial rates versus substrate concentration yields a rectangular hyperbola described by the Michaelis-Menten equation:

$$v = \frac{[E]_t k_p [S]}{K_M + [S]}$$

The Michaelis constant, K_M, represents the substrate concentration at which the initial rate is half of the maximum velocity. Under steady-state conditions, K_M may approximate the binding affinity of substrate to enzyme if product formation is slow relative to dissociation of substrate from the enzyme. The affinity an enzyme has for a particular substrate is described by a dissociation constant, K_D. Formation of ES and E+S are described by rate constants, k_1 and k_{-1}, respectively:

$$E + S \underset{k_{-1}}{\overset{k_1}{\rightleftarrows}} ES$$

K_D is represented as:

$$K_D = \frac{k_{-1}}{k_1}$$

When describing the reaction in full, a rate for product formation must be included:

$$E + S \underset{k_{-1}}{\overset{k_1}{\rightleftarrows}} ES \overset{k_p}{\rightarrow} E + P$$

Thus, the definition of K_M is:

$$K_M = \frac{k_{-1} + k_p}{k_1}$$

In the case where k_{-1} is much greater than k_p, K_M will approach the value of K_D. In other words, in situations where the substrate dissociation rate is much greater than the rate of catalysis, K_M approximates K_D.

These mathematical equations form the backbone of steady-state kinetics and allow researchers to quantify and model inhibitor mechanisms. It is important to note that the model is appropriate for reactions containing only a single species of enzyme.

In contrast to steady-state kinetics where initial, linear rates are required for analysis, it is possible to determine all kinetic parameters from a single progress curve with non-linear regression [93]. This process, however, is prone to complications from changes in the enzyme's environment or denaturation of the enzyme. The analyses, in the presence of inhibitors also become a computational challenge for software. For these reasons, classical steady-state kinetic techniques are preferred for modelling enzymatic activity.

2.3 Reversible inhibitor mechanisms

Enzymes are large proteins made of numerous amino acids, providing potential areas for small molecules to bind. Some of these molecules will bind and inhibit the enzyme directly in the active site (competitive inhibition), while others may bind at distant sites and affect the ability of the enzyme to catalyse the reaction (allosteric). Determination of the mechanism of an inhibitor can provide important insight into therapeutic targets available on enzymes. Classically, four types of general inhibition exist: competitive, non-competitive, uncompetitive, and mixed inhibition. All these inhibition forms appear differently in kinetic experiments. Using mathematical equations representing each model can help to determine kinetic parameters and elucidate how an inhibitor works. In all these forms of inhibition, the inhibitors bind rapidly and reversibly to the enzyme.

2.3.1 Competitive inhibition

Competitive inhibitors reduce substrate turnover by preventing binding of the substrate to the enzyme in a mutually exclusive fashion. In other words, binding of substrate to the active site completely blocks the inhibitor from binding, while binding of inhibitor completely blocks the ability of substrate to bind. In most cases, this form of inhibition occurs because the inhibitor binds directly in the active site. The similarity of binding between substrate and inhibitor is frequently due to similarity in structure, with the inhibitor

unable to undergo catalysis. Describing this form of inhibition in a model makes the mutually exclusive relationship obvious:

$$\begin{array}{ccccc} & & K_s & & \\ E + S & \leftrightharpoons & ES & \rightharpoonup & E + P \\ + & & & & \\ I & & & & \\ K_i \updownarrow & & & & \\ EI & & & & \end{array}$$

This model shows the dissociation constants for the inhibitor (K_i) and for substrate (K_s). The model also makes it clear that as the concentration of inhibitor increases, the equilibrium shifts towards the formation of EI and away from ES. The EI form of the enzyme is unable to yield product, leading to inhibition. Importantly, increasing substrate concentrations are able to surmount any inhibition caused by an inhibitor. An equation describing this form of inhibition is:

$$v = \frac{V_{MAX}[S]}{K_M\left(1 + \frac{[I]}{K_i}\right) + [S]}$$

The above equation describes an inhibitor that modifies only K_M. Thus, the apparent K_M changes in the presence of an inhibitor. It is important to note that experimentally, measurement of K_M is achieved through kinetic assays. This value can approximate a dissociation constant (K_s) under certain conditions (See Section 2.2.3).

2.3.2 Non-competitive inhibition

Independent binding of substrate and inhibitor at different sites results in non-competitive inhibition. Binding of inhibitor in this scenario renders the enzyme unable to catalyse the reaction, but has no effect on the ability of substrate to bind. The result is a decrease in V_{MAX} that is insurmountable by increases in substrate concentration, but with no change in the K_M value. The model for such inhibition is:

$$\begin{array}{ccccc} & & K_s & & \\ E & + S \leftrightharpoons & ES & \rightharpoonup & E + P \\ + & & + & & \\ I & & I & & \\ K_i \updownarrow & & K_s & \updownarrow K_i & \\ EI & + S \leftrightharpoons & ESI & & \end{array}$$

Similar to competitive inhibition, inhibitor-bound enzyme is unproductive (EI, ESI). The ability of inhibitor and substrate to bind randomly and independently results in no apparent change in affinities secondary to equilibrium shifts. This is represented mathematically by:

$$v = \frac{V_{MAX}[S]}{K_M\left(1 + \frac{[I]}{K_I}\right) + [S]\left(1 + \frac{[I]}{K_I}\right)}$$

From this equation, it appears that a change in inhibitor concentration is capable of affecting the apparent K_M value in relation to velocity. Rearranging the equation, however, makes it clear that only V_{MAX} is affected:

$$v = \left(\frac{V_{MAX}}{\left(1 + \frac{[I]}{K_I}\right)}\right)\left(\frac{[S]}{K_M + [S]}\right)$$

This rearranged equation makes it clear that the concentration of inhibitor changes the *fraction* of maximum velocity the enzyme is capable of yielding, but any given substrate concentration will always yield the same fraction of maximal velocity. In other words, this form of inhibition is insurmountable.

2.3.3 Uncompetitive inhibition

Uncompetitive inhibition requires the sequential binding of substrate prior to the binding of the inhibitor. The model can be described:

$$\begin{array}{c} \overset{K_s}{E + S \leftrightharpoons ES} \rightharpoonup E + P \\ + \\ I \\ \downuparrows K_i \\ ESI \end{array}$$

Oddly, this form of inhibition results in a decrease in measured K_M values when inhibitor is present. Consider the binding of I to ES shifts the equilibrium to favour ESI, resulting in a shift of the equilibrium between E + S and ES to favour ES. This increase in occupation of E by S decreases K_S and results in an apparent lower K_M when measured kinetically. The equation describing this model is:

$$v = \frac{V_{MAX}[S]}{K_M + [S]\left(1 + \frac{[I]}{K_i}\right)}$$

2.3.4 Mixed inhibition

Mixed inhibition is similar to noncompetitive inhibition, except the binding of substrate or inhibitor proportionally changes the binding of the other respective ligand by a similar degree. In other words, binding of substrate to enzyme will change the apparent K_i of the inhibitor by a factor (in this case represented by α). The binding of inhibitor to free enzyme affects the apparent K_s by the same factor:

$$\begin{array}{ccccc} & & \overset{K_s}{} & & \overset{k_p}{} \\ E & + & S & \leftrightharpoons & ES & \rightharpoonup & E & + & P \\ + & & & & + & & & & \\ I & & & & I & & & & \\ K_i \uparrow\downarrow & & & & \alpha K_s \uparrow\downarrow & & \alpha K_i & & \\ EI & + & S & \leftrightharpoons & ESI & & & & \end{array}$$

This form of enzyme inhibition can be described mathematically by the equation:

$$v = \frac{V_{MAX}[S]}{K_M\left(1 + \frac{[I]}{K_i}\right) + [S]\left(1 + \frac{[I]}{\alpha K_i}\right)}$$

2.3.5 Partial inhibition

The previous sections described four distinct forms of inhibition. In all cases, the binding of an inhibitor rendered the enzyme unable to yield product. Consider a situation wherein an inhibitor does not completely halt turnover, but slows turnover. Such a situation is referred to as partial inhibition. In such a case, the complex of enzyme (E), substrate (S) and inhibitor (I) still yields a product albeit at a different rate than enzyme with substrate alone. The

schematic below represents a partial-mixed inhibition, where the ESI complex yields product at different rate than ES by a factor of β:

$$\begin{array}{ccccc} & & \overset{K_s}{} & & \overset{k_p}{} \\ E & + & S & \leftrightharpoons & ES \rightharpoonup E + P \\ + & & & & + \\ I & & & & I \\ {\scriptstyle K_i}\uparrow\downarrow & & & & {\scriptstyle \alpha K_s}\uparrow\downarrow{\scriptstyle \alpha K_i} \\ EI & + & S & \leftrightharpoons & ESI \rightharpoonup EI + P \\ & & & & {\scriptstyle \beta k_p} \end{array}$$

The above model represents a situation wherein binding of substrate affects the binding of inhibitor (and *vice versa*) by a factor of α, and the rate of product formation while bound to inhibitor by a factor of β. In the case of α=1 and β=0, the inhibition is purely non-competitive. The equation describing this model kinetically is:

$$v = \frac{V_{MAX}[S]\left(1 + \frac{\beta[I]}{\alpha K_i}\right)}{K_s\left(1 + \frac{[I]}{K_i}\right) + [S]\left(1 + \frac{I}{K_i}\right)}$$

2.4 Transient-state kinetics

Steady-state analyses depend on the rapid equilibration between substrate and the enzyme-substrate complex. This transient phase between initial mixing and equilibrium can provide valuable kinetic information regarding the interaction between substrate and enzyme. Measuring the changes occurring prior to equilibrium requires the use of stopped-flow kinetics.

2.4.1 Stopped-Flow kinetics

The method of determining kinetic constants from a pre-equilibrium state requires the fast mixing of two solutions. In a laboratory setup, two syringes hold reactant mixtures (one a substrate mixture, the other an enzyme mixture) prior to mixing. Depressing the plungers of the syringes, the contents are forced into a common chamber where they are mixed. After mixing, the flow of the substances is abruptly stopped, and changes in absorbance or fluorescence occurring in the substrate-enzyme mixture are measured by spectroscopy.

Measurement of pre-steady-state kinetics in MAO-B with stopped-flow analyses revolves around the unique spectral properties of the riboflavin. In an oxidised form, the flavin absorbs light maximally at 450 nm. As the flavin is reduced, this absorption maximum diminishes in a process referred to as "bleaching"[94]. Measurement of the changes in absorption of the MAO-B flavin

under anaerobic conditions provides important information on how MAO-B handles substrates (See Section 2.5 for more details).

None of experiments presented herein used stopped-flow methods. It is, however, an important technique that has been utilised by researchers in the characterisation of MAO kinetics. Information presented in the literature from stopped-flow experiments provides extra information about the way MAO-B handles substrates. This information is used in conjunction with steady-state data to provide a comprehensive model of MAO-B inhibition by numerous inhibitors.

2.4.2 Isotope effects

There are many steps in the process of an enzyme catalysing the breakdown of substrate to a product. Substrate must proceed to the active site, bind within the active site, become distorted to induce bond breakage, bonds must be broken, and the product must be released. Determining which of these steps is rate limiting is an important aspect of elucidating a mechanism for an enzyme. One way to determine if the rate-limiting step is the breakage of a bond within the substrate is to use an isotopic substitution at the location where the bond breakage is occurring[95]. Addition of an isotope, for example replacing a hydrogen with deuterium, changes the vibrational frequencies of the affected bonds and decreases the ease of bond breakage[95].

If the rate-limiting step in catalysis is the breaking of the bond, a substrate that possesses a deuterated group at the site of bond break will proceed with

an overall rate decrease compared to a non-deuterated form of the substrate. If no decrease in reaction rate occurs with the deuterated substrate, it is unlikely that the bond-breakage process is rate limiting in the catalysis of the reaction[95].

The effect of isotopes are seen mostly through a decrease in rate, and a decrease in affinity for the enzyme should not be seen (remember that since K_M does not necessarily approximate K_S and that reaction rate may contribute to the magnitude of K_M, a change in K_M is possible with isotope effects since the rate of reaction is changing).

Isotope effects should not change the way an inhibitor appears to impair turnover, nor should the constants of the inhibitor change between the deuterated and non-deuterated forms of the substrate.

2.5 Development of reaction scheme for MAO-B

2.5.1 Classical reaction scheme

Understanding how MAO-B handles substrates is essential for developing accurate models of inhibition that describe observations in a consistent manner. Major contributions to understanding the catalytic mechanism of MAO-B have been made in the past 60 years, with enzyme kinetics providing sufficient information for researchers to believe the enzyme follows a ping-pong mechanism (shown in Figure 2.5.1.1)[96]. In such a model, one substrate binds and is catabolised before the second substrate can bind and be catabolised.

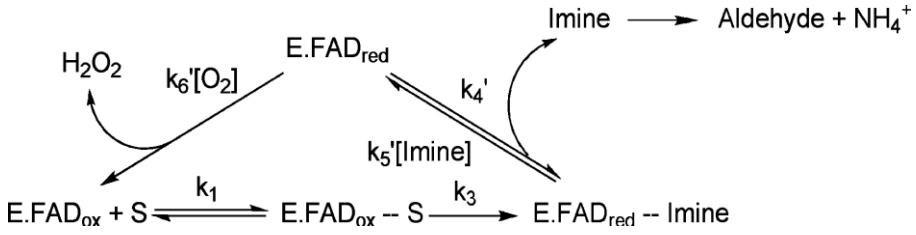

Figure 2.5.1.1 Classical ping-pong mechanism for MAO-B
Scheme of MAO-B oxidation of amines as a simple ping-pong mechanism. E.FADox represents free enzyme with an oxidised flavin and E.FADred refers to free enzyme with the flavin in reduced form. S represents substrate, Imine represents the product of the reaction which is converted to an aldehyde via non-enzymatic hydrolysis.

In a study designed to confirm a ping-pong mechanism for MAO-B, Husain *et al.* used stopped-flow analyses to probe MAO-B[97]. The experiments yielded some very interesting observations, which the scheme presented in Figure 2.5.1.2 incorporates.

Comparing V_{MAX} values for benzylamine and D_2-benzylamine at saturating amine and oxygen concentrations, D_2-benzylamine turnover is 6.7-fold lower[97], suggesting that oxidation of the substrate is rate-limiting.

Comparing V_{MAX} values for phenylethylamine and D_2-phenylethylamine at saturating amine and oxygen concentrations yields a ratio of 1, suggesting that oxidation of the flavin is rate-limiting[97].

At atmospheric oxygen, V_{MAX} for benzylamine is 3.3 fold higher than phenylethylamine. At saturating concentrations of oxygen, however, the V_{MAX} for phenylethylamine is 1.7 times greater than benzylamine[97].

The K_M for oxygen when phenylethylamine is substrate is 10-fold larger than when benzylamine is substrate[97].

Upon entering the steady state, 40 and 80-90 percent of the enzyme is in the reduced state when benzylamine and phenylethylamine are substrate, respectively[97].

Enzyme reduced with either a slight excess of benzylamine or dithionite under anaerobic conditions reoxidises at a rate slower than benzylamine turnover, suggesting that benzylamine forms an enzyme-product complex that undergoes flavin reoxidation faster than reduced enzyme alone[97].

An attempt to form a reduced enzyme-imine complex through a massive excess of benzylamine under anaerobic conditions, followed by rapid mixing of oxygen yielded a biphasic reaction. The first phase was a 25% reoxidation of the flavin, which occurred at the same rate as free enzyme. The other 75% of the reoxidation activity occurred at a rate 4-fold slower [97].

The rate of enzyme reduction with β-phenylethylamine (referred to hereafter as phenylethylamine) as substrate is 30-fold faster than the maximal rate of catalytic turnover[97].

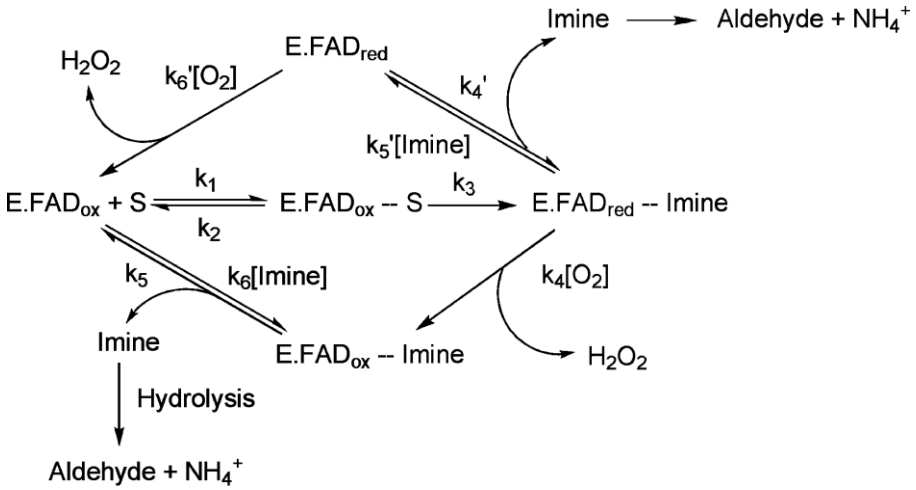

Figure 2.5.1.2 Model of MAO-B mechanism following stopped-flow data collection

From reference [98]. Scheme of MAO-B oxidation of amines. E.FADox represents free enzyme with an oxidised flavin and E.FADred refers to free enzyme with the flavin in reduced form. S represents substrate, Imine represents the product of the reaction which is converted to an aldehyde via non-enzymatic hydrolysis.

The scheme presented in Figure 2.5.1.2 for amine oxidation by MAO-B suggests that upon binding $E.FAD_{ox}$, substrate undergoes oxidation to produce an imine. Certain substrates, such as phenylethylamine, are suggested to most frequently produce an imine that is released, yielding unbound $E.FAD_{red}$ that is then oxidised back to $E.FAD_{ox}$ (upper pathway in Figure 2.5.1.2)[97]. Other substrates, such as benzylamine, typically produce an imine that remains in the active site while $E.FAD_{red}$ is oxidised (lower pathway in Figure 2.5.1.2)[97].

This model of amine turnover continues to be quoted as the mechanism as late as 2009 even though improvements have been made [98,99].

2.5.2 Updating the reaction scheme

The classical scheme appropriately explains the data obtained by the researchers at the time. In 1987, however, further stopped-flow analyses by Ramsay showed that at high concentrations, substrate binds $E.FAD_{red}$ and speeds up the rate of flavin oxidation[100,101]. She incorporated this result into the classical reaction scheme to yield the schematic in Figure 2.5.2.1[101].

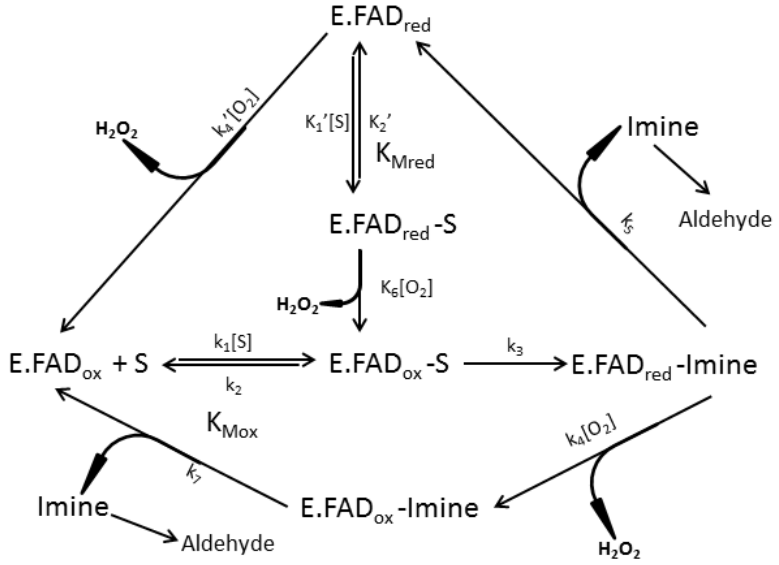

Figure 2.5.2.1 Modification of MAO-B mechanism to incorporate $E.FAD_{red}$-S

Comprehensive model of amine catabolism by MAO-B. Evidence from Ramsay[100,101] indicates that substrate can bind $E.FAD_{red}$ to form $E.FAD_{red}$-S which is capable of being reoxidised to form $E.FAD_{ox}$-S.

The ability of $E.FAD_{red}$ to participate in the catabolism of amines requires reconsideration of the observations from the initial stopped-flow experiments. The addition of the $E\text{-}FAD_{red}$-S to $E.FAD_{ox}$-S pathway by Ramsay provides an explanation for her observation alone. The addition of her observation that substrate binding to E.FADred speeds up the rate of flavin oxidation allows us to reinterpret the previously obtained stopped-flow data as well. As a part of reconciling the full array of evidence, we propose a major

shift in interpretation of the data, summarised in Table 2.5.1, that suggests the existence of E.FAD$_{red}$-Imine being reduced by oxygen prior to imine release is no longer required in the model.

The observation that benzylamine turnover by MAO-B occurs at a rate greater than the rate of oxidation of the flavin in free enzyme was originally used to justify the existence of an E.FADred-Imine species [97]. This E.FAD$_{red}$-Imine species was thought to form a ternary complex with oxygen and result in faster oxidation of the flavin, thus explaining how the presence of benzylamine results in a faster catalytic rate than the rate of flavin oxidation alone[97]. With the knowledge that substrate actually binds to E.FAD$_{red}$ to yield a complex that oxidises the flavin faster than the oxidation in the absence of substrate[99,100], the need for a ternary imine-containing complex no longer exists.

The 10-fold increase in K_M for oxygen when phenylethylamine is substrate was previously interpreted to suggest that E.FAD$_{red}$ has a lower K_M for oxygen than does E.FAD$_{red}$-Imine[97]. The known existence of E.FAD$_{red}$-S no longer requires the model to have an E.FAD$_{red}$-Imine component to explain the change in observed K_M for oxygen in the presence of different substrates. Instead, the explanation can be simply that when phenylethylamine is substrate, the K_M for oxygen is significantly different depending on whether the enzyme is in the E.FAD$_{red}$ or E.FADred-S form. Binding of benzylamine to E.FAD$_{red}$ may cause a shift in the K_M for oxygen as well, but not to the same degree as phenylethylamine.

The inclusion of an E.FAD$_{red}$-S pathway allows *all* of the observations from the original paper [97] to be explained *without* inclusion of the E.FAD$_{ox}$-Imine step. For this reason, the scheme used for the derivation of steady state equations and analyses throughout this writing do not include an E.FAD$_{ox}$-Imine complex (scheme shown in Figure 2.5.2.2). That is not to say that E.FAD$_{ox}$-Imine is a completely benign entity, but rather it represents an unnecessary level of complexity without just reason. A table of original observations leading to the development of the model in Figure 2.5.1.2 along with interpretation supporting the modified schematic (Figure 2.5.2.2) can be found in Table 2.5.1.

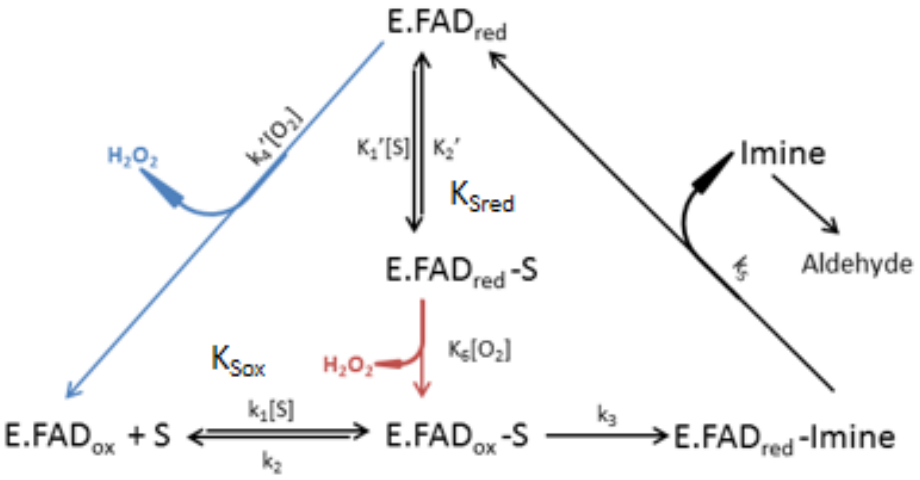

Figure 2.5.2.2 Proposed MAO-B mechanism incorporating all evidence
Simplified scheme of amine turnover by MAO-B. To help define which pathway is being referred to, K_{Sox} and K_{Sred} are labelled. The blue line represents product formation associated with V_{MAXox}. The

red line represents product formation associated with V_{MAXred}. The selection of hydrogen peroxide as an indicator of product formation is for technical reasons discussed in Section 2.6.2.

Interpretation of Evidence for Model Development			
	Evidence	**Classical Interpretation**	**New Intepretation**
1	Comparing V_{MAX} values for benzylamine and D_2-benzylamine at saturating amine and oxygen concentrations, D_2-benzylamine turnover is 6.7-fold lower, sugesting that the oxidation of substrate is rate-limiting	$E.FAD_{red}$-Imine reoxidises faster than $E.FAD_{ox}$-S goes to $E.FAD_{red}$-Imine	With oxidation as the rate-limiting step in benzylamine oxidation, flow through the model is held up at $E.FAD_{ox}$-S complex, thus increasing the fraction of enzyme in the oxidised form
2	Comparing V_{MAX} values for phenylethylamine and D_2-phenylethylamine at saturating amine and oxygen concentrations yields a ratio of 1, suggesting that oxidation of the flavin is rate-limiting.	E.FADred to E.FADox occurs slowly compared with E.FADox to E.FADred-Imine	With oxidation of the flavin as the rate-limiting step, flow through the model is slowed at $E.FAD_{red}$ and $E.FAD_{red}$-S, thus increasing the fraction of enzyme in the reduced form
3	At atmospheric oxygen, V_{MAX} for benzylamine is 3.3-fold higher than phenylethylamine. At saturating concentrations of oxygen, however, the V_{MAX} for phenylethylamine is 1.7 times greater than benzylamine.	$E.FAD_{red}$ to $E.FAD_{ox}$ is much faster than when imine is present IF oxygen concentrations are high. This is based upon the K_M for oxygen at $E.FAD_{red}$ being lower than at $E.FAD_{red}$-Imine.	When phenylethylamine is substrate, $E.FAD_{red}$-S oxidation is extremely fast, as long as oxygen concentration is high enough. The rate when benyzlamine is substrate is not as fast, however more occurs at a low oxygen concentrations
4	The K_M for oxygen when phenylethylamine is substrate is 10-fold larger than when benzylamine is substrate	$E.FAD_{red}$ has a lower KM for oxygen than $E.FAD_{red}$-Imine	As above (point 3)
5	Upon entering the steady state, 40 and 80-90 percent of the enzyme is in the reduced state when benzylamine and phenylethylamine are substrate, respectively	$E.FAD_{red}$-Imine is rapidly reoxidised to $E.FAD_{ox}$-Imine compared to $E.FAD_{red}$ to $E.FAD_{ox}$	As explained above (points 1 and 2)
6	Enzyme reduced with either a slight excess of benzylamine or dithionite under anaerobic conditions reoxidises at a rate slower than benzylamine turnover, suggesting that benzylamine forms and enzyme-product complex that reoxidises the flavin faster than reduced enzyme alone.	Imine must speed up reoxidation of flavin	As above (point 3)
7	A quarter of $E.FAD_{red}$-Imine reoxidation occurs at the same rate as free $E.FAD_{red}$ and the remaining 75% reoxidises 4-fold slower.	Interpreted as technical difficulties associated with creating imine. Evidence was not incorporated into the model	Intepreted to suggest that imine pathway likely plans a minimal role
8	The rate of enzyme reduction with phenylethylamine as substrate is 30-fold faster than the maximal rate of catalytic turnover	Presence of imine must speed up reoxidation of flavin	E.FADox-S to E.FADred occurs much faster than reoxidation of flavin, leading to a build-up of reduced enzyme when phenylethylamine is substrate

Table 2.5.1 Summary of evidence from stopped-flow experiments

Summary of the evidence from the classical 1982 stopped-flow experiments by Husain *et al*[97]. The original interpretation of the evidence are listed along side any new interpretations that have occurred as a result of the existence of $E.FAD_{red}$-S.

2.5.3 Implications of a New Model

The application of a Michaelis-Menten model requires a single catalytic enzyme to be valid, as mentioned previously in Section 2.2.3. Given that the model for MAO-B catabolism of substrates possesses two distinct enzyme species ($E.FAD_{red}$ and $E.FAD_{ox}$) with different rates of reaction, the application of the Michaelis-Menten model is no longer valid. The inappropriate use of Michaelis-Menten kinetics to determine enzymatic parameters continues, with publications as late as 2011 utilizing the technique[65]. Part of the reason for this is that the enzyme does appear to yield a kinetic curve similar to that described by the Michaelis-Menten equation if an insufficient number of data points is used.

As an example, Figure 2.5.3.1 shows the catabolism of benzylamine under both high and low oxygen conditions using minimal points to define the curve. Linear-regression yields K_M values of 180 and 130μM for high and low oxygen, respectively. The substrate range spans approximately ten times the K_M value.

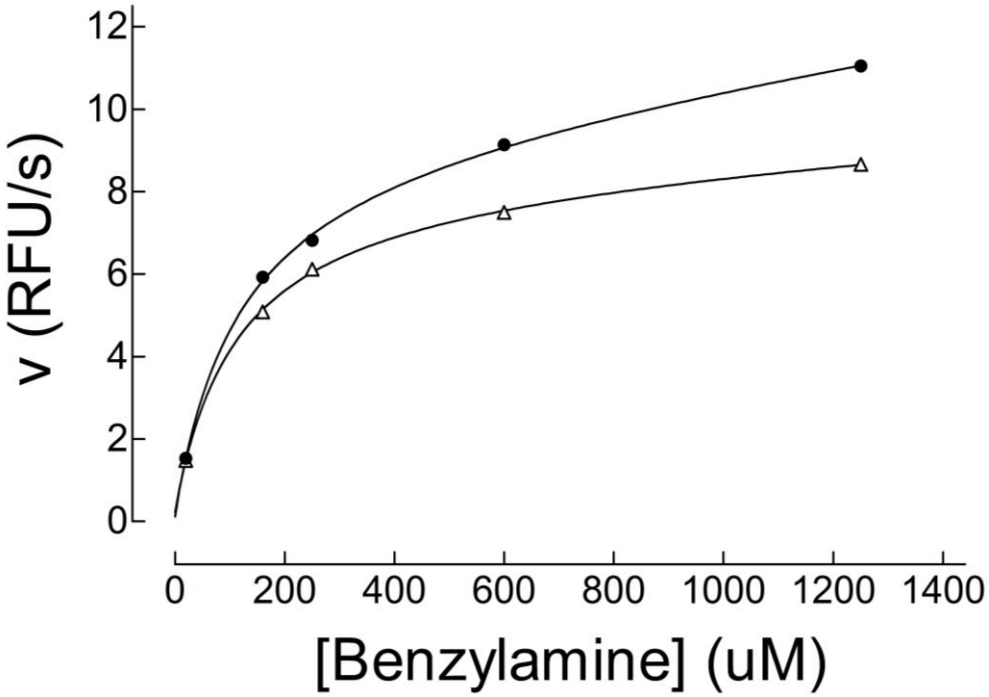

Figure 2.5.3.1 Curve fitting with minimal data points

Oxidation of benzylamine (10-1250 μM) by hMAO-B (1nM) under 100 μM oxygen (Δ) and 500 μM oxygen (●) fitted to a one site hyperbola (Michaelis-Menten Equation)

Using so few points allows the Michaelis-Menten equation approximately to fit the data. The addition of more points within the same concentration range allows the systematic differences between the data and the Michaelis-Menten model to be seen. Figure 2.5.3.2 is similar to Figure 2.5.3.1 with the exception that more data points are included to fill in the gaps. The dotted line represents a Michaelis-Menten model, while the solid line shows a two-site fit.

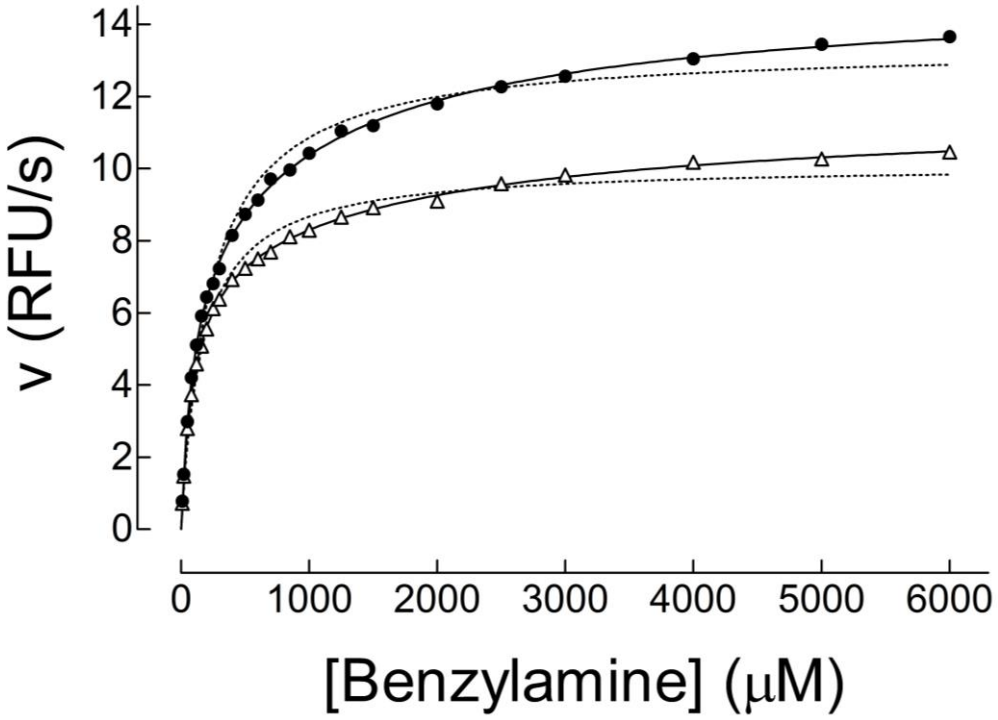

Figure 2.5.3.2 Curve fitting with multiple data points

Oxidation of benzylamine (10-1250 μM) by hMAO-B (1nM) under 94 μM oxygen (△) and 526 μM oxygen (●) fitted to a one-site hyperbola (dotted line) and a two-site hyperbola (solid line).

The differences seen between the fits appear very small, but show that MAO-B follows a two-site model more closely than it does a one-site model. This has major implications for interpretation of kinetic behaviour and understanding of inhibitor mechanisms.

Classically, inhibitor mechanisms have been determined using a transformation of the Michaelis-Menten equation to a linear form. This linearization allows the mechanism of the inhibitor to be determined visually. A commonly used linearization technique is that of Lineweaver and Burk. The method takes the reciprocal of the Michaelis-Menten equation, allowing the data to be linearized as a double reciprocal plot. The transformation is represented mathematically as:

$$\frac{1}{v} = \frac{K_M}{V_{max}[S]} + \frac{1}{V_{max}}$$

This equation also represents a model with only one enzyme species present and cannot be applied on its own to determine the mechanisms of MAO-B inhibitors. Nonetheless, this transformation has been used extensively in MAO-B kinetics. Upon close inspection of published Lineweaver-Burk plots, as well as of transformations of our own data, we observe consistently that the re-plots are not linear, but slightly curved. This curve is a significant problem for creating a line of best fit, which is an essential part of using a Lineweaver-Burk plot to determine an inhibitor mechanism. It is no surprise, therefore, that there are inconsistencies in the literature regarding the mechanisms of certain inhibitors of MAO-B.

Clearly, the application of the classical Michaelis-Menten equation is not to use in analysis of MAO-B. We set out to develop a mathematical model that more closely represented the data observed for MAO-B activity.

2.5.4 Mathematical Modeling of the New Reaction Scheme

The scheme presented in Figure 2.5.2.2 represents the simplest, accurate model of MAO-B turnover of amines based upon the information in the literature. Currently, there are no mathematical models developed specifically to describe the steady-state kinetics of this model. Even with the acceptance of a complicated reaction scheme for MAO-B, researchers continue to apply Michaelis-Menten kinetics designed to describe the simple reaction scheme:

$$\boldsymbol{E + S \leftrightarrow ES \rightarrow E + P}$$

Substrate (S) binds to enzyme (E) to form an enzyme substrate complex (ES). The rate of product formation resulting from ES formation is k_p. Using this scheme, the Michaelis-Menten equation, shown in Eq. 2.1, can be derived.

$$v = \frac{V_{MAX}[S]}{K_M + [S]} \qquad \text{Eq. 2.1}$$

The Michaelis-Menten equation describes the velocity of a reaction as a function of substrate concentration, K_M and a maximum velocity (a number obtained by multiplying the concentration of enzyme by k_p). The function yields a rectangular hyperbola wherein K_M describes the concentration of substrate required to obtain fifty-percent of maximum velocity. Unfortunately, this equation describes a simple reaction scheme with only one enzyme form available for binding substrate. Applications of this equation to MAO-B kinetic data cannot possibly obtain accurate kinetic parameters, especially when attempting to determine a mechanism for an inhibitor.

To develop an equation that adequately describes the steady state kinetics of MAO-B, the reaction scheme shown in Figure 2.5.2.1 is separated into two velocities, one coming from substrate binding $E.FAD_{ox}$ and the from substrate binding $E.FAD_{red}$.

$$\text{E. FADox} + \text{S} \leftrightarrow \text{E. FADox} - \text{S} \rightarrow \text{E. FADred} + \text{P} \qquad v_{ox} = \frac{V_{MAX_{ox}}[S]}{K_{M_{ox}} + [S]} \qquad \text{Eq. 2.2}$$

$E.\text{FADred} + S \leftrightarrow E.\text{FADred} - S \rightarrow\rightarrow \text{E.FADred} + \text{P}$ $\quad v_{red} = \frac{V_{MAX_{red}}[S]}{K_{M_{red}} + [S]}$ Eq. 2.3

Equation 2.2 describes the velocity contribution from the pathway where $E.FAD_{red}$ oxidises directly to $E.FAD_{ox}$, with K_{Mox} describing the formation of $E.FAD_{ox}$-S from $E.FAD_{ox}$ and V_{MAXox} being the maximum rate of product formation through the pathway. Equation 2.3 describes the reaction where substrate binds $E.FAD_{red}$ to form $E.FAD_{red}$-S, where K_{Mred} is for the formation of $E.FAD_{red}$ and V_{MAXred} represents the rate of product formation from the pathway when substrate concentration is saturating. It remains possible, however, that some of the flux still proceeds via conversion of $E.FAD_{red}$ to $E.FAD_{ox}$ without substrate binding first.

As is evident from the schematic, entrance into the $E.FAD_{red}$-S pathway occurs at the expense of the $E.FAD_{ox}$ pathway. Therefore, as flux through v_{red} increases, flux through v_{ox} must decrease proportionally. This is most easily done by defining the flux through the $E.FAD_{red}$ pathway as a fraction (F_{red}). The derivation of such an equation is shown.

Summation of the two velocities with a multiplicative function to reduce v_{ox} as enzyme enters the v_{red} pathway.

$$v_{tot} = V_{ox}\{1 - F_{red}\} + V_{red} \quad \text{Eq. 2.4}$$

Substitution of v_{ox} and v_{red} to solvable kinetic parameters.

$$v_{tot} = \frac{V_{MAX_{ox}}[S]}{K_{M_{ox}} + [S]}\{1 - F_{red}\} + \frac{V_{MAX_{red}}[S]}{K_{M_{red}} + [S]} \quad \text{Eq. 2.5}$$

Fraction of the enzyme consumed by the $E.FAD_{red}$ pathway

$$F_{red} = \frac{v_{red}}{V_{MAX_{red}}} \quad \text{Eq. 2.6}$$

Substitution of F_{red}

$$v_{tot} = \frac{V_{MAX_{ox}}[S]}{K_{M_{ox}} + [S]}\left\{1 - \frac{v_{red}}{V_{MAX_{red}}}\right\} + \frac{V_{MAX_{red}}[S]}{K_{M_{red}} + [S]} \quad \text{Eq. 2.7}$$

Conversion of v_{red}/V_{MAXred} to variables already used in non-linear regression

$$\frac{v_{red}}{V_{MAX_{red}}} = \frac{[S]}{K_{M_{red}} + [S]} \quad \text{Eq. 2.8}$$

Final equation with all substitutions

$$v_{tot} = \frac{\mathrm{V_{MAX_{ox}}[S]}}{\mathrm{K_{M_{ox}} + [S]}}\left\{1 - \frac{\mathrm{[S]}}{\mathrm{K_{M_{red}} + [S]}}\right\} + \frac{\mathrm{V_{MAX_{red}}[S]}}{\mathrm{K_{M_{red}} + [S]}} \quad \text{Eq. 2.9}$$

Equation 2.9 mathematically describes the velocity of product formation for the scheme presented in Figure 2.5.2.2 during steady state at a given concentration of substrate. Non-linear regression analyses can provide kinetic constants from kinetic curves using Eq. 2.9. The equation will also serve as the backbone for determining the mechanisms and characteristics of novel inhibitors that exhibit extremely interesting properties in MAO-B kinetic assays. Much of this chapter is dedicated to empirically testing the validity of this formula and the model it represents through a battery of assays under various conditions. Throughout this section, the equation provides insight into the complicated workings of MAO-B, although it should be recognised that it is a simplification rather than a precise representation of MAO-B substrate turnover.

2.6 Application of the model to data

2.6.1 Hypotheses

The model that has been proposed above is based upon the data available in the published literature on MAO-B. The amalgamation of the results from Tan and Ramsay[99] and Husain *et al.*[97] has allowed for the removal of a ternary complex from the model, which significantly reduces the complexity of describing the kinetics mathematically. As described previously, the ternary complex is no longer required to explain the results seen by Husain *et al*.

To investigate the validity of this new model, purified human MAO-B control kinetic curves with two different substrates were done. Phenylethylamine and benzylamine were chosen because of the compatibility with the assays as well as the mountain of literature that suggests the two substrates are handled differently by MAO-B. It is expected that the new mathematical model will provide significantly better fits than the Michaelis-Menten equation does. It is also expected that the two K_M values for each substrate are reasonable and the amount of flux through each pathway fits reasonably within the known parameters from stopped flow experiments. Since the stopped flow experiments found that the degree of flux can be influenced by oxygen concentration, we expect to see similar results during our steady-state analysis as well.

2.6.2 Materials

Purified preparations (hMAO-B) and mitochondrial membrane fractions (WT-hMAO-B) of human MAO-B from *Pichia pastoris* (yeast) were graciously donated by

Dr. Dale Edmondson (Emory University, Atlanta, Georgia). Amplex Red was obtained from Invitrogen (Burlington, ON, Canada). 2-BFI was purchased from Tocris-Cookson (Ellisville, MO). All other substrates, inhibitors and reaction constituents were obtained from Sigma–Aldrich (Oakville, ON, Canada).

2.6.3 Methods

For all experiments in this section, the activities of purified preparations or membrane fractions from *P. pastoris* yeast were measured continuously in 96-well plates with a SpectraMax Gemini XPS microplate reader by following the fluorescence related to the peroxidase-coupled formation of resorufin from AmplexRed[102]. Each reaction was run at 30°C in a total volume of 200 µL. The temperature of 30°C was chosen over 37°C because the uneven heating of microplates at 37°C increased error within experimental replicates. Amine substrate was prepared on the day of the experiment using colourless Eppendorf™ micocentrifuge tubes for the dilutions. All dilutions were done in water.

The MAO-B/AmplexRed™/peroxidase solution was prepared by diluting MAO-B from a batch stock into a solution of 100 mM HEPES buffer. This was then mixed 1:1 with an AmplexRed™/peroxidase solution made up at four times the concentration required for the experiment. The MAO-B/AmplexRed™/peroxidase solution was prepared to be used in entirety for a single experiment and was made fresh each time. During experiments involving more than one plate, enzyme was stored in the fridge until it was required in the experiment.

Plates were warmed to 30˚C prior to commencing the experiment. Assays were started by rapid addition of enzyme/AmplexRed/peroxidase mixture using an 8-channel pipette. Experiments were carried out under atmospheric oxygen unless otherwise stated.

Initial (pseudolinear) rates of product formation were determined by linear regression (SoftMax Pro v. 4.8) and were fitted to equations via the nonlinear regression function of GraphPad Prism v. 5.0c for Windows (GraphPad Software Inc., San Diego, CA).

2.6.4 Non-linear Regression to fit Models to Data

All curve fitting was carried out using the non-linear regression functionality of GraphPad Prism 5.0 (GraphPad Software Inc., San Diego, CA). For single-site hyperbola models (standard Michaelis-Menten kinetics) and sigmoidal inhibitor plots, the standard equations supplied with Prism 5 are used. These equations are:

$$Y = Vmax * X/(K_M + X)$$

For non-linear regression of single-site hyperbolas

$$Y = Bottom\ +\ (Top - Bottom)/(1 + 10^{\{LogEC_{50} - X\}})$$

For non-linear regression of sigmoidal plots

$$Y = Bottom\ +\ (Top - Bottom)/(1 + 10^{\{LogEC_{50} - X) * HillSlope\}})$$

For sigmoidal plots with a variable Hill-slope

$$SPAN = -Bottom + Top$$
$$Part1 = Span * Fraction1/(1 + 10^{\{X - LogEC_{50_1}\}})$$
$$Part2 = Span * (1 - Fraction1)/(1 + 10^{\{X - LogEC_{50_2}\}})$$
$$Y = Bottom\ +\ PART1\ + PART2$$

For two-site sigmoidal plots

Wherein EC_{50} is the concentration at which 50% of the effect is achieved. In the inhibitor plots used in the analysis of the data presented herein, EC_{50} is referred to as an IC_{50}. IC_{50} is the concentration at which the inhibitor has 50% of its maximal effect. In cases where the two site sigmoid is used, the activities are broken into two distinct "activities", each with a corresponding IC_{50} for the ability of the inhibitor to reduce the velocity of the respective activity by 50%.

In cases where a Michaelis-Menten equation did not adequately describe the data, the equation described in Eq. 2.9 is implemented using Prism's *User Defined Equation* function.

Application of a novel equation is a two-step process: 1) programming the equation into Prism 5, and 2) providing initial parameter values to initiate the regression process. In all cases, initial estimates were based upon literature values or previous experiments.

2.6.5 Phenylethylamine Turnover by hMAO-B (Purified Enzyme)

All values presented throughout Section 2 have been compiled into Table 2.6.1 Kinetic Constants for hMAO-B and WT-MAO-B, which contains all kinetically derived values with errors.

Evidence from Ramsay and Tan suggests that phenylethylamine is capable of undergoing oxidation via the $E.FAD_{red}{\cdot}S$ pathway in addition to the $E.FAD_{ox}{\cdot}S$ pathway[99]. Literature data suggest that the substrate produces a simple hyperbolic curve (ie. Michaelis-Menten kinetics). In a basic confirmatory experiment, the oxidation of phenylethylamine by MAO-B was examined kinetically. Activity was measured in environments of high oxygen (≅500 μM) and low oxygen (≅100 μM) with the intention of influencing the flux through each pathway, thus elucidating

two separate K_M values. The results, shown in Figure 2.6.5.1, indicate that the data collected were not able to discriminate two distinct K_M values at each oxygen concentration.

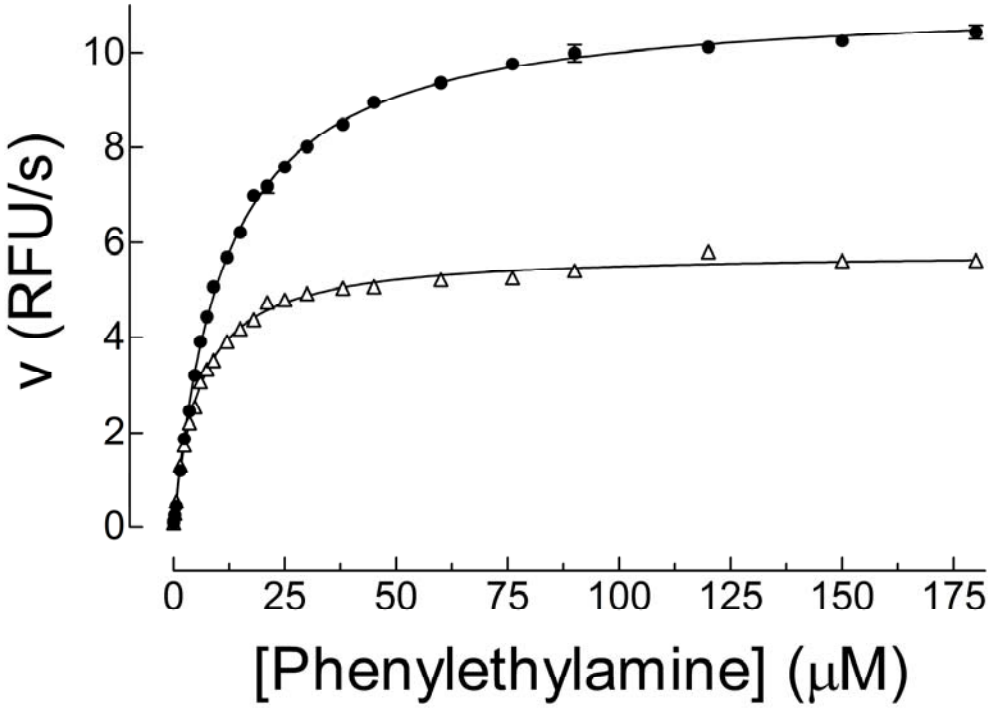

Figure 2.6.5.1 Control kinetics for phenylethylamine turnover by hMAO-B
Oxidation of phenylethylamine (0.3μM-175μM) by hMAO-B (1nM) under 100 μM (△) and 500 μM oxygen (●) (n=4). The oxidation of phenylethylamine is fitted to a single-site hyperbolic equation yielding a K_M of 5.6±0.1μM and 11.6±0.2μM for 100 μM and 500 μM oxygen, respectively. The V_{MAX} values increased from 5.81±0.02 RFU/s to 11.55±0.05 RFU/s with the 5-fold increase in oxygen concentration. Error bars are shown as SEM.

Two-site modelling using Eq 2.9 was attempted, but provided fits no better than those done with a single-site model (Michaelis-Menten equation). Two options are left to explain this: 1) phenylethylamine turnover proceeds predominantly through the $E.FAD_{red}{\cdot}S$, or 2) the values for K_{Mox} and K_{Mred} must be so similar in that non-linear regression is unable to discern two separate values from these data.

The steady state kinetics of phenylethylamine provide no evidence for the proposed model on their own. It is important, however, to note that the data do not

disagree with the model. The data also yielded K_M values consistent with values published in the literature[105].

2.6.6 Benzylamine Turnover by hMAO-B (Purified Enzyme)

Benzylamine, a non-endogenous substrate, shows different kinetic properties than phenylethylamine[97]. Preliminary data suggest that benzylamine oxidation by MAO-B does not fit a single hyperbola, but may fit a two-site hyperbola. To produce sufficient data to fit the data to a two-site model appropriately and to obtain accurate K_M values, a 24-point kinetic curve was produced over a wide range of benzylamine concentrations.

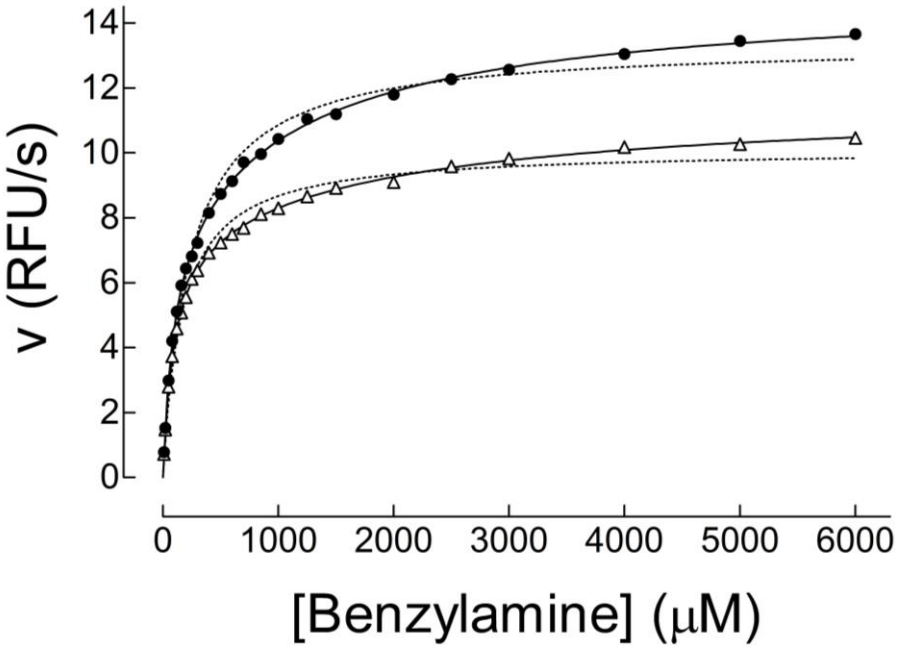

Figure 2.6.6.1 Control kinetics for benzylamine turnover by hMAO-B
Oxidation of benzylamine (10-6000μM) by hMAO-B (1nM) under 100 μM oxygen (Δ) and 500μM oxygen (●) fitted to a two-site hyperbolic equation (solid line) described in Eq. 2.9 and a one-site hyperbola (dashed line) (n=4). The two-site fit yields a K_{Mox} of 90±6μM and 92±8μM for 100μM and 500μM oxygen, respectively. The K_{Mred} was found to be 2.06±0.53mM for 100μM oxygen and 1.25±0.18mM for 500μM oxygen. V_{MAXred} increased from 11.6±0.2 RFU/s to 14.9±0.2 RFU/s with the increase in oxygen. V_{MAXox} values remained consistent between treatments at 7.3±0.4 RFU/s. The dotted line shows the best fit of a one-site hyperbolic equation. Error bars are shown as SEM.

Figure 2.6.6.1 clearly shows that benzylamine does not fit to a single-site reaction model (dashed line). The two-site model described in Eq. 2.9 is fitted to the data (solid line) and provides a superior fit of the data compared to a single-site model. Importantly, the K_{Mox} value remains stagnant when oxygen is increased while the K_{Mred} decreases slightly (from 2mM to 1.25 mM). It is possible that oxygen decreases the K_{Mred} via an uncompetitive mechanism (ordered binding, explained in Section 2.3.3). The only place in the model where this can occur is, like phenylethylamine, at $E.FAD_{red}$-S going to $E.FAD_{ox}$-S. That a shift in the value of $K_{Mred,}$ but not in K_{Mox}, occurs in response to increased oxygen concentrations is very promising for the validity of the mathematical representation of the model.

The stagnation in V_{MAXox} values is also significant. It suggests that, if the model is correct, oxidation of free $E.FAD_{red}$ is nearly saturated at low concentrations of oxygen, although the reaction occurs at a relatively slow rate. The increase in the V_{MAXred}:V_{MAXrox} ratio towards the favour of V_{MAXred} with an increase in oxygen concentration suggests that $E.FAD_{red}$-S to $E.FAD_{ox}$-S is not saturated with oxygen. This also suggests that in the presence of substrate, flavin oxidation occurs much more rapidly, since this is one way to increase V_{MAXred}.

The increase in V_{MAXred} (1.28 fold) with the change in oxygen concentration is significantly smaller than the change in V_{MAX} seen with phenylethylamine (2-fold). This could represent the difference in the rate of flavin oxidation in the presence of each substrate, but without precise affinities for oxygen available for calculations, this is purely speculation.

2.6.7 Benzylamine Turnover by WT-hMAO-B (Mitochondrial Membrane Particles from Pichia pastoris)

The results in Figure 2.6.7.1 were obtained from purified enzyme that lacks the anchoring to a charged lipid membrane environment where MAO-B is typically found. Although working with purified MAO-B is logistically much simpler than the membrane-bound counterparts, it is imperative to ensure that the two-site results are not an artefact of the purified form. The experiment from Figure 2.6.7.1 was, therefore, repeated using membrane-bound, wild type, human MAO-B.

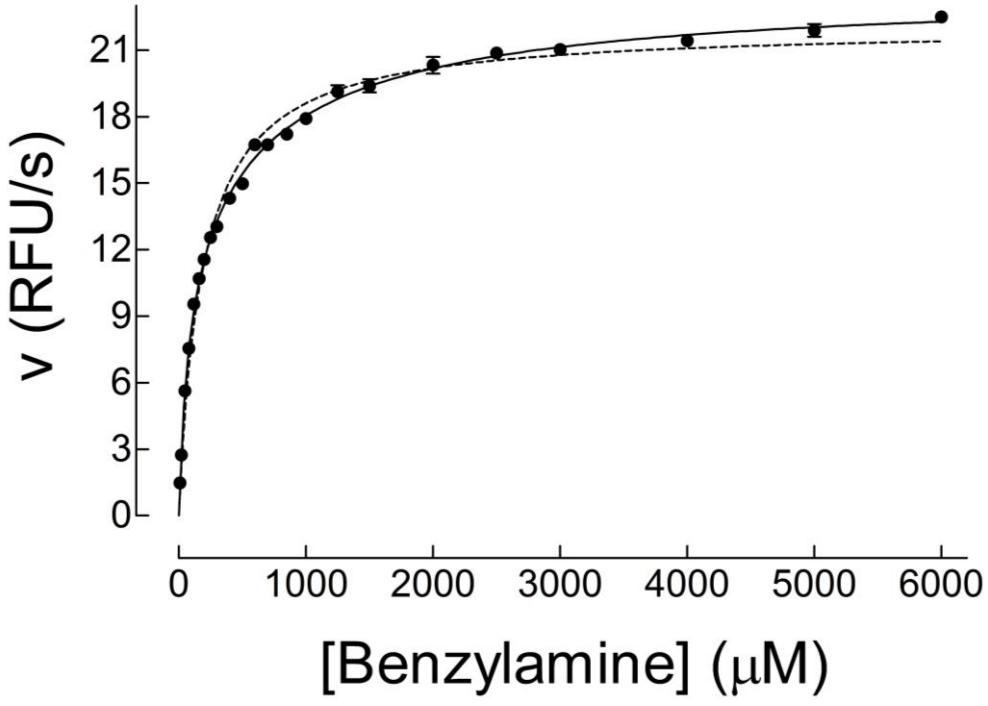

Figure 2.6.7.1 Control kinetics for WT-h-MAO-B when benzylamine is substrate
Oxidation of benzylamine (10-6000μM) by WT-hMAO-B (800μg/mL) under atmospheric conditions (n=4) fitted to a two-site hyperbolic equation (solid line) described by Eq. 2.9 and a one-site model (dashed line). The two-site model yields a K_{Mox} value of 81±11μM and a K_{Mred} value of 814±183μM. V_{MAXox} and V_{MAXred} were found to be 12.0±1.4 and 23.7±0.7 RFU/s, respectively. Error bars represent SEM.

Results from Figure 2.6.7.1 show that membrane-bound human MAO-B also produces kinetic fits to a two-site model with kinetic constants that are very similar to those of the purified enzyme. The K_{Mox} value for membrane-bound enzyme of 81±11 μM is within error of the purified enzyme under either high or low oxygen. The K_{Mred} is also very similar. Interestingly, V_{MAXred}:V_{MAXox} is significantly larger than in purified enzyme. Reasons for this could include a decrease in K_M for oxygen at E.FAD_{red}-S, a slower rate of oxidation (or drastically increased K_M for oxygen) at E.FAD_{red}, or an increase in oxidation rate at E.FAD_{red}-S. Although interesting, no research was done into the reason for this change in membrane particles.

In general, the purified enzyme mimics the membrane-bound form in the catalysis of benzylamine oxidation, and the continued use of purified enzyme in kinetic assays is justified.

2.6.8 Kinetic Constants for hMAO-B and WT-MAO-B

Purified hMAO-B

	Michaelis-Menten Kinetics			Two-Site Model					
Substrate	K_M (μM)	V_{MAX} (RFU· s^{-1}· 200 $amol_{MAOB}^{-1}$)	R^2	K_{Mox} (μM)	K_{Mred} (μM)	V_{MAXox}	V_{MAXred}	V_{MAXred}:V_{MAXox}	R^2
Phenylethylamine (High Oxygen)	11	11.6	0.9951						
Phenylethylamine (Low Oxygen)	6	5.7	0.9979						
Benzylamine (High Oxygen)	233	13.4	0.9841	92	1248	7.4	14.9	2.0	0.9978
Benzylamine (Low Oxygen)	167	10.1	0.9809	91	2062	7.3	11.6	1.6	0.9957

WT hMAO-B Membrane Particles

	Michaelis-Menten Kinetics			Two-Site Model					
Substrate	K_M (μM)	V_{MAX} (RFU· s^{-1}· 1.6 $pg_{Particles}^{-1}$)	R^2	K_{Mox} (μM)	K_{Mred} (μM)	V_{MAXox}	V_{MAXred}		R^2
Benzylamine (Atmospheric)	187	22.1	0.9862	81	814	12.0	23.7	1.975	0.9956

Table 2.6.1 Kinetic Constants for hMAO-B and WT-MAO-B
Compilation of the kinetic constants obtained in Sections 2.6.5 through 2.6.7

2.6.9 Concluding remarks

The data obtained from steady-state analyses using Eq 2.9 provide very comparable results to data obtained through transient-state experiments already published in the literature [97,101]. Husain *et al.* found that the rate-limiting step in phenylethylamine turnover was the reoxidation of the flavin[97]. In a steady-state

model, we would expect that the concentration of oxygen would increase the V_{MAX} of phenylethylamine turnover significantly. Figure 2.2.7 shows that V_{MAX} was increased 2-fold by increasing oxygen concentration. On the other hand, Husain *et al*. found that benzylamine turnover was limited by the reductive half-reaction. We would, therefore, not expect a significant change in the V_{MAX} values for benzylamine turnover when the concentration of oxygen is modified[97]. This is precisely what is observed using the two-site model described by Eq. 2.9.

The preliminary exploration of the MAO-B kinetic mechanism was very successful in a basic proof-of-principle sense. To validate further the model presented in Eq. 2.9, inhibitors must be introduced and the results must be equally robust.

2.7 Competitive Inhibition of MAO-B

2.7.1 Background

As described in Section 2.2, enzyme kinetics is the study of rate in the presence of controlled or varied conditions. One way to probe the way an enzyme works is to introduce a drug that changes the rate of catalysis in a concentration-dependent manner to produce a rate versus substrate concentration curve at each concentration of the drug. The large number of data points obtained from these experiments allows for determination of the mechanism of interaction between the substrate and the inhibitor drug, whether it is at the active site or a separate site. Numerous models of reversible enzyme inhibition exist, but the simplest is competitive inhibition wherein the substrate and inhibitor directly compete for binding at the active site. In order to validate our model, we selected two classical competitive inhibitors of MAO-B, amphetamine and amitriptyline.

Amphetamine is a phenylethylamine derivative with a methyl group on the α-carbon, preventing catabolism by MAO-B (see Figure 1.1.7.1 and Figure 1.1.7.2 for structures of phenylethylamine and amphetamine, respectively). Published experiments with amphetamine have shown varied results ranging from competitive inhibition to mixed inhibition [103,104]. The modes of inhibition have differed based upon which substrates were used and the concentrations of oxygen[104].

Amitriptyline is classified as a tricyclic compound and has been found to be competitive with benzylamine under normal atmospheric conditions, but non-

competitive with phenylethylamine under identical conditions[105]. Clearly, this cannot be the case; the inhibitory mechanism should remain consistent and independent of substrate.

The model is then applied to confirm the mechanism of a novel inhibitor of MAO-B, di(2-hydroxyethyl)methyldodecylammonium (DiHEMDA), that we discovered from investigations of leachates from plasticware[106].

2.7.2 Derivation of Competitive Inhibition Equation for MAO-B

The derivation of an equation for competitive inhibition of MAO-B using the two-site model requires applying the basic principles of enzyme inhibition as described in Section 2.3. Both velocities, v_{ox} and v_{red}, are again summed, but this time the velocities need to be a function not only of substrate concentration, but also of the concentration of inhibitor. Using the application of the equations for competitive inhibition described in Section 2.3.1, Eq. 2.11 and 2.12 represent the effect of inhibitor concentration on each of v_{ox} and v_{red} as mutually exclusive pathways. In the control equation, the fraction of enzyme available for the $E.FAD_{ox}$ pathway was defined simply as 1-(fraction of catalysis proceeding through $E.FAD_{red}$). With the addition of an inhibitor, binding of inhibitor to $E.FAD_{red}$ also lowers the portion of enzyme available to the $E.FAD_{ox}$ pathway. To account for this inhibition, a factor for the *fraction* of *inhibition* caused by a *competitive* inhibitor, represented as F_{Ic}, is introduced to the overall scheme, shown in Eq. 2.10. F_{Ic} is essentially defined (Eq. 2.13) as the fraction of enzyme bound to inhibitor in the presence of a second ligand, which in the case of the enzyme is a substrate.

Substitution of the constituents of Eqs. 2.11, 2.12, and 2.13 into Eq. 2.10 yields Eq. 2.14, which is used in the analysis of all ligands in Section 2.7.

Inclusion of F_{Ic}

$$v_{tot} = v_{ox}\{1 - F_{red} - F_{I_c}\} + v_{red} \quad \text{Eq. 2.10}$$

Inhibition of v_{ox}

$$v_{ox} = \frac{V_{MAX_{ox}}[S]}{K_{M_{ox}}\left(1 + \frac{[I]}{K_{I_{ox}}}\right) + [S]} \quad \text{Eq. 2.11}$$

Competitive Inhibition for v_{red}

$$V_{red} = \frac{V_{MAX_{red}}[S]}{K_{M_{red}}\left(1 + \frac{[I]}{K_{I_{red}}}\right) + [S]} \quad \text{Eq. 2.12}$$

Defining F_{Ic}

$$F_{I_C} = \frac{[I]}{K_{I_{red}}\left(1 + \frac{[S]}{K_{M_{red}}}\right) + [I]} \quad \text{Eq. 2.13}$$

$$v_{tot} = \frac{V_{MAX_{ox}}[S]}{K_{M_{ox}}\left(1 + \frac{I}{K_{I_{ox}}}\right) + [S]}\left\{1 - \frac{[S]}{K_{M_{red}}\left(1 + \frac{[I]}{K_{I_{ox}}}\right) + [S]} - \frac{[I]}{K_{I_{red}}\left(1 + \frac{[S]}{K_{M_{red}}}\right) + [I]}\right\} + \frac{V_{MAX_{red}}[S]}{K_{M_{red}}\left(1 + \frac{[I]}{K_{I_{red}}}\right) + [S]}$$

Eq. 2.14 Mathematical description of competitive inhibition
Derivation of Eq. 2.14 involves substituting Eqs. 2.11, 2.12 and 2.13 into Eq. 2.10

Equation 2.14 describes amine catabolism by MAO-B in the presence of an inhibitor that works by reversibly binding to the active site. A different derivation method of this equation has also been published, yielding an identical equation[107]. This equation only estimates, mathematically, what is occurring kinetically with MAO-B. It is expected, however, that if both the model and the mathematics that

represent it are valid, the parameter estimates for substrates and inhibitors will remain similar across different combinations. In other words, for all competitive inhibitors analysed, a correct model should consistently yield similar values for a parameter (K_I in this case) regardless of substrate used. The same should be true for substrates, in that the K_M values should be similar regardless of the competitive inhibitor used. To test the validity of this mathematical model, Section 2.7 focuses on kinetic assays and the application of Eq. 2.14 to the datasets. The model can then be used to verify the mechanism of novel inhibitors.

2.7.3 Hypotheses

The observation that amphetamine has differential modes of inhibition depending on the substrate used does not satisfactorily describe it as an inhibitor. The structure of amphetamine is similar to that of phenylethylamine, with the exception of the presence of an α-methyl, which is sufficient to prevent oxidation of amphetamine. Based on its structural similarity, phenylethylamine is expected to act as a competitive inhibitor.

Past analyses in the literature have relied on the incorrect application of Michaelis-Menten kinetics and the linearization techniques associated with it. We expect the application of the updated model, which takes into account the existence of two distinct MAO-B species ($E.FAD_{ox}$ and $E.FAD_{red}$), to describe the inhibitor activity more consistently. The use of an appropriate equation describing competitive inhibition of MAO-B should yield parameters for amphetamine (i.e. K_{Iox} and K_{Ired}) that will be similar regardless of the substrate used. This is because the K_I

represents the dissociation constant for the inhibitor, a parameter used to describe the affinity of an inhibitor for an enzyme. If the inhibitory mechanism of amphetamine is purely competitive, affinity of the inhibitor should not change regardless of the substrate used.

Amitriptyline also possesses some interesting properties as an inhibitor of MAO-B activity that could potentially be explained more completely with the application of the new model. In 1976, Roth observed that changing the concentration of oxygen resulted in change in mode of inhibition of MAO-B by amitriptyline[105]. Using phenylethylamine as substrate, Roth found that at high concentrations of oxygen, amitriptyline inhibits MAO-B competitively [105]. At atmospheric concentrations of oxygen, this inhibition appeared to be non-competitive in nature[105]. This "change" in mechanism could be explained using the new model if amitriptyline binds to one form of the enzyme with higher affinity than the other form. Based on the information used to develop our current model, we felt the observations by Roth were best explained by amitriptyline binding to $E.FAD_{ox}$ with a much higher affinity than to $E.FAD_{red}$, since increasing oxygen concentrations would increase the likelihood of $E.FAD_{red}$ oxidising to $E.FAD_{ox}$ prior to substrate binding. Similar to our expectations with phenylethylamine, we expected that the affinity parameter (K_{Iox}) to remain consistent regardless of substrate used.

Appropriate and consistent fits with different substrates will provide significant evidence in favour of the proposed model accurately depicting the steady state mechanism of MAO-B and will confirm amphetamine and amitriptyline as competitive inhibitors. The model could then be applied to determine accurately if

a novel MAO-B inhibitor, DiHEMDA, inhibits MAO-B in a competitive manner. We predicted that DiHEMDA was likely to act as a competitive inhibitor based on its structural similarity to lauryldimethylamine N-oxide (LDAO) (structure shown in Figure 1.1.7.2). LDAO was found to bind in the active site of MAO-B, with its aliphatic chain extending into the entrance channel[61].

It is not unreasonable that inhibitors may have different affinities for the different forms of MAO-B, even in cases where K_{Mox} and K_{Mred} for a substrate are similar. It is expected, therefore, that a two-site model will fit phenylethylamine data better than a single-site model and may provide valuable insight into the kinetic mechanism of phenylethylamine turnover by MAO-B.

2.7.4 Materials and Methods

Purified preparations (hMAO-B) and mitochondrial membrane fractions (WT-hMAO-B) of human MAO-B from *Pichia pastoris* (yeast) were graciously donated by Dr. Dale Edmondson (Emory University, Atlanta, Georgia). Dr. Edmondson also provided deuterated phenylethylamine and deuterated benzylamine. Amplex Red was obtained from Invitrogen (Burlington, ON, Canada). 2-BFI was purchased from Tocris-Cookson (Ellisville, MO). All other substrates, inhibitors and reaction constituents were obtained from Sigma–Aldrich (Oakville, ON, Canada).

For all experiments in this section, the activities of purified preparations or membrane fractions from *P. pastoris* yeast were measured continuously in 96-well plates with a SpectraMax Gemini XPS microplate reader by following the

fluorescence related to the peroxidase-coupled formation of resorufin from AmplexRed[102]. Each reaction was run at 30°C in a total volume of 200 µL. Amine substrate was prepared on the day of the experiment using colourless Eppendorf™ micocentrifuge tubes for the dilutions. Inhibitor solutions were prepared in an identical manner. All dilutions were done in water.

The MAO-B/AmplexRed™/peroxidase solution was prepared by diluting MAO-B from a batch stock into a solution of 100 mM HEPES buffer. This was then mixed 1:1 with an AmplexRed™/peroxidase solution made up at four times the concentration required for the experiment. The MAO-B/AmplexRed™/peroxidase solution was prepared to be used in entirety for a single experiment and was made fresh each time. During experiments involving more than one plate, enzyme was stored in the fridge until it was required in the experiment.

Plates were warmed to 30˚C prior to commencing the experiment. Assays were started by rapid addition of enzyme/AmplexRed/peroxidase mixture using an 8-channel pipette. Experiments were carried out under atmospheric oxygen unless otherwise stated.

Initial (pseudolinear) rates of product formation were determined by linear regression (SoftMax Pro v. 4.8) and were fitted to equations via the nonlinear regression function of GraphPad Prism v. 5.0c for Windows (GraphPad Software Inc., San Diego, CA).

2.7.5 Non-linear Regression to fit Models to Data

All curve fitting was carried out using the non-linear regression functionality of GraphPad Prism 5.0 (GraphPad Software Inc., San Diego, CA). All data were fitted using the global analysis function in Prism 5 to Eq. 2.14 using initial value estimates from the literature and previous experiments.

2.7.6 Inhibition of MAO-B by Amphetamine

Amphetamine (α-methyl-phenylethylamine) has been well established as an inhibitor of MAO-B. Based on its structure, it is reasonable to suggest that amphetamine directly competes with phenylethylamine at the active site. The presence of an α-methyl prevents oxidation from occurring. Interestingly, Pearce and Roth indicate that amphetamine inhibits monoamine oxidase turnover of phenylethylamine in a mixed fashion[104]. At the time this was proposed, Lineweaver-Burk plots were used extensively to determine the mode of inhibition. Lineweaver-Burk plots are a linearisation of a single enzyme-state model. It is possible that the two-site nature of MAO-B produces data that are easily misinterpreted by single-site derived analyses, thus yielding an outcome of mixed inhibition.

Although control kinetics for phenylethylamine turnover by MAO-B are well described by a single-site equation, it is possible that the presence of an inhibitor will "reveal" two distinct enzyme activities. Consider that in order for a Lineweaver-Burk plot to show linear competitive inhibition from a model with two enzyme species, the inhibitor must possess a ratio between the two species (K_{Iox}:K_{Ired}) that is identical to the ratio between the affinities of the substrate for the same species (K_{Mox}:K_{Mred}). In such a case, K_{Mox}:K_{Mred} for phenylethylamine needs to equal the

K_{Iox}:K_{Ired} for amphetamine for the inhibition to appear competitive using a Michaelis-Menten model. The fact that previously published Lineweaver-Burk plots have not shown competitive inhibition suggests that it is likely the two ratios will be different. To investigate, we performed kinetic assays with phenylethylamine in the presence of amphetamine.

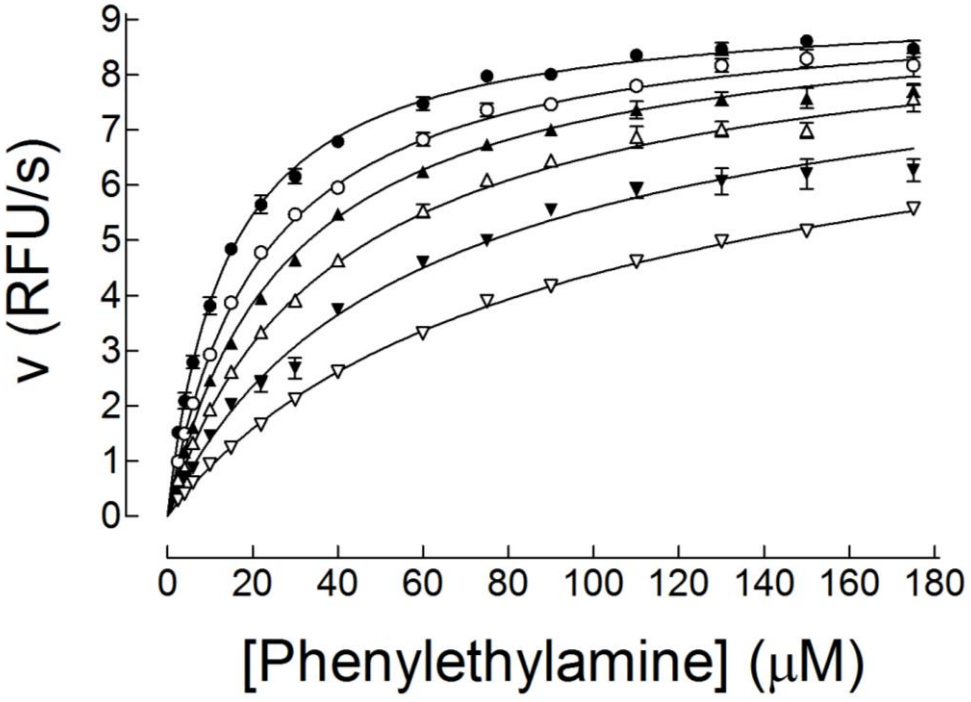

Figure 2.7.6.1 Inhibition of hMAO-B by amphetamine versus phenylethylamine
Oxidation of phenylethylamine (3-175μM) by hMAO-B (1nM) in the presence of 0(●), 200(○), 600(▲), 1200(△), 2400(▼) and 5000(▽)μM (+)Amphetamine (n=3) globally fitted to a two-site model with competitive inhibition at each site (***Eq. 2.14***). Error bars represent SEM. Fits yielded a value of 12±1 and 16±1 μM for K_{Mox} and K_{Mred}, respectively. K_{Iox} and K_{Ired} were found to be 260±90 and 1950±790 μM. The global R^2 was 0.9932.

The data obtained fit a full competitive model of inhibition at two enzyme species, as described by Equation 2.14. The presence of an inhibitor allows more data points and, for the first time, discrimination of two different K_M values for phenylethylamine. The inability to see two sites in the absence of amphetamine is

due to the extreme closeness between the two values (12 and 16 μM for K_{Mox} and K_{Mred}, respectively).

V_{MAXred}:V_{MAXox} was found to be 1, which is lower than the ratio for benzylamine under low oxygen. This fits well with the data that indicate phenylethylamine turnover is rate-limited by oxidation of the flavin compared to benzylamine which is rate-limited by the reductive half-reaction[97]. Consider that the contribution of E.FAD_{red}-S to the total velocity when phenylethylamine is substrate under atmospheric conditions is only marginally greater than the contribution by reoxidation of free reduced enzyme. Increasing oxygen concentration increases the maximum catalytic rate of phenylethylamine[99,97], suggesting that E.FAD_{red}-S reoxidation is extremely fast, but highly limited by oxygen concentrations. This also fits with the data that indicate the K_M for oxygen is increased 10-fold for phenylethylamine as substrate when compared to benzylamine[97].

Using the model in Figure 2.5.2.2, saturating phenylethylamine concentrations force the majority of the enzyme to E.FAD_{red}-S. This explains why 80-90% of the flavin is bleached upon entering the steady state when phenylethylamine is substrate[97].

It should be noted that these data are not inconsistent with the literature that have shown mixed inhibition[104]. The data suggest that amphetamine decreases V_{MAX} and increases K_M, which is characteristic of mixed inhibition. The inappropriate analyses in the literature, however, have misled researchers to believe that amphetamine acts via a mixed mechanism[104].

An important aspect of validating a model is that the results are consistent between substrates. MAO-B has been known to exhibit sensitivity to isotopes, particularly deuterated amines[97]. It is expected that the deuterated form of phenylethylamine will result in only a moderate change in the sum of the V_{MAX} values since bond breakage has not been reported to be the rate limiting step in its catabolism[97] (see Section 2.4.2 for background information on isotope effects). A change in the V_{MAXred}:V_{MAXox} may occur based on the rate limiting steps for each enzyme species potentially being different. For example, if the majority of the velocity of phenylethylamine turnover is contributed from the $E.FAD_{red}$-S pathway and this pathway is rate-limited by flavin reoxidation, the total V_{MAX} for the enzyme will not change at saturation. In such a case it is possible for the $E.FAD_{ox}$ pathway to be rate limited by bond breakage, but if the contribution of V_{MAXox} to the total V_{MAX} is small, this decrease in rate could be hard to differentiate looking at total V_{MAX} alone. The K_I values for amphetamine, however, should remain consistent across all substrates.

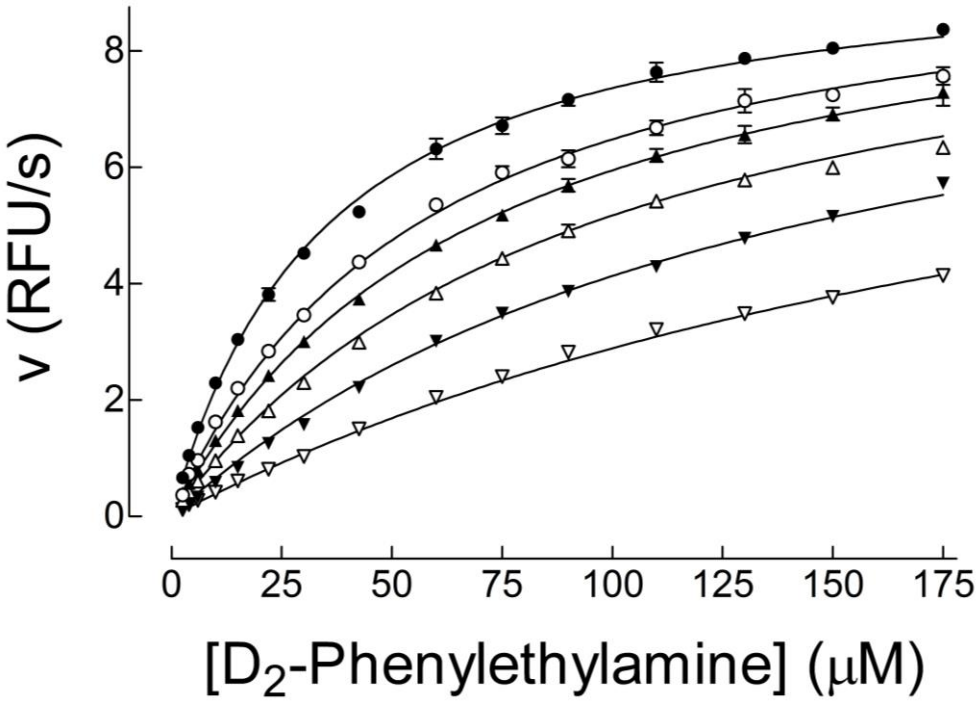

Figure 2.7.6.2 Inhibition of hMAO-B by amphetamine versus D_2-phenylethylamine

Oxidation of D_2-phenylethylamine (3-175μM) by hMAO-B (1nM) in the presence of 0(●), 200(○), 600(▲), 1200(△), 2400(▼) and 5000(▽)μM (+)Amphetamine (n=3) globally fitted to a two-site model with competitive inhibition at each site (***Eq. 2.14***). Error bars represent SEM. Fits yielded a value of 29±5 and 62±6 μM for K_{Mox} and K_{Mred}, respectively. K_{Iox} and K_{Ired} were found to be 320±90 and 1600±190 μM. V_{MAXox} was found to be 3.7±0.6 RFU/s and V_{MAXred} was found to be 10.1±0.1 RFU/s. The global R^2 was 0.9961.

Oxidation of D_2-phenylethylamine by MAO-B yields almost identical values for K_{Iox} and K_{Ired} as for phenylethylamine when fitted with a competitive two-site model. Due to differences in MAO-B concentrations in different experiments, the V_{MAX} values are not comparable between experiments. What can be examined, however, is the ratio of V_{MAXox}:V_{MAXred}. With phenylethylamine, this ratio ranges from 0.4 to 1.4 (see Figure Table 2.8.1 for compilation of results). The deuterated form has a V_{MAXred}:V_{MAXox} ratio of 2.4, indicating an isotope effect on the velocity associated with the $E.FAD_{ox}$ pathway. This may suggest that bond breakage is rate-limiting for phenylethylamine in the $E.FAD_{ox}$ pathway.

As mentioned previously, it is important in verifying a model that K_I values for an inhibitor be consistent across all substrates. In the same literature that suggests amphetamine exhibits mixed inhibition of phenylethylamine, the authors indicate that benzylamine is inhibited competitively[104]. Recall that inhibition would appear competitive in Lineweaver-Burk plots for MAO-B data *if* the inhibitor has a K_{Ired}:K_{Iox} similar to the K_{Mred}:K_{Mox}. A kinetic assay with benzylamine as substrate and amphetamine as the inhibitor was carried out, with the results shown in Figure 2.7.6.3.

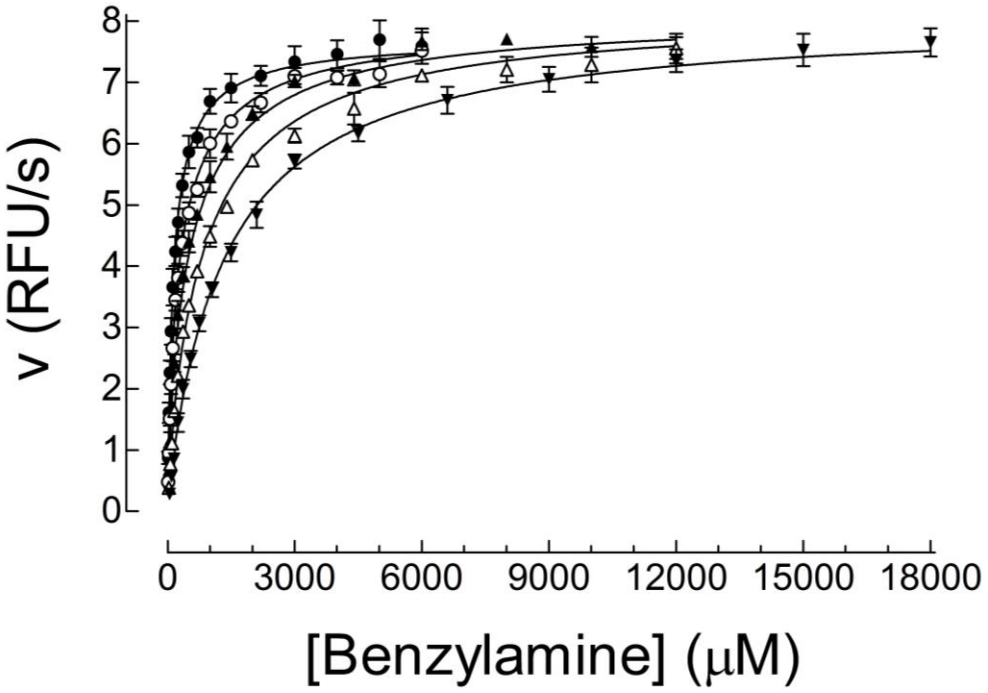

Figure 2.7.6.3 Inhibition of hMAO-B by amphetamine versus benzylamine

Oxidation of benzylamine (15-18000μM) by hMAO-B (1nM) in the presence of 0(●), 300(○), 800(▲), 2000(△), and 5000(▼)μM (+)Amphetamine (n=3) globally fitted to a two-site model with competitive inhibition at each site (Eq. 2.14). Error bars represent SEM. Fits yielded a value of 110±10 and 730±90 μM for K_{Mox} and K_{Mred}, respectively. K_{Iox} and K_{Ired} were found to be 730±90 and 5000±900 μM. The global R^2 was 0.9829.

Visually, the data appear to follow a competitive trend with there being a change in K_M but no change in V_{MAX}. The values from global non-linear regression

using Eq. 2.14 are consistent with the values determined in the control kinetics (K_{Mox} and K_{Mred}). Values for K_{Iox} and K_{Ired} are higher than seen previously (730 and 5000 μM, respectively), which may speak to the limitations of some of the assumptions made in developing Eq. 2.14. The K_{Ired}:K_{Iox}, however, is consistent with other experiments. K_{Mred}:K_{Mox} and K_{Ired}:K_{Iox} are extremely close in value. K_{Ired}:K_{Iox} is 6.8 and K_{Mred}:K_{Mox} is 6.7. Ignoring the fact that a properly created Lineweaver-Burk plot with benzylamine would produce curved rather than straight lines, it is possible that inhibition of benzylamine by amitriptyline would look competitive because of the similarity in these ratios.

There is some concern that the K_I values are higher than previously observed, although this can be somewhat settled by the similar K_{Ired}:K_{Iox} to other experiments. As a whole, the evidence suggests that MAO-B is inhibited competitively by amphetamine. The mathematical model resolves to values that are very reasonable and consistent, supporting its usage. Many of the strange results seen in early kinetic assays involving amphetamine are well explained in light of a model that accounts for both $E.FAD_{ox}$ and $E.FAD_{red}$ species, emphasising the importance of proper kinetic modelling when determining inhibition mechanisms by steady-state kinetics.

2.7.7 Inhibition of MAO-B by Amitriptyline

Amitriptyline, a tricyclic antidepressant, has interesting documented properties as an MAO-B inhibitor. In a 1976 paper[105], amitriptyline was found to inhibit catabolism of phenylethylamine non-competitively, and of benzylamine

catabolism competitively at atmospheric oxygen. Elevating oxygen concentrations converts the form of inhibition versus phenylethylamine to competitive[105]. With the current two-site model in mind, the modes of inhibition can be explained by amitriptyline binding preferentially to $E.FAD_{ox}$.

Oxidised enzyme exists at relatively high concentrations during benzylamine turnover. Binding of amitriptyline to $E.FAD_{ox}$ would, therefore, competitively inhibit much more benzylamine turnover than it would phenylethylamine turnover, since phenylethylamine appears to cause more of the enzyme to be in the reduced state at equilibrium. Increasing oxygen concentrations could cause an equilibrium shift in phenylethylamine turnover such that more oxidised enzyme exists when compared to lower concentrations of oxygen. This shift would come because of an increased likelihood that oxygen binds $E.FAD_{red}$ over substrate based on the increased concentration of oxygen. Any equilibrium modification in the favour of $E.FAD_{ox}$ creation provides more opportunity for amitriptyline to bind. The larger the percentage of total velocity yielded through the $E.FAD_{ox}$ rather than the $E.FAD_{red}$ pathway, the closer amitriptyline will appear to be a competitive inhibitor of phenylethylamine turnover. That is not to say that oxygen is capable of causing a complete shift in equilibrium, but rather just enough of a shift to cause a change in Lineweaver-Burk plots observed by Roth in 1976[105].

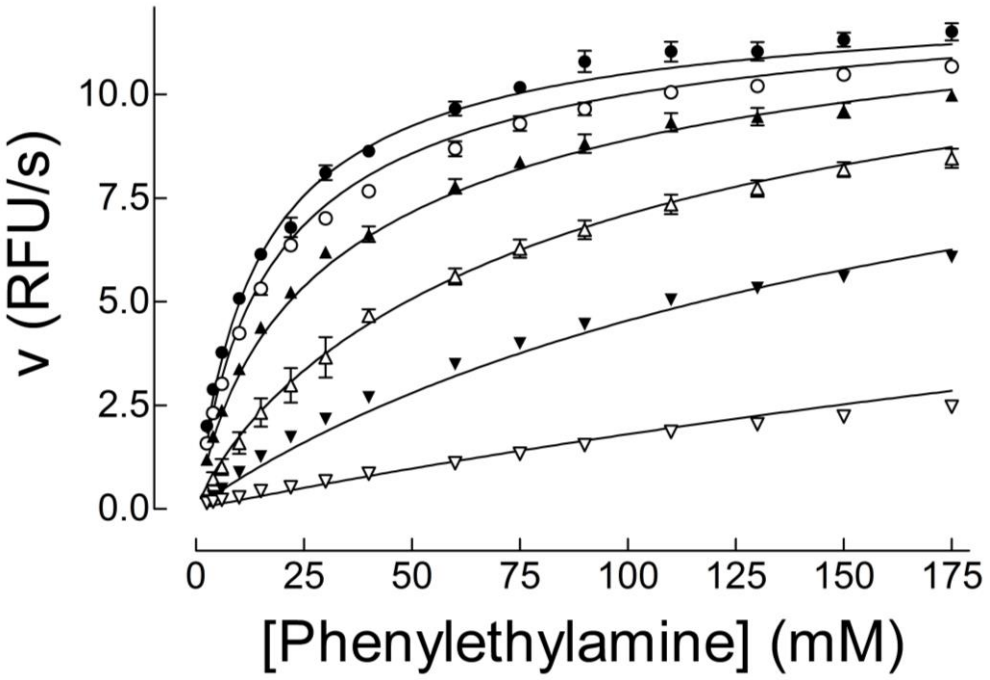

Figure 2.7.7.1 Inhibition of hMAO-B by amitriptyline versus phenylethylamine

Oxidation of phenylethylamine (2.5-200uM) by hMAO-B (3nM) in the presence of 0(●), 10 (○), 46.4(▲), 215(△), 1000(▼) and 4640(▽)μM amitriptyline (n=4) globally fitted to a two-site model with competitive inhibition at $E.FAD_{ox}$ and $E.FAD_{red}$ (Eq. 2.14). Error bars represent SEM. Fits yielded a value of 12±1 and 71±6 μM for K_{Mox} and K_{Mred}, respectively. K_{Iox} and K_{Ired} were found to be 58±6 and 630±60 μM, respectively. The global R^2 was 0.9675.

Visually, inhibition of phenylethylamine oxidation by amitriptyline clearly shows aspects of classical non-competitive inhibition, wherein V_{MAX} decreases and K_M remains the same. When analysed by non-linear regression, a model of inhibition where amitriptyline only binds at one form of the enzyme ($E.FAD_{ox}$) fits the data very well at atmospheric oxygen concentrations. With a K_{Ired} and K_{Iox} of 58±6 and 630±60 μM, respectively, amitriptyline shows a much higher affinity for $E.FAD_{ox}$ over $E.FAD_{red}$. This value is also significantly larger than the K_{Mred}:K_{Mox} value and is expected to display two sites in a sigmoidal plot.

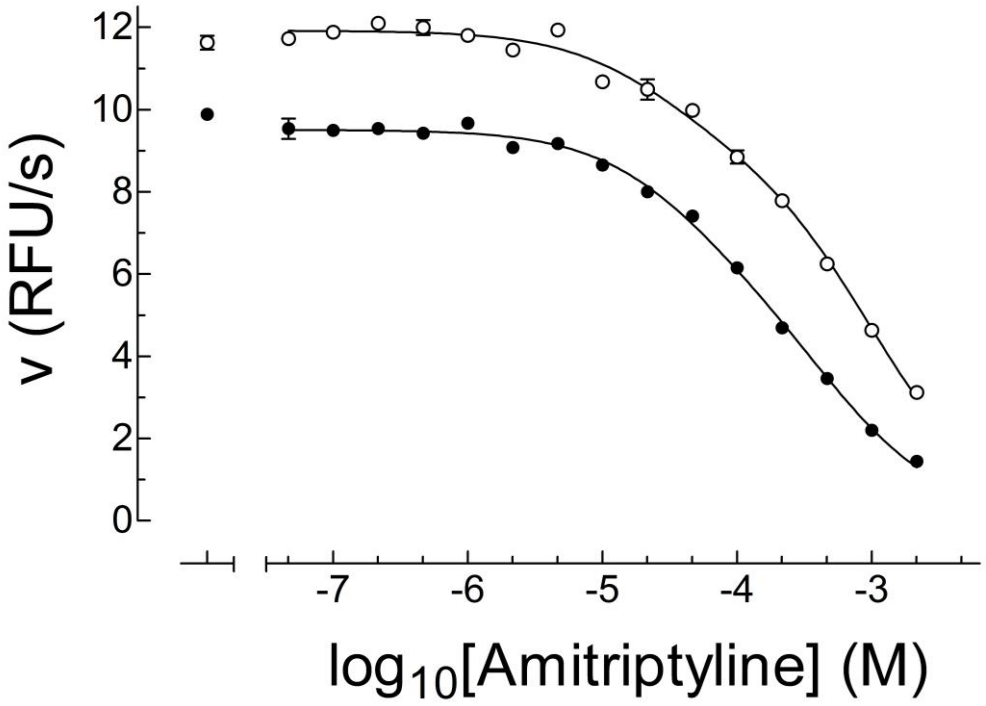

Figure 2.7.7.2 Inhibitor plots of amitriptyline versus phenylethylamine
Oxidation of 30(●) and 90(○)μM phenylethylamine by hMAO-B (3nM) in the presence of amitriptyline (n=3) fitted to a biphasic sigmoid with both Hill-slopes constrained to -1.0. 30 μM PEA produced an $IC_{50\text{-}1}$ of 33.9 μM and an $IC_{50\text{-}2}$ of 500 μM. 90 μM PEA yielded 34.1 and 1042 μM for $IC_{50\text{-}1}$ and $IC_{50\text{-}2}$, respectively. Fractions were 0.33 and 0.26 for 30 and 90 μM, respectively with overlapping errors. Error bars represent SEM.

The curves in Figure 2.7.7.2 were originally fitted to a monophasic sigmoid equation with a variable Hill-slope. Shallow Hill-slopes (-0.61) suggested that the curves may represent two sigmoids combined into one. Data were then fitted to the biphasic curves shown with $IC_{50\text{-}1}$ and $_{\text{-}2}$ representing the the high and low affinity sites, respectively.

The $IC_{50\text{-}1}$ values for 30 μM PEA and 90 μM PEA were both calculated to be 34 μM. The lack of change in $IC_{50\text{-}1}$ values when there has been a 3-fold increase in substrate concentration suggests a non-competitive mechanism of inhibition. The fraction value relates to the amount of flux contributed by catabolism from the

higher affinity pathways. In this case, the fraction value is relatively small (0.33 and 0.26 for 30 and 90 μM, respectively). This number corresponds well with the fraction of the flavin in the oxidised form when phenylethylamine is substrate.

The results also fit with $E.FAD_{ox}$ being the site for which amitriptyline has the highest affinity. It is worth noting that the change in fraction is relatively small, which fits well with previously published data that suggest the fraction of phenylethylamine going through $E.FAD_{red}$-S is largely determined by the concentration of oxygen rather than the concentration of substrate[97]. When benzylamine is substrate, however, the fraction of enzyme in the reduced form ($E.FAD_{red}$) is likely dictated by concentration of benzylamine[97]. This suggests that the degree of change in the fraction value from inhibitor plots should increase when benzylamine is substrate (see Figure 2.7.7.6).

As mentioned previously, the literature suggests that amitriptyline yields competitive inhibition of benzylamine, regardless of oxygen conditions. If the model in Figure 2.5.2.2 is correct, curve fitting on benzylamine kinetic data in the presence of amitriptyline should yield kinetic parameters consistent with values obtained using phenylethylamine as a substrate. This should occur under both high and low oxygen conditions.

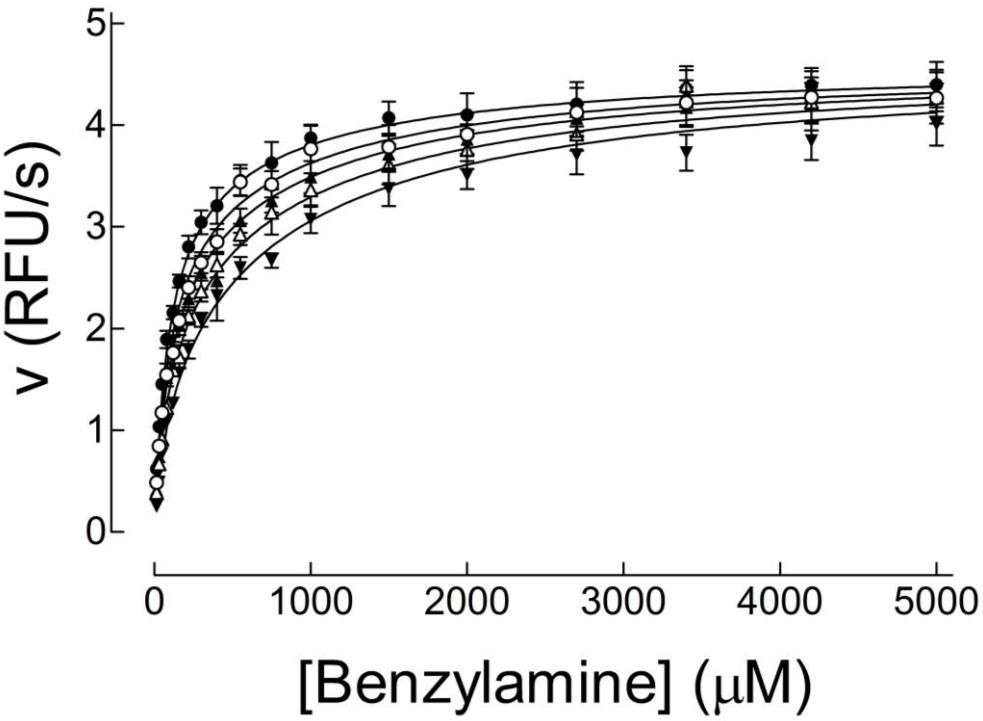

Figure 2.7.7.3 Inhibition of hMAO-B by amitriptyline versus benzylamine under low oxygen

Oxidation of benzylamine (15-5000μM) by hMAO-B (1nM) under 100 μM oxygen in the presence of 0(●), 15 (○), 30(▲), 60(△) and 120(▼) μM amitriptyline (n=3) globally fitted to a two-site model with competitive inhibition at $E.FAD_{ox}$ and $E.FAD_{red}$(Eq. 2.14). Error bars represent SEM. Fits yielded a value of 65±3 and 1110±110 μM for K_{Mox} and K_{Mred}, respectively. K_{Iox} was found to be 170±10 μM. K_{Ired} was exceedingly large and could not be determined. The global R^2 was 0.9919.

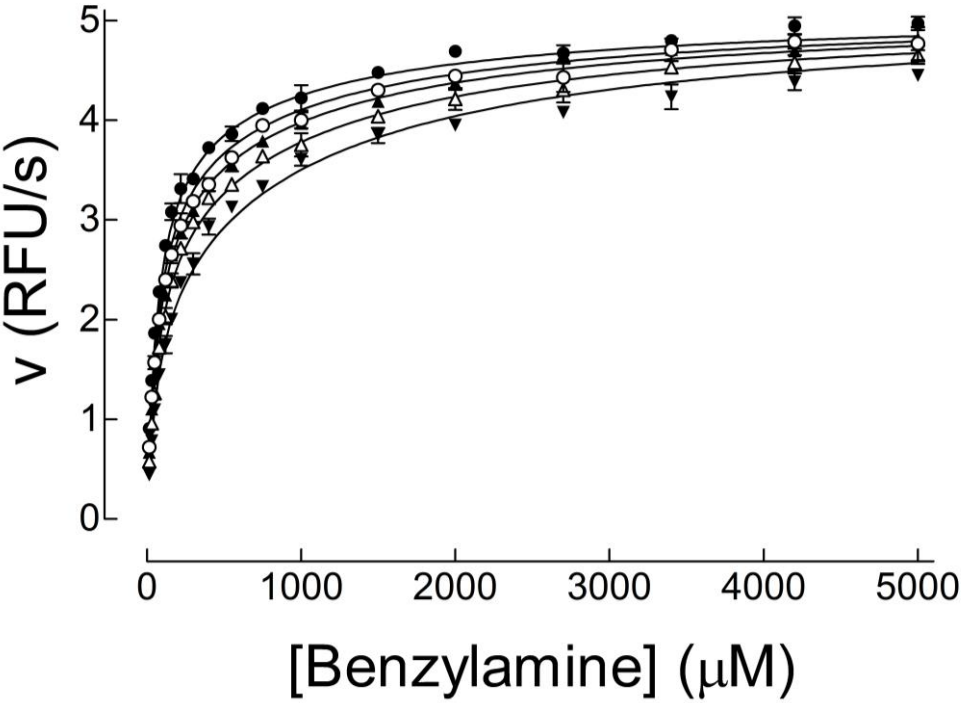

Figure 2.7.7.4 Inhibition of hMAO-B by amitriptyline versus benzylamine under high oxygen

Oxidation of benzylamine (15-5000μM) by hMAO-B (1nM) under 500 μM oxygen in the presence of 0(●), 15(○), 30(▲), 60(△) and 120(▼) μM amitriptyline (n=3) globally fitted to a two-site model with competitive inhibition at $E.FAD_{ox}$ (*Eq. 2.14*). Error bars represent SEM. Fits yielded values of 85±0 and 890±150 μM for K_{Mox} and K_{Mred}, respectively. K_{Iox} was found to be 100±20μM. K_{Ired} was exceedingly large and could not be determined. The global R^2 was 0.9674.

As suggested by previously published work[105], MAO-B catabolism of benzylamine appears to be competitively inhibited by the presence of amitriptyline. The values obtained from benzylamine are in agreement with those determined from phenylethylamine oxidation. None of the values between the two experiments were significantly different, although K_{Mred} did increase under low oxygen concentrations (K_{Mred}:K_{Mox} of 17.2). This is similar to the results seen in the control kinetics where the K_{Mred}:K_{Mox} ratio was 22.6.

The kinetic curves in Figure 2.7.7.3 and Figure 2.7.7.4 did not use high enough inhibitor concentrations to define K_{Ired} adequately, although they did provide

consistent results. The kinetic curve was repeated with higher concentrations of amitriptyline under atmospheric conditions to determine a K_{Ired}.

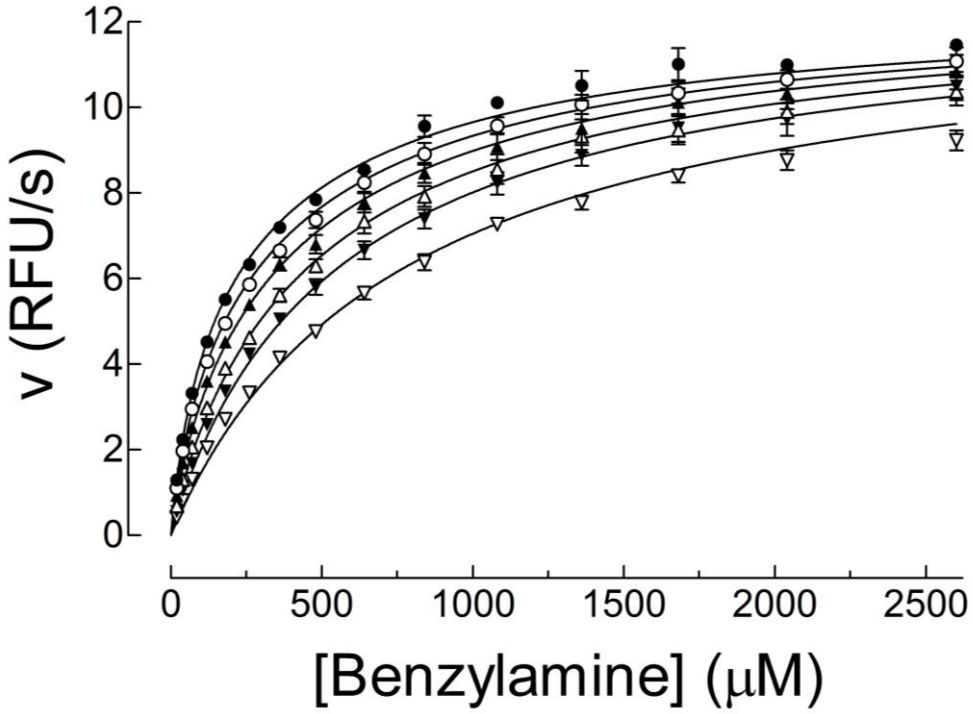

Figure 2.7.7.5 Inhibtion of hMAO-B by amitriptyline versus benzylamine under atmospheric oxygen
Oxidation of benzylamine (20-2600μM) by hMAO-B (2 nM) under atmospheric conditions in the presence of 0(●), 10 (○), 30(▲), 100(△), 300(▲), 1000(▽) μM amitriptyline (n=3) globally fitted to a two-site model with competitive inhibition at $E.FAD_{ox}$ (Eq. 2.14). Error bars represent SEM. Fits yielded a value of 82±13 and 500±30 μM for K_{Mox} and K_{Mred}, respectively. K_{Iox} and K_{Ired} were found to be 34±6 and 1800±250 μM. The global R^2 was 0.9868.

An increased range of amitriptyline concentrations was used to allow the equation to determine a value for K_{Ired} (1800±250 μM), although the concentrations of amitriptyline used were still too low to define the parameter accurately. Non-linear regression provides a value for K_{Iox} of 34±6 μM, which is in line with the value determined when phenylethylamine is substrate. K_{Mox} and K_{Mred} values were found to be similar to previous experiments.

As done with phenylethylamine, sigmoidal plots were done to ensure the values obtained through the mathematical model of the MAO-B reaction scheme are reasonable.

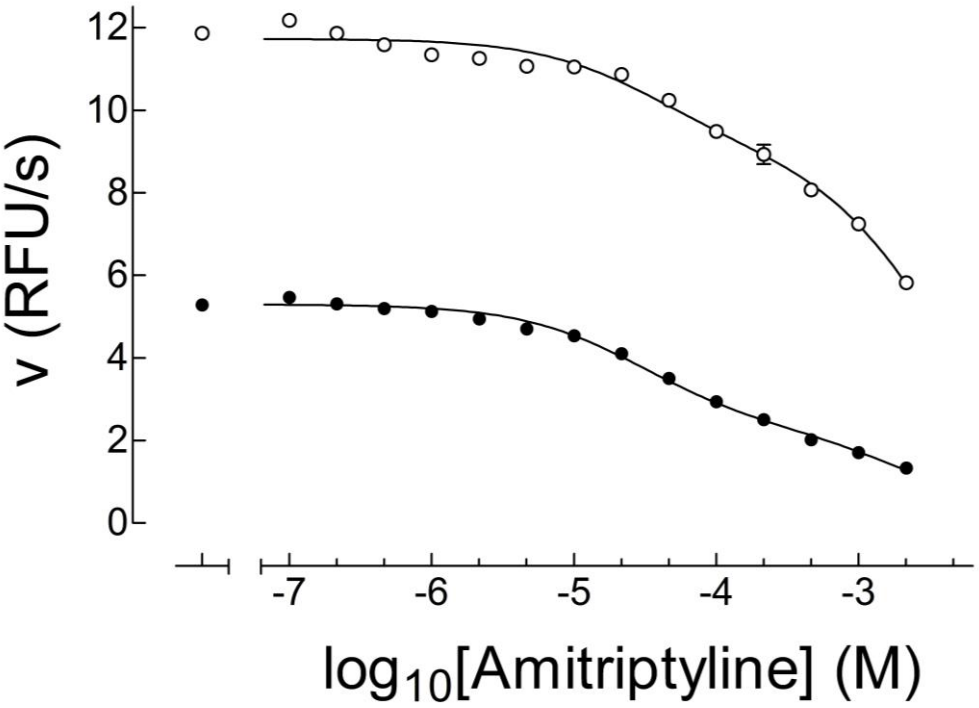

Figure 2.7.7.6 Inhibitor plots of amitriptyline versus benzylamine

Oxidation of 70(●) and 700(○) µM benzylamine by hMAO-B (0.3nM) in the presence of amitriptyline (n=3) fitted to a biphasic sigmoid with both Hill-slopes constrained to -1.0. 70 µM benzylamine produced an $IC_{50\text{-}1}$ of 31 µM and an $IC_{50\text{-}2}$ of 2290 µM. 700 µM benzylamine yielded 34 µM and 3723 µM for $IC_{50\text{-}1}$ and $IC_{50\text{-}2}$, respectively. Fractions were 0.57 and 0.23 for 70 and 700 µM, respectively with overlapping errors. Error bars represent SEM.

The concentrations of benzylamine in the inhibitor plots shown in Figure 2.7.7.6 were based upon K_{Mox} and K_{Mred} values obtained from previous experiments. The IC_{50} values for amitriptyline obtained from these data are also very similar to those obtained with phenylethylamine and relate well to K_I values obtained from kinetic analyses.

A major difference between the sigmoids produced with phenylethylamine and benzylamine is the degree of change in the fraction value. Benzylamine shows a large shift from 0.57 to 0.23 with increased substrate concentration, suggesting that the fraction of enzyme in the reduced form increases as benzylamine concentration increases. This likely stems from benzylamine binding to $E.FAD_{red}$ more frequently as substrate concentration increases, thus retaining more of the enzyme population in the reduced pathway. In turn, this reduces the amount of $E.FAD_{ox}$ available for amitriptyline binding.

The sigmoidal data suggest that at 70 μM benzylamine, about 57% of the activity is associated with the $E.FAD_{ox}$ pathway. Increasing the concentration of benzylamine to 700 μM causes a shift such that less than a quarter of all activity is via the $E.FAD_{ox}$ pathway.

Assuming competitive inhibition, if K_{Mox} is taken to be 70 μM, the Cheng-Prusoff equation *estimates values* of 17 and 3.1 μM for K_{Iox} at 70 and 700 μM, respectively. This apparent increase in potency can be attributed to benzylamine inhibiting its own catabolism through the $E.FAD_{ox}$ pathway by increasing flux through the $E.FAD_{red}$-S pathway as substrate concentration increases.

The amitriptyline experiments provide consistent evidence in support of the mathematical model as well as some evidence in favour of the proposed schematic. The evidence also shows the difficulty in interpreting plots from an enzyme with $E.FAD_{ox}$ and $E.FAD_{red}$ components that are each capable of binding amine substrate and yielding products at different rates. In many respects, the sigmoids appear to yield a result of non-competitive inhibition if a classical Michaelis-Menten enzyme

model is used. In our modified model, which accounts for both $E.FAD_{ox}$ and $E.FAD_{red}$, the results are well-explained by a competitive inhibition model.

2.7.8 Inhibition of MAO-B by DiHEMDA

DiHEMDA, di(2-hydroxyethyl)methyldodecylammonium, is an MAO-B inhibitor that leaches from plasticware[106]. Preliminary experiments with DiHEMDA suggest it is a relatively potent MAO-B inhibitor. As mentioned previously, we expected DiHEMDA to act as a competitive inhibitor based upon the similarity in structure to LDAO, an aliphatic chain amine known to bind to the active site of MAO-B based on crystallographic data. Using the competitive inhibition model, the inhibitor mechanism of DiHEMDA was characterised.

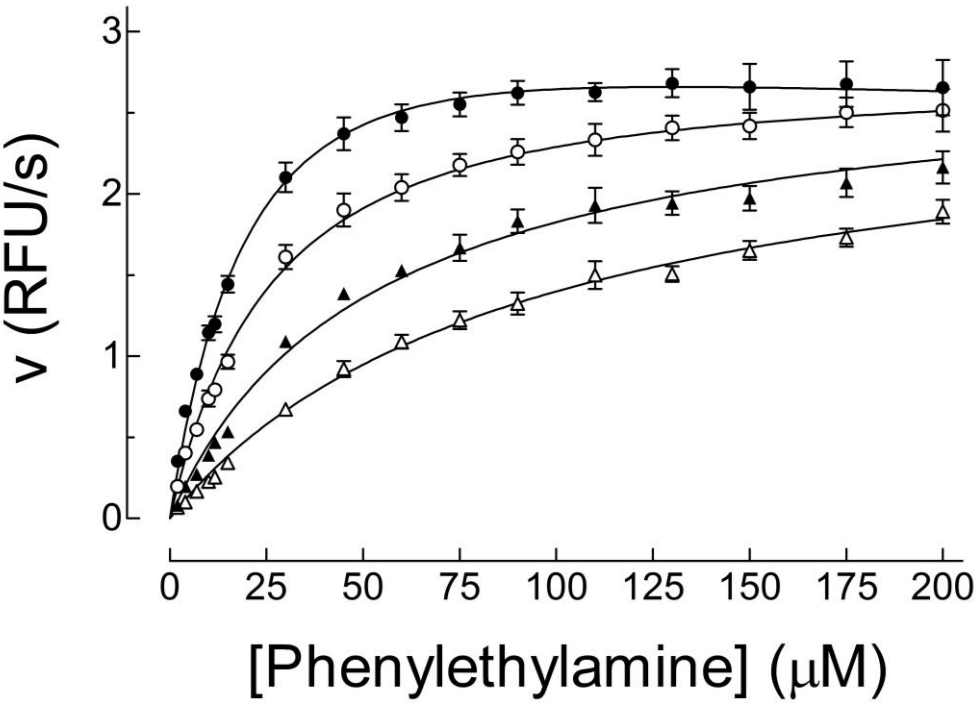

Figure 2.7.8.1 Inhibition of hMAO-B by DiHEMDA versus phenylethylamine

Oxidation of phenylethylamine (2-200μM) by hMAO-B (2nM) in the presence of 0(●), 2(○), 8(▲), and 20(△) μM DiHEMDA (n=3) globally fitted to a two-site model with competition at both (***Eq. 2.14***). Error bars represent SEM. Fits yielded a value of 38±9 and 54±10 μM for K_{Mox} and K_{Mred}, respectively. K_{Iox} and K_{Ired} were found to be 2.8±0.6 and 14±4 μM, respectively. The global R^2 was 0.9672.

The results displayed in Figure 2.7.8.1 come from an experiment performed by Owen Degenhardt. The K_M values for phenylethylamine are about 2-fold higher than observed in the control curves, however the K_{Mred}:K_{Mox} ratio of about 1.3 is maintained. The results provide evidence of competitive inhibition at both E.FAD_{ox} and E. FAD_{red} and it appears that DiHEMDA is a more potent competitive inhibitor than either amitriptyline or amphetamine.

Probing further into DiHEMDA, two sigmoidal curves were produced with phenylethylamine as the substrate.

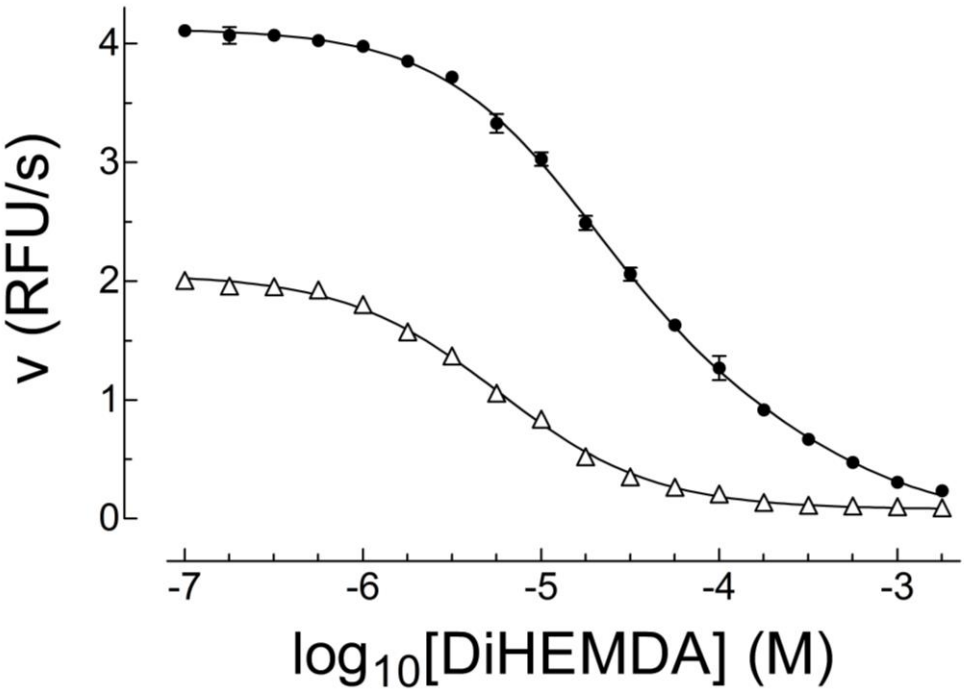

Figure 2.7.8.2 Inhibitor plots of DiHEMDA versus phenylethylamine

Oxidation of 120(●) and 6(Δ) μM phenylethylamine by hMAO-B (1 nM) in the presence of DiHEMDA (n=4) fitted to a biphasic sigmoid with each Hill-slope constrained to -1.0. 6 μM phenylethylamine produced an $IC_{50\text{-}1}$ of 5.7 μM without a second site being seen. 120 μM phenylethylamine produced $IC_{50\text{-}1}$ of 18 μM, an $IC_{50\text{-}2}$ 370 of μM. Error bars represent SEM.

The 6 μM phenylethylamine sigmoid fits nicely to a monophasic sigmoid, while the 120 μM curve requires a biphasic curve to describe the data. The 120 μM sigmoid is very close to monophasic except for at the highest concentrations of DiHEMDA. The bottom required constraining to zero to be able to fit the biphasic curve. One important thing to consider is that DiHEMDA is a detergent, and at high concentrations it may have an effect on the membrane-associated MAO-B. The constraining requirement and large fraction of inhibition from the high affinity site support using a one-site model for analysis.

At first glance, it appears that a twenty-fold increase in substrate concentration causes less than a five-fold shift in the IC_{50} values. In a one-site system, this would be taken to suggest that some form of non-competitive inhibition is occurring. It is

important to remember that when dealing with a two-site model, it may be possible to have such a result from competitive inhibition at one site.

When selecting the concentrations for phenylethylamine, the K_M values for both $E.FAD_{ox}$ and $E.FAD_{red}$ were considered. A concentration of 6 μM phenylethylamine was selected with the hope of having the enzyme proceed predominantly through $E.FAD_{ox}$, thus determining an IC_{50} most closely related to K_{Iox}. Using a concentration of 120 μM phenylethylamine, it was our intention to have MAO-B proceed predominantly through $E.FAD_{red}$, and thus allow sufficient data points to allow accurate determination of an $IC_{50\text{-}2}$.

Using the Cheng-Prusoff equation to convert the IC_{50} values to *estimate* K_I values, 4.4 μM and 12.2 μM are obtained for the 6 and 120 μM phenylethylamine sigmoids, respectively. The calculations use 20 μM and 42 μM for K_{Mox} and K_{Mred}, respectively (based on averages from Table 2.8.1 Compilation of Kinetic Values Determined from Kinetic Analyses). The results concur with the kinetic fits done previously and help support the idea of two pathways with distinct kinetic parameters.

It is also important to note that one of the reasons that there is no clear sign of biphasic inhibition in this case is that the K_I values have a very similar ratio as K_{Mox}:K_{Mred}. The "K_I" values from this experiment have a ratio of 2.8 and the average of phenylethylamine constants produces a K_{Mox}:K_{Mred} of 2.7. DiHEMDA's ability to inhibit both $E.FAD_{ox}$ and $E.FAD_{red}$ at a ratio similar to that with phenylethylamine's K_M values causes the inhibition to appear as a one-site system.

DiHEMDA was also analysed with benzylamine as substrate. Kinetic curves were produced under both high and low oxygen conditions and fitted with non-linear regression to Eq 2.14.

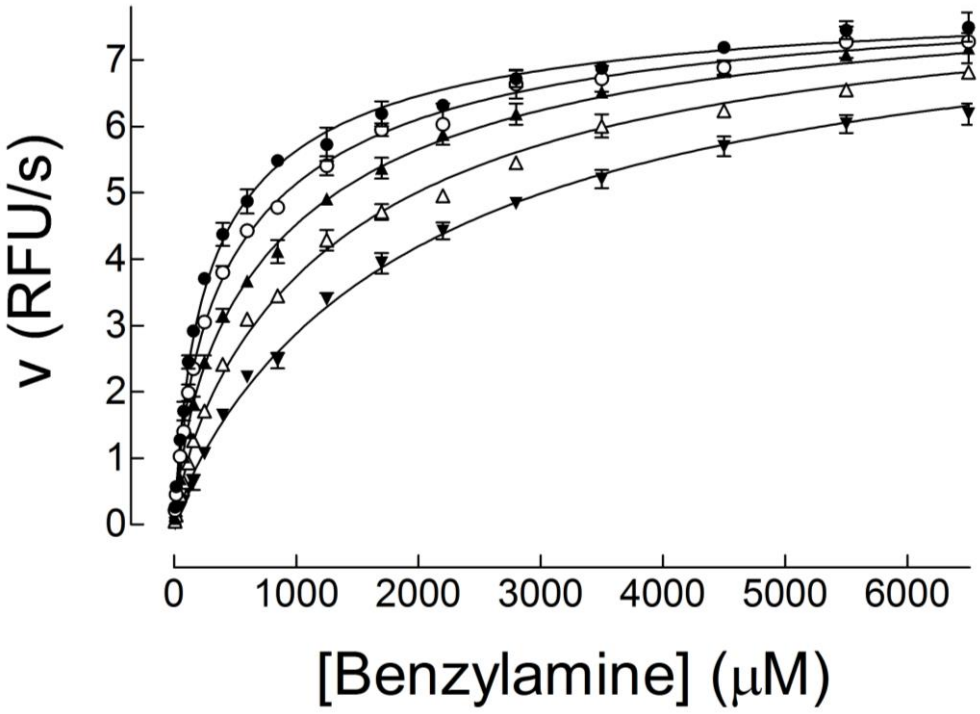

Figure 2.7.8.3 Inhibition of MAO-B by DiHEMDA versus benzylamine under high oxygen

Oxidation of benzylamine (10-6500μM) by hMAO-B (1 nM) under 500 μM oxygen in the presence of 0(●), 1(○), 3 (▲), 8(△) and 20(▼) μM DiHEMDA (n=3) globally fitted to a two-site model with competitive at both $E.FAD_{ox}$ and $E.FAD_{red}$ (***Eq. 2.14***). Error bars represent SEM. Fits yielded a value of 170±20 and 1200±100 μM for K_{Mox} and K_{Mred}, respectively. K_{Iox} and K_{Ired} were found to be 3.9±0.4 and 30±5 μM. The global R^2 was 0.9939.

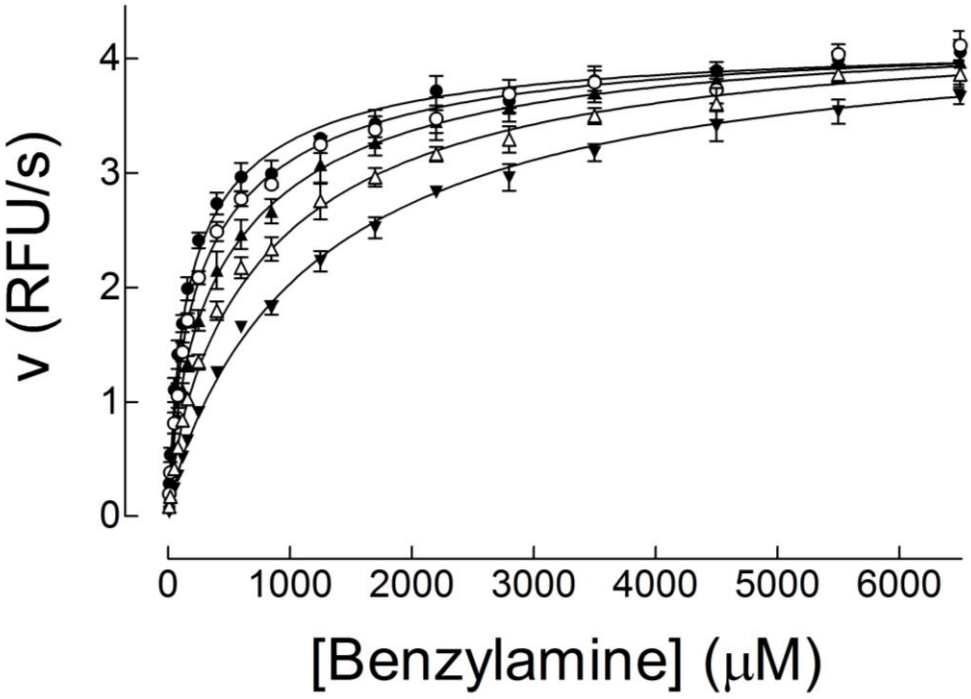

Figure 2.7.8.4 Inhibition of hMAO-B by DiHEMDA versus benzylamine under low oxygen

Oxidation of benzylamine (10-6500μM) by hMAO-B (1 nM) under 100 μM oxygen in the presence of 0(●), 1(○), 3 (▲), 8(△) and 20 (▼) μM DiHEMDA (n=3) globally fitted to a two-site model with competitive at both $E.FAD_{ox}$ and $E.FAD_{red}$ (***Eq. 2.14***). Error bars represent SEM. Fits yielded a value of 100±10 and 780±90 μM for K_{Mox} and K_{Mred}, respectively. K_{Iox} and K_{Ired} were found to be 5.3±0.8 and 32±7μM. The global R^2 was 0.9829.

The values for K_{Iox} and K_{Ired}, as determined by non-linear regression, are nearly identical under high- and low-oxygen. K_{Iox} values of 3.9 and 5.3 μM and K_{Ired} values of 30 and 32 μM were determined for high oxygen and low oxygen, respectively. Visually, it appears that DiHEMDA is a more effective inhibitor when oxygen levels are increased even though K_I values remain constant. The presence of elevated oxygen may increase the probability that free $E.FAD_{ox}$ exists. DiHEMDA has a higher affinity for $E.FAD_{ox}$ than $E.FAD_{red}$, so as flux through $E.FAD_{ox}$ increases, so does the apparent degree of inhibition by DiHEMDA.

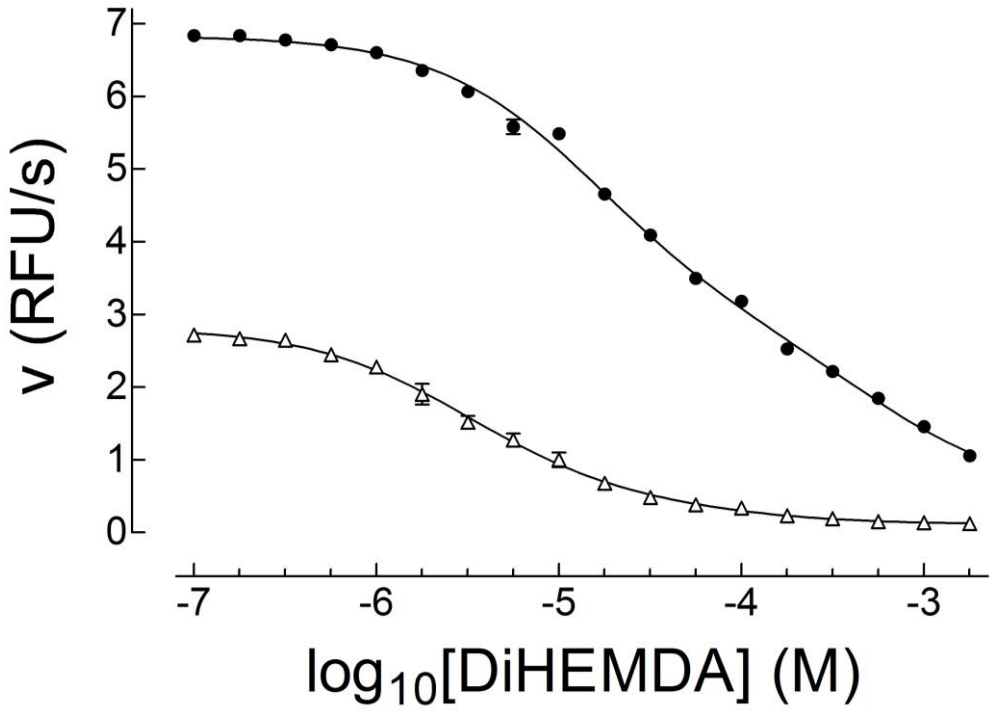

Figure 2.7.8.5 Inhibitor plots of DiHEMDA versus benzylamine

Oxidation of 90(△) and 1800(●) μM benzylamine by hMAO-B (1 nM) in the presence of DiHEMDA (n=4) fitted to a biphasic sigmoid with both Hill-slopes constrained to -1.0. 90 and 1800 μM phenylethylamine produced an $IC_{50\text{-}1}$ and $IC_{50\text{-}2}$ of 3.3 and 22 μM, and 12.9 and 52 μM respectively. Error bars represent SEM.

Unlike phenylethylamine, inhibition of benzylamine by DiHEMDA does not yield perfectly monophasic sigmoidal curves across high and low concentrations. At 90 μM, IC_{50} values for the two sites are 3.3 and 22 μM, although there is a wide range of error on the second IC_{50} value. Increasing benzylamine concentrations by 20-fold only causes a shift in IC_{50} values to 12.9 and 52 μM. Some basic calculations can explore whether the increases are appropriate for a competitive inhibitor at two sites.

First, the values of 3.3 and 22 μM are likely IC_{50} values loosely corresponding to K_I values at $E.FAD_{ox}$ and $E.FAD_{red}$, respectively. The Cheng-Prusoff equation with values of 103.5 and 1020 μM for K_{Mox} and K_{Mred}, respectively (based on averages

from Table 2.8.1 Compilation of Kinetic Values Determined from Kinetic Analyses), yields a K_{Iox} and K_{Ired} of 1.8 and 20.2 μM, respectively. Using the same constants for the IC_{50} values of 12.9 and 52 μM, K_{Iox} and K_{Ired} are calculated to be 0.70 and 18.8 μM, respectively. With the exception of K_{Iox} calculated from the turnover of 1800 μM benzylamine (and to some extent K_{Iox} from the turnover of 90 μM benzylamine), the values come out exactly where expected.

One final confirmatory experiment was done with D_2-benzylamine as a deuterated isotope (see Section 2.4.2). The results, once again, were very consistent with previously obtained data.

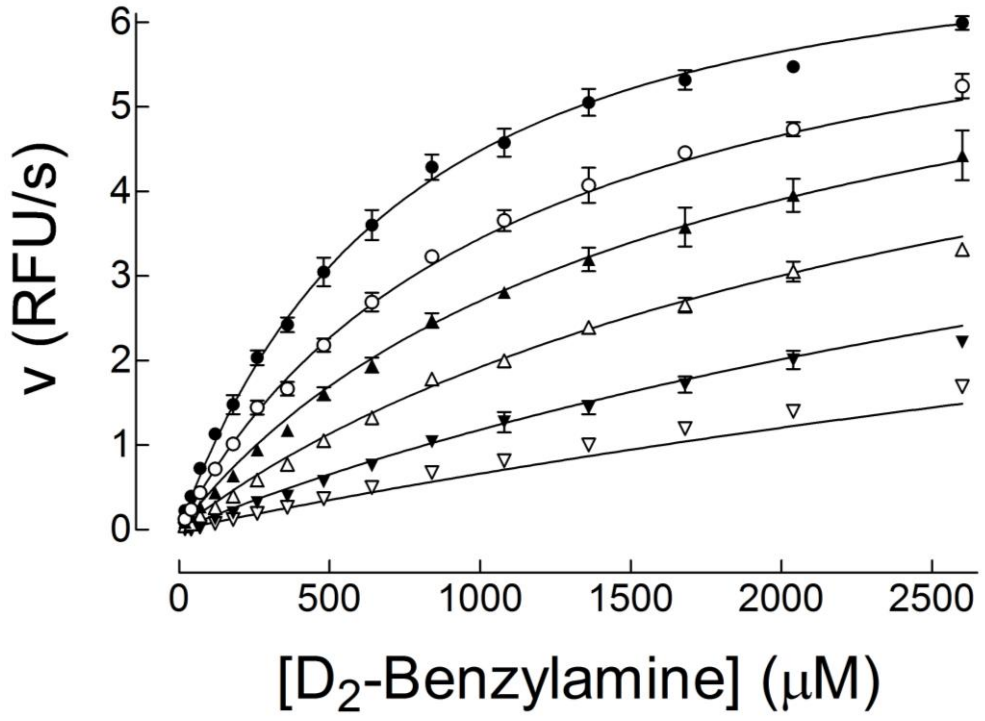

Figure 2.7.8.6 Inhibition of hMAO-B by DiHEMDA versus D_2-benzylamine

Oxidation of D_2-benzylamine (20-2600μM) by hMAO-B (1 nM) in the presence of 0(●), 3(○), 7.5(▲), 18(△) 44(▼) and 100(▽) μM DiHEMDA (n=3) globally fitted to a two-site model with competitive at both $E.FAD_{ox}$ and $E.FAD_{red}$ (***Eq. 2.14***). Error bars represent SEM. Fits yielded a value of 1100±300 and 1900±400 μM for K_{Mox} and K_{Mred}, respectively. K_{Iox} and K_{Ired} were found to be 5.1±0.8 and 24±4 μM. The global R^2 was 0.9913.

The results from the sigmoids of DiHEMDA inhibition of benzylamine are very consistent with values obtained from other substrates. Together, with the support of sigmoid plots, the evidence strongly supports a mechanism of competitive inhibition by DiHEMDA. The results of all experiments have been compiled into Table 2.8.1.

2.8 Concluding Remarks

For the first time, much of the literature on MAO-B kinetics has been consolidated into one comprehensive explanation. The differences between phenylethylamine and benzylamine as substrates are adequately described by the model presented in Section 2.5.2. It appears that benzylamine has a K_{Mox} value of approximately 100 μM and a K_{Mred} value of approximate 700 μM with a V_{MAXred}:V_{MAXox} ratio between 1.4 and 3.0. Phenylethylamine appears to have a K_{Mox} of around 15 μM and a K_{Mred} of between 20 and 80 μM, although it is difficult to accurately determine the K_M values precisely because the V_{MAXred}:V_{MAXox} is relatively close to 1.0, making the system appear more like a classical Michaelis-Menten model of enzyme catalysis.

The model has been shown to be valuable in determining the kinetic parameters for inhibitors as well. The most potent competitive inhibitor, DiHEMDA, had affinities for both forms of MAO-B in the low micromolar range. Application of this mathematical model to future inhibitors of MAO-B will likely provide valuable insight into the mechanism of both the inhibitor and of MAO-B, and will offer a substantial improvement over use of the Michaelis-Menten equation.

It is hoped that with appropriate use of our new model, the mechanism of inhibition of MAO-B by 2-BFI can be elucidated and the role of the I_2 site on MAO-B can be clarified. Application of Michaelis-Menten kinetics to past data has yielded inconsistent results and questions remain regarding how the 2-BFI acts as an inhibitor and why this inhibition occurs at micromolar concentration when 2-BFI appears to have nanomolar affinity for MAO-B in radioligand binding experiments. To begin our investigation into this discrepancy of binding and inhibitor action, we performed radioligand binding experiments which are presented in Chapter 3, *MAO-B through the "I" of Radioligands*.

Data from all the experiments are compiled into *Table 2.8.1 Compilation of Kinetic Values Determined from Kinetic Analyses* (below).

Amphetamine											
		Two-Site Model, Competitive at both									
Substrate	Figure Number	K_{Mox} (μM)	K_{Mred} (μM)	V_{MAXox}	V_{MAXred}	K_{Iox} (μM)	K_{Ired} (μM)	KIred:KIox	KMred:KMox	VMAXred:VMAXox	R^2
Phenylethylamine (Atmospheric)	2.7.6.1	12 ± 1	16 ± 1	4.4 ± 1.5	4.5 ± 4.9	**262 ± 90**	**1950 ± 800**	**7.44**	**1.39**	**1.01**	0.9932
D_2-Phenylethylamine (Atmospheric)	2.7.6.2	29 ± 5	62 ± 6	3.7 ± 0.6	10.1 ± 0.6	**320 ± 90**	**1600 ± 190**	**5.00**	**2.11**	**2.75**	0.9961
Benzylamine (Atmospheric)	2.7.6.3	110 ± 12	730 ± 90	5.4 ± 0.3	7.7 ± 0.1	**730 ± 90**	**5000 ± 900**	**6.85**	**6.65**	**1.42**	0.9820
Amitriptyline											
		Two-Site Model, Competitive at both									
Substrate	Figure Number	K_{Mox} (μM)	K_{Mred} (μM)	V_{MAXox}	V_{MAXred}	K_{Iox} (μM)	K_{Ired} (μM)	KIred:KIox	KMred:KMox	VMAXred:VMAXox	R^2
Phenylethylamine (Atmospheric)	2.7.7.1	12 ± 1	71 ± 6	8.6 ± 0.3	12.5 ± 0.2	**58 ± 6**	630 ± 60	10.9	5.9	1.4	0.9917
Benzylamine (Low Oxygen)	2.7.7.3	65 ± 3	1110 ± 110	3.7 ± 0.1	5.1 ± 0.0	**170 ± 10**	∞		17.2	1.4	0.9919
Benzylamine (High Oxygen)	2.7.7.4	85 ± 0	890 ± 150	3.2 ± 0.2	4.6 ± 0.1	**100 ± 20**	∞		10.6	1.5	0.9674
Benzylamine (Atmospheric)	2.7.7.5	82 ± 13	500 ± 30	4.4 ± 0.3	12.4 ± 0.1	**34 ± 6**	1800 ± 250	53.2	6.1	2.8	0.9868
DiHEMDA											
		Two-Site Model, Competitive at both									
Substrate	Figure Number	K_{Mox} (μM)	K_{Mred} (μM)	V_{MAXox}	V_{MAXred}	K_{Iox} (μM)	K_{Ired} (μM)	KIred:KIox	KMred:KMox	VMAXred:VMAXox	R^2
Phenylethylamine (Atmospheric)	2.7.8.1	38 ± 10	54 ± 10	5.6 ± 2.4	2.3 ± 0.2	**2.8 ± 0.6**	**14 ± 4**	**5.11**	**1.44**	**0.41**	0.9683
Benzylamine (High Oxygen)	2.7.8.3	170 ± 20	1200 ± 100	4.4 ± 0.2	8.0 ± 0.1	**3.9 ± 0.4**	**30 ± 5**	**7.56**	**7.06**	**1.81**	0.9939
Benylamine (Low Oxygen)	2.7.8.4	100 ± 10	780 ± 90	2.4 ± 0.2	4.2 ± 0.0	**5.3 ± 0.8**	**32 ± 7**	**6**	**8**	**2**	0.9878
D_2-Phenylethylamine (Atmospheric)	2.7.8.6	1100 ± 300	1900 ± 400	6.6 ± 1.1	6.9 ± 0.5	**5.1 ± 0.8**	**24 ± 4**	**5**	**2**	**1**	0.9919
AVERAGE						**4.3**	**25.0**				

Table 2.8.1 Compilation of Kinetic Values Determined from Kinetic Analyses

3 MAO-B through the "I" of Radioligands

3.1 Publications

Data and findings presented in this chapter have been published previously:

On the formation and nature of the imidazoline I2 binding site on human monoamine oxidase-B. **McDonald GR**, Olivieri A, Ramsay RR, Holt A. *Pharmacol Res*. 2010 Dec;62(6):475-88.

Potentiation of ligand binding through cooperative effects in monoamine oxidase B. Bonivento D, Milczek EM, **McDonald GR**, Binda C, Holt A, Edmondson DE, Mattevi A. *J Biol Chem*. 2010 Nov 19;285(47):36849-56

3.2 Background

In vitro and MAO knockout mice studies have provided evidence of I_2 localisation on MAO-B[79]. Binding and displacement studies with [^{3}H]2-BFI and [^{3}H]clonidine, however, consistently produce IC_{50} values in the low nanomolar range while kinetics of inhibition by the ligands only occurs at significantly higher concentrations (two to four orders of magnitude). More puzzling is that only a fraction of MAO-B in tissue samples used by researchers appear to possess a high affinity I_2 binding site, but imidazolines are capable of producing complete inhibition of amine oxidation. Furthermore, Steinberg and Weist (1997) found that preincubation with tranylcypromine (TCP) increased the number of I_2 binding sites in rat brain samples[83].

Crystallographic models of human MAO-B (hMAO-B) show the enzyme possesses two cavities separated by an isoleucine residue (Ile199). This residue is thought to act as a gate between the active site and a substrate entrance channel (Edmondson et al., 2009). Photoaffinity labelling of hMAO-B with the compound

[^{125}I]AZIPI identified a region between lysine 149 and methionine 222 as the region to which imidazolines bind[108,109]. Contained within that region of residues are Ile199 and other amino acids that line the substrate entrance channel but none contributes to the substrate binding cavity within the active site[109]. Crystal structures indicate that incubation of MAO-B with the irreversible inhibitor tranylcypromine leads to adduct formation with the flavin cofactor of the enzyme and a resultant shift in both Ile199 and glutamine 206 (Gln206) (see Figure 2.7.8.1)[61].This shift appears to force the two residues to close the opening into the substrate-binding site, creating a unique cavity in the entrance cavity. Based on the information contained in the literature, we proposed that [^{3}H]2-BFI binds in the cavity formed by the closure of the gating residues. Herein, [^{3}H]2-BFI is used as a high affinity I_2 ligand to probe the I_2-site on MAO-B in hopes of characterising the site and providing direct confirmatory evidence that the site is located in the entrance cavity.

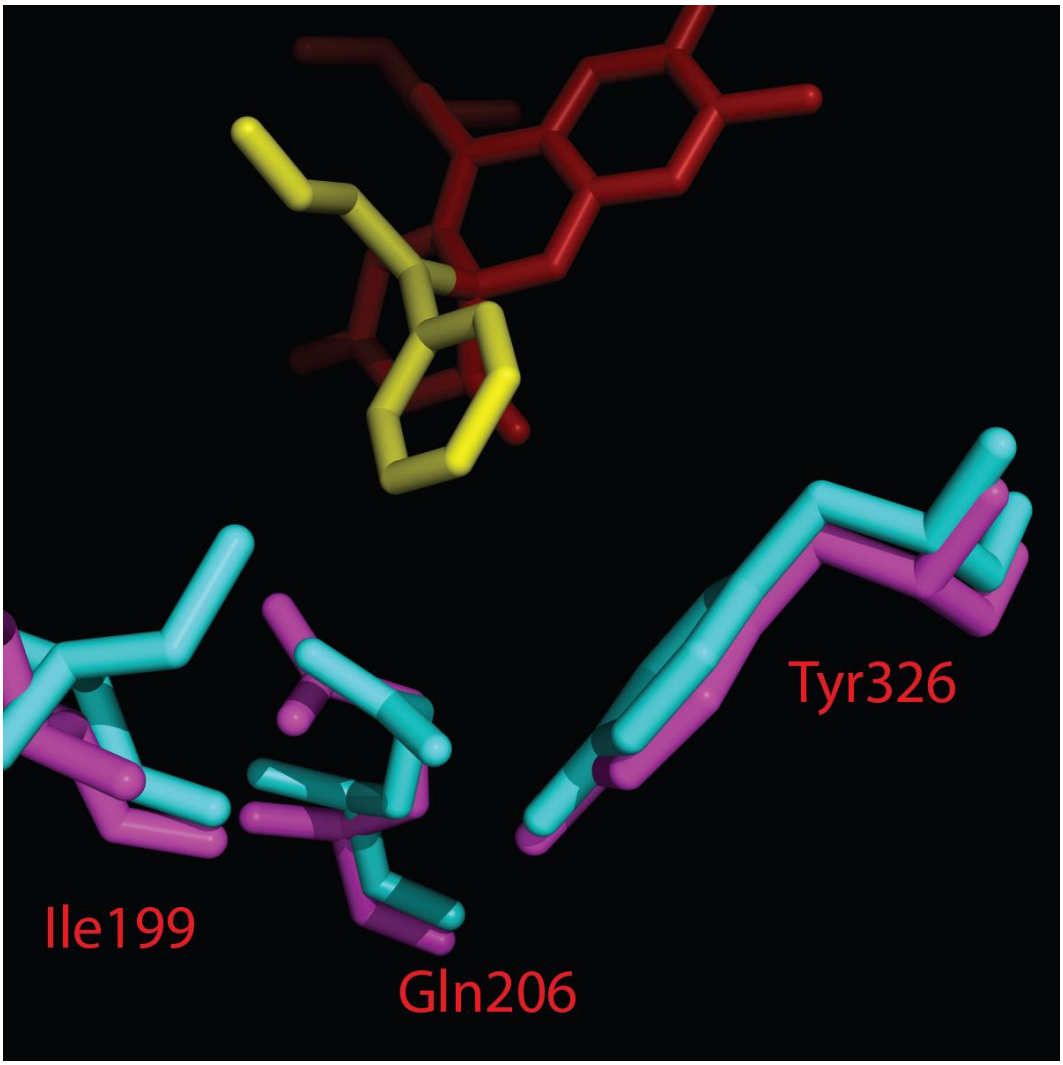

Figure 2.7.8.1 Changes in MAO-B when TCP is bound

Three important residues (Ile199, Gln206, and Tyr326) in MAO-B (purple) versus when TCP is covalently bound to the flavin (blue). The flavin is show in red and TCP in yellow[61]. Binding of TCP to the flavin appears to shift Ile199 and Gln206 significantly, closing the opening between the substrate-binding site and the entrance cavity.

3.3 Control Binding of [^{3}H]2-BFI MAO-B

3.3.1 Hypotheses

Based upon the numerous studies involving human platelets and the presence of the I_2 binding site, it was expected that purified enzyme would also possess the binding site[83,86,87]. We expected to find an affinity in the low nanomolar range, confirming a site similar to that extracted from endogenous human sources.

3.3.2 Materials

[^{3}H]2-BFI ([5,7-(n)-^{3}H]2-(2-benzofuranyl)-2-imidazoline hydrochloride; 67 Ci mmol^{-1}) was purchased from Amersham Biosciences (Little Chalfont, U.K.; product discontinued - now available from Moravek Biochemicals, Brea, CA). [^{3}H]Benzylamine ([2,2,4-^{3}H]benzylamine hydrochloride; 60 Ci mmol^{-1}) was purchased from American Radiolabeled Chemicals (St. Louis, MO). 2-BFI was purchased from Tocris-Cookson (Ellisville, MO). Cytoscint scintillation fluid was purchased from MP Biomedicals, Santa Ana, CA. Rasagiline was a gift from Prof. Dale Edmondson. All other substrates, inhibitors and reaction constituents were obtained from Sigma-Aldrich (Oakville, ON, Canada). Buffer salts were of molecular biology grade.

Mitochondrial membrane homogenates of human (WT-hMAO-B) and mutant MAO-B were a gift from Dr. Dale Edmondson (Emory University, Atlanta, GA). Enzymes used in binding assays were associated with a membrane fraction from a culture of *Pichia pastoris* yeast[110].

3.3.3 Methods

Radioligand binding assays were carried out using deep-well polypropylene 96-well plates. To each experimental well 25 µl of 30nM [^{3}H]2-BFI (5 nM final concentration and 4.19 µCi/nmol) and either 25 µl of water (total binding) or 2-BFI (15 µM final concentration, to define non-specific binding) were added. In competition assays, 25 µl of competing ligand were added to wells containing [^{3}H]2-BFI in order of ascending concentration first and then wells containing 2-BFI in order of ascending concentration to prevent contamination of total binding well with high concentrations of 2-BFI displacer. In experiments without competing ligands, 25 µl of water were added to all wells. To commence binding, 75 µl of *P. pastoris* membrane homogenate containing 2.7 mg protein per ml of hMAO-B made up in 100mM intracellular HEPES buffer (pH 7.4) were added with a multichannel pipette. The choice of 2-BFI as a displacing agent to define non-specific binding resulted from concern regarding non-competitive displacement of 2-BFI with other imidazoline ligands. By using 2-BFI as both the radiolabeled ligand and displacing agent, competitive displacement was guaranteed despite the potential for displacing non-specific (low affinity) binding.

Incubations not involving substrate lasted for 30 minutes at 25°C before filtration through Whatman GF/B filter paper (Brandel Inc. Gaithersburg, MD) which were soaked in 0.5% polyethyleneimine for one hour prior to extraction onto filter papers using a Brandel cell harvester. In binding experiments where substrates were included to determine their effects on [^{3}H]2-BFI, incubations occurred for 60 minutes on ice to prevent substrate turnover prior to filtration.

Filters were briefly washed with ice-cold 50 mM potassium phosphate buffer (pH 7.4) before being counted for tritium content in 3 ml of Cytoscint. Standards were prepared for all experiments as a check to ensure dilutions and specific activity was correct.

As with all kinetic experiments, solutions and dilutions were carried out in colourless Eppendorf™ tubes to reduce the chance of introducing contaminants.

3.3.4 Binding of [^{3}H]2-BFI binding to WT-hMAO-B

The literature supporting binding of [^{3}H]2-BFI to MAO-B has typically relied upon rat brain homogenates or human platelets as the source material. With access to purified, human MAO-B produced in yeast, defining the K_D for 2-BFI at a site on *human* MAO-B is essential to confirm the presence of a high affinity binding site. Binding data from the literature suggest that high affinity [^{3}H]2-BFI binding appears only on 5-10% of the MAO-B present in tissues, although different tissues report different fractions of MAO-B possessing I_2-sites.

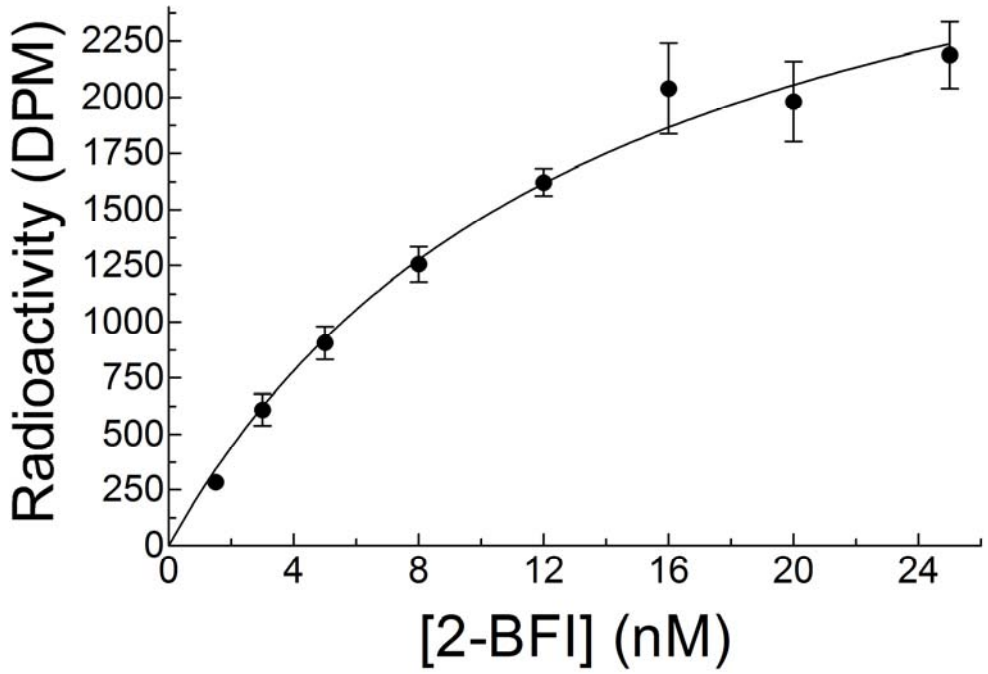

Figure 3.3.4.1 Binding of [³H]2-BFI to WT-hMAO-B

Specific binding of [³H]2-BFI (14 Ci/mmol) to WT-hMAO-B membrane fractions fitted to a rectangular hyperbola by non-linear regression. The K_D was determined to be 14±2 μM and the B_{MAX} was determined to be 280 amol/μg. Error bars represent SEM.

[³H]2-BFI displays an affinity of 14 nM for MAO-B in the preparation used, in agreement with values determined in human platelets by Weist and Steinberg in 1997. Based on the specific activity of the standards (and a B_{MAX} of 3464 dpm), there appears to be an I_2-site concentration of 279 amol/μg protein. This is less than 1% of the expected binding based on activity level in the samples, which is somewhat consistent with observations from the literature using homogenates. The binding does confirm the presence of a high-affinity site on *human* MAO-B, but provides the same baffling result seen in the literature wherein only a small fraction of MAO-B appears to possess a high affinity I_2 site. The results of the binding alone appear to be similar to the results seen from human platelets, but this does not mean that the site [³H]2-BFI is binding to is identical to the site endogenously formed in humans.

3.4 Modulation of [^{3}H]2-BFI binding to WT-MAO-B

3.4.1 Hypothesis

Numerous researchers had found that preincubation with TCP led to increased exposure of I_2 binding sites[86,87]. We expected to see similar results using the purified enzyme, showing undoubtedly that TCP exposes a site for [^{3}H]2-BFI to bind to on MAO-B.

3.4.2 Materials and Methods

Many of the experiments in this section were performed in a manner identical to the methods described in Section 3.3.2. All experiments requiring preincubation of the ligand (TCP and phenylethylamine) with MAO-B had the excess ligand removed by three separate centrifugations (15,000 relative centrifugal force (RCF) for 5 min followed by resuspension in HEPES buffer) prior to inclusion in the assay. These experiments were carried out such that the MAO-B concentrations remained at 2.7 mg protein per ml in 100mM HEPES prior to inclusion in the 96-well plate.

For experiments involving kinetics determinations, the activities of purified preparations or membrane fractions from *P. pastoris* yeast were measured continuously in 96-well plates with a SpectraMax Gemini XPS microplate reader by following the fluorescence related to the peroxidase-coupled formation of resorufin from AmplexRed[102]. Each reaction was run at 30°C in a total volume of 200 μL. Amine substrate was prepared on the day of the experiment using colourless Eppendorf™ micocentrifuge tubes for the dilutions. All dilutions were done in water.

The MAO-B/AmplexRed™/peroxidase solution was prepared by diluting MAO-B from a batch stock into a solution of 100 mM HEPES buffer. This was then mixed 1:1 with an AmplexRed™/peroxidase solution made up at four-times the concentration required for the experiment. The MAO-B/AmplexRed™/peroxidase solution was prepared to be used in entirety for a single experiment and was made fresh each time. During experiments involving more than one plate, enzyme was stored in the fridge until it was required in the experiment.

Plates were warmed to 30˚C prior to commencing the experiment. Assays were started by rapid addition of enzyme/AmplexRed/peroxidase mixture using an 8-channel pipette. Experiments were carried out under atmospheric oxygen unless otherwise stated.

Data were fitted to equations via the nonlinear regression function of GraphPad Prism v. 5.0c for Windows (GraphPad Software Inc., San Diego, CA).

3.4.3 Non-linear Regression to fit Models to Data

All curve fitting was carried out using the non-linear regression functionality of GraphPad Prism 5.0 (GraphPad Software Inc., San Diego, CA). For single-site hyperbola models (standard Michaelis-Menten kinetics) and sigmoidal inhibitor plots, the standard equations supplied with Prism 5 are used. These equations are:

$$Y = Vmax * X/(K_M + X)$$

For non-linear regression of single-site hyperbolas

$$Y = Bottom + (Top - Bottom)/(1 + 10^{\{LogEC_{50} - X\}})$$

For non-linear regression of sigmoidal plots

$$Y = Bottom + (Top - Bottom)/(1 + 10^{\{LogEC_{50} - X) * HillSlope\}})$$

For sigmoidal plots with a variable Hill-slope

$$Y = Y0 + (Plateau - Y0) * (1 - exp(-K * x))$$

For one-phase exponential association

3.4.4 I_2-site Formation by Tranylcypromine

Reports of TCP potentiation of [^{3}H]2-BFI, but not [^{3}H]idazoxan, binding to MAO-B found in human brain homogenates and platelets[83,87] were published in the late 1990s (see Section 1.3 for details). The authors found no potentiation in homogenates derived from rats. It was also found that other irreversible inhibitors, such as pargyline and deprenyl, *do not* potentiate binding of 2-BFI.

The unique properties of 2-BFI led the authors to suggest that inhibition of *human* MAO-B with TCP may cause a conformation change in the enzyme such that an otherwise masked site is exposed for 2-BFI. A cryptic I_2 site or a different site on MAO-B have been given as explanations for the lack of potentiation of [^{3}H]idazoxan binding by TCP[83].

The crystal structure of human MAO-B was published in 2001[58], followed shortly by the structure with TCP in 2003[61](see

Figure 2.7.8.1 for image). Using the photoaffinity labelling results from 1989 [77], we felt the most likely place for 2-BFI to bind is the substrate entrance channel. Overlaying the crystal structures of both TCP-bound and non-TCP-bound human MAO-B shows shifts in two substrate entrance channel amino acids: Gln206 and Ile199 (see Figure 2.7.8.1).Recently, the crystal structure of MAO-B bound to TCP was redone, showing TCP bound to a different site of the flavin (PBD ID 2XFN).

To probe and characterise the I_2-site on human MAO-B, replication of the original potentiation data was done to ensure the results were not an artefact of using human tissue homogenate.

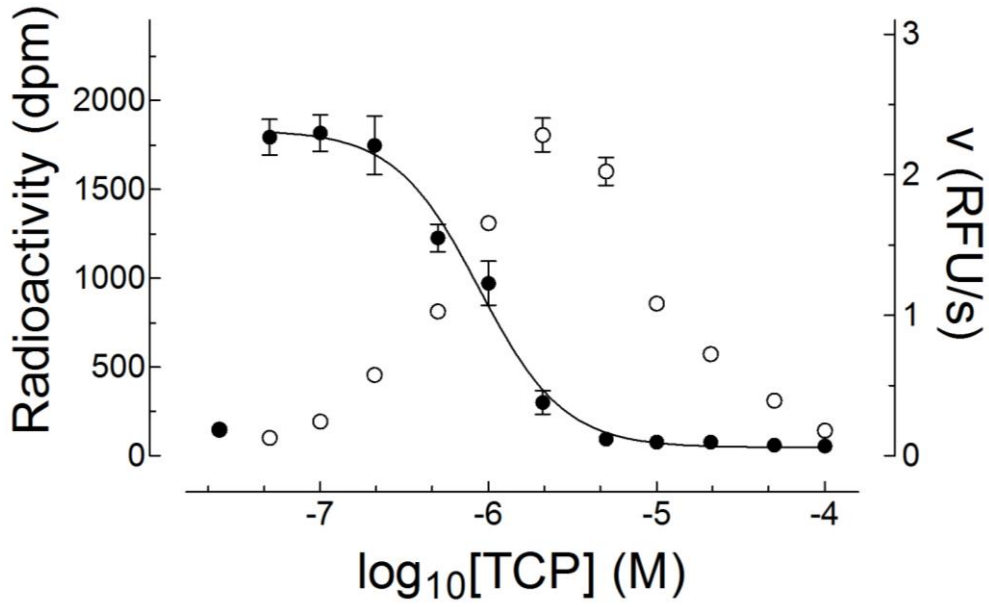

Figure 3.4.4.1 Potentiation of [^{3}H]2-BFI binding to WT-hMAO-B by TCP
Activity (●) and [^{3}H]2-BFI(○) binding to membrane-fractions of human monoamine oxidase following incubation with TCP for 30 minutes at room temperature. Error bars represent SEM.

Preincubation with TCP increased the specific binding of [^{3}H]2-BFI nearly 12-fold. The binding peak corresponds to nearly complete inhibition of activity, suggesting that occupation of the active site by TCP is responsible for the increase in binding. As indicated by Weist and Steinberg, the inhibition of [^{3}H]2-BFI binding by TCP appears to be irreversible.

There are two potential explanations for the results seen in Figure 3.4.4.1: 1) Binding may be increased by increasing the available number of binding sites (increasing B_{MAX}) or by 2) increasing the affinity of MAO-B for 2-BFI (decreasing K_D).

To investigate whether potentiation was a result of increasing B_{MAX} or decreasing K_D, MAO-B was preincubated with 20 μM TCP (peak of the potentiation) for 30 minutes at room temperature. Following the preincubation, the samples were washed by centrifugation (as described previously) and used in a binding assay to determine the affinity (K_D) of 2-BFI for the TCP-induced I_2 binding site.

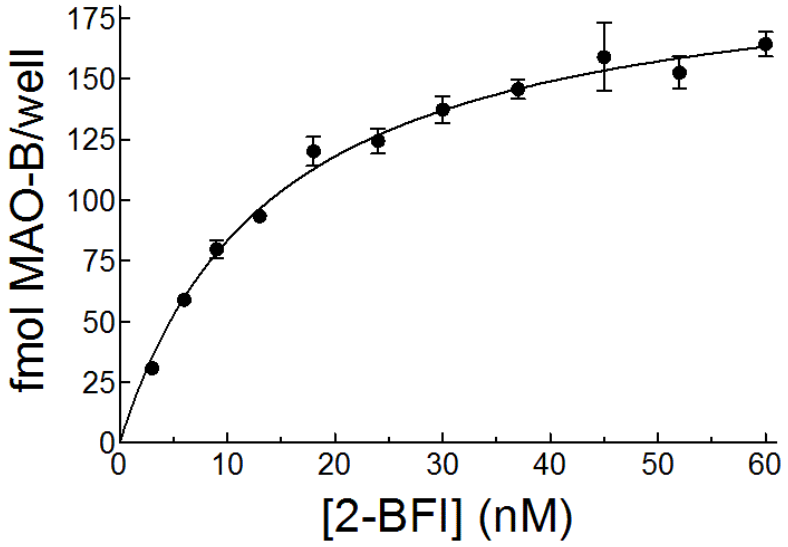

Figure 3.4.4.2 Binding of [³H]2-BFI to the TCP-induced I_2 site on WT-hMAO-B

Binding of [³H]2-BFI to human MAO-B following preincubation with TCP (20μM) for 30 minutes at room temperature. Samples were washed as described previously prior to inclusion in binding wells. The K_D was found to be 14±1 μM and B_{MAX} was found to be 210±6 fmol/well (450 pmol/mg protein).

The data clearly show that TCP potentiation is a result of increasing binding sites as B_{MAX} is increased nearly 161-fold. Interestingly, the K_D (14±1 μM) was found to be similar to the K_D seen in untreated enzyme (14±2 μM), suggesting that the site created by TCP is identical to the site created *in vivo*. The report by Weist and Steinberg, however, suggested that the induced I_2-site was not identical to the site occurring *in vivo* based on TCP's inability to potentiate the binding of idazoxan[83,86].

That TCP potentiates the binding of 2-BFI but not idazoxan suggests that the site is not identical to the site found *in vivo*. The experiments supporting such an idea were done in homogenates of human tissue and do not represent binding purely to MAO-B. To confirm that the site created by TCP is different than the *in vivo* site a competition binding assay was carried out using 5nM [^{3}H]2-BFI with and without preincubation with TCP.

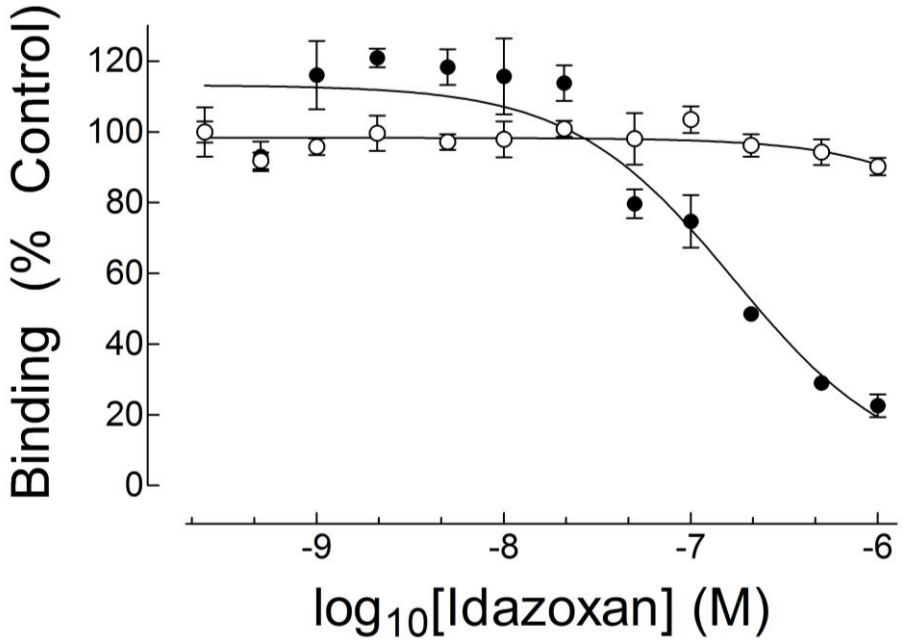

Figure 3.4.4.3 Displacement of [^{3}H]2-BFI from TCP-induced I_2 site on WT-hMAO-B by idazoxan
Inhibition of 5nM [^{3}H]2-BFI by idazoxan with (○)or without(●) pretreatment with 3.13 µM TCP for 30 minutes at room temperature. Data are expressed as percent control due to the potentiation caused TCP. Fits are the result of monophasic sigmoids with Hill-slope constrained to -1. IC_{50} values were found to be 170 nM and >1 µM for without and with TCP pretreatment, respectively. Error bars represent SEM.

In agreement with observations in the literature, there is a staggering difference between the two treatments. It should be noted that there is no accuracy in the IC_{50} value determined for idazoxan inhibition of [^{3}H]2-BFI binding to MAO-B following pretreatment with TCP because of the lack of definition of a curve.

The site formed by TCP differs in such a way that the deviations in structure between idazoxan and 2-BFI cause a massive difference in affinities at the *in vivo* site compared to the TCP site.

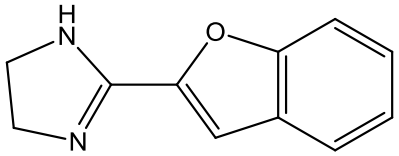

2-BFI

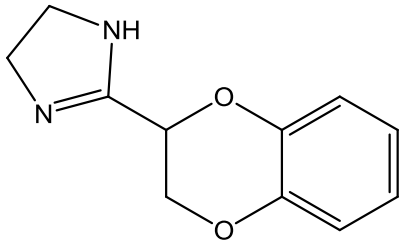

Idazoxan

Figure 3.4.4.4 Structures of 2-BFI and Idazoxan

The major difference between idazoxan and 2-BFI is the presence of an extra oxygen. 2-BFI is also significantly more rigid than idazoxan . Although mostly speculation, the I_2-site formed by tranylcypromine likely produces a relatively hydrophobic environment that cannot accommodate the extra oxygen on idazoxan.

Preliminary data from our lab suggested that benzylamine, phenylethylamine, dopamine and nonylamine are capable of displacing [^{3}H]2-BFI binding from the *in vivo* I_2-site. This is extremely interesting because the binding is occurring at values 50- to 100-fold lower than K_M values. To see if substrates continue to bind with high affinity to the TCP-induced site, MAO-B was preincubated with TCP and competition binding experiments were carried out with phenylethylamine and benzylamine.

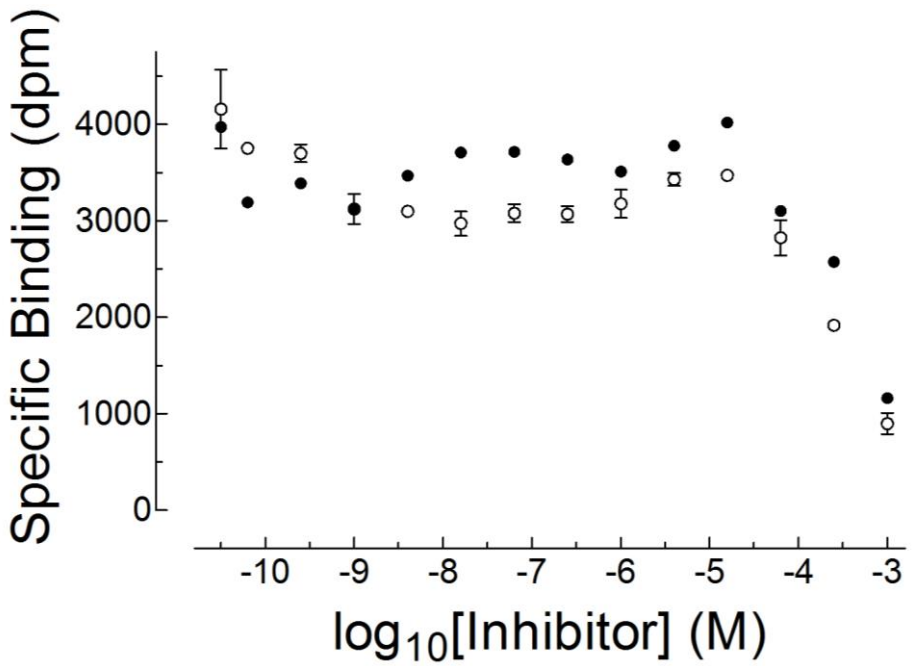

Figure 3.4.4.5 Displacement of [³H]2-BFI from the TCP induced site by phenylethylamine and benzylamine
Inhibition of 5 μM[³H]2-BFI binding by phenylethylamine(●) and benzylamine(○) following pretreatment of MAO-B with 3.2 μM TCP for 30 minutes. Error bars represent SEM.

The presence of TCP in the active site prevents the turnover of benzylamine and phenylethylamine. There may be some high affinity displacement of [³H]2-BFI by both benzylamine and phenylethylamine, corresponding to displacement from the *in vivo* site. The displacement of [³H]2-BFI at the inducible site appears to occur at similar benzylamine and phenylethylamine concentrations.

Benzylamine, phenylethylamine and idazoxan all displace [³H]2-BFI from an *in vivo* created site on MAO-B with greater affinity than on a TCP created site (data not shown). DiHEMDA, a competitive, reversible inhibitor of MAO-B activity was also tested in competition with [³H]2-BFI.

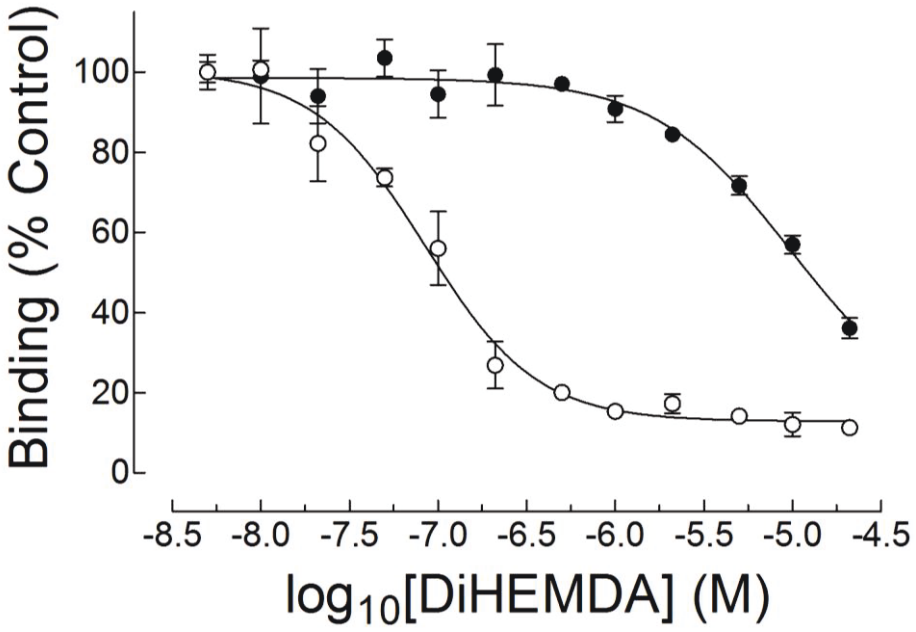

Figure 3.4.4.6 Displacement of [^{3}H]2-BFI from WT-hMAO-B by DiHEMDA

Inhibition of 5 nM [^{3}H]2-BFI binding to MAO-B in the presence of DiHEMDA following preincubation with (●) or without(○) TCP (3.13 µM). Non-linear regression was used to fit monophasic sigmoids with a Hill-slope of -1 to the data. IC_{50} values were found to be 84 nM and 9.6 µM for without and with TCP, respectively. Error bars represent SEM.

Without pre-treatment of MAO-B with TCP, DiHEMDA exhibits a nanomolar affinity similar to that of the substrates for displacing [^{3}H]2-BFI. Following pre-treatment with TCP, a massive shift occurs and an IC_{50} of 9.6 µM is obtained. The shifted IC_{50} value is remarkably similar to the K_{Iox} value obtained through kinetic assays and poses an interesting supposition. The structures of benzylamine, phenylethylamine and tranylcypromine are shown in Figure 3.4.4.7.

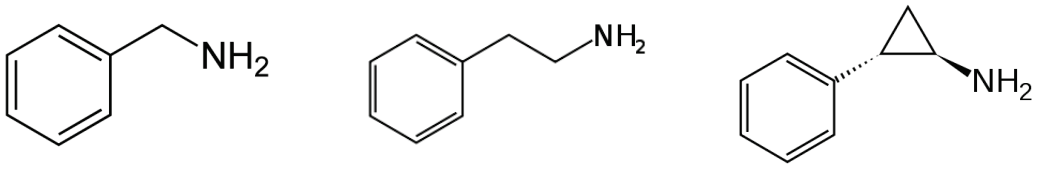

Benzylamine Phenylethylamine Tranylcypromine

Figure 3.4.4.7 Structures of benzylamine, phenylethylamine and tranylcypromine.

When in the substrate cavity, benzylamine, phenylethylamine and tranylcypromine are aligned such that the phenyl ring pushes out towards the entrance cavity. In the case of TCP and phenylethylamine, the distance between the phenyl ring and the entrance cavity is nearly identical, potentially contributing to a very similar binding pocket formation for each molecule. It may be possible that DiHEMDA binds to the induced site and causes inhibition without binding to the active site. The requirement of an ordered reaction (phenylethylamine entering before DiHEMDA can bind) would typically result in uncompetitive inhibition. In this situation, however, substrate appears to bind at the induced site as well, making the inhibition appear kinetically as competitive inhibition. For such a case to be considered, phenylethylamine must produce a site similar to that produced by tranylcypromine when bound to the active site.

To explore whether phenylethylamine is capable of producing an imidazoline site similar to the one created by TCP, two treatments of MAO-B were prepared. To prevent substrate turnover (and binding of substrate to the active site), MAO-B was incubated with 7 μM pargyline for 20 minutes at room temperature. A control was run concurrently with a 20-minute incubation using water in place of pargyline. Following the incubation, both pargyline and control treatments were pipetted into wells containing a range of phenylethylamine concentrations and incubated *on ice* to reduce substrate turnover in the control. The results are show in Figure 3.4.4.8.

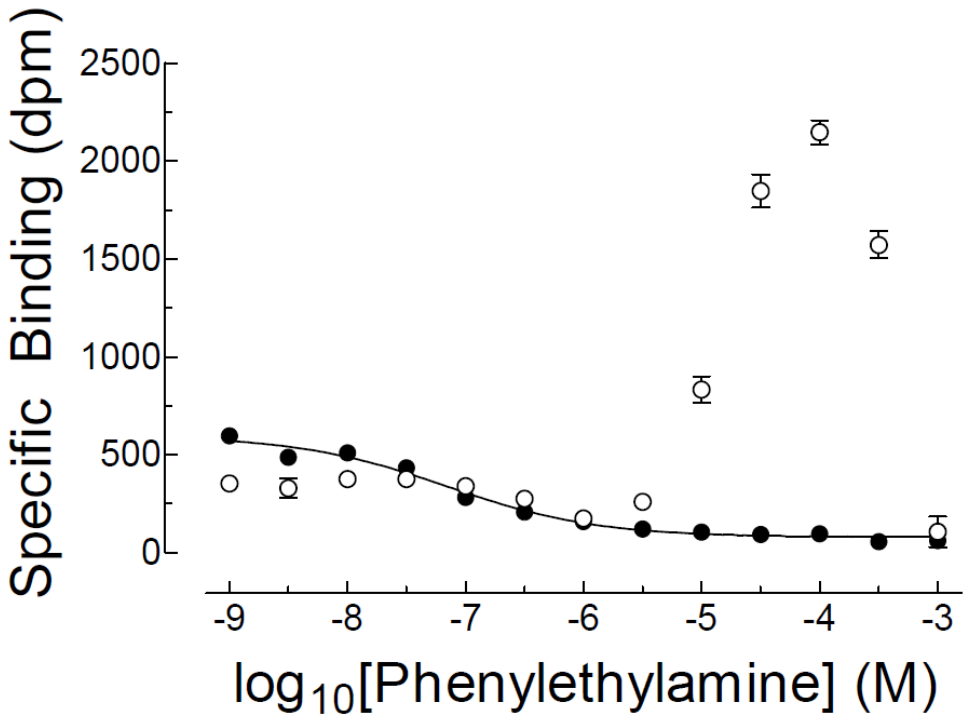

Figure 3.4.4.8 Phenylethylamine-induced I_2-site on WT-hMAO-B

Binding of 5 nM [^{3}H]2-BFI to human MAO-B in the presence of phenylethylamine with (●) and without (○) pargyline pretreatment. The pargyline treatment is fitted to a monophasic sigmoid, yielding an IC_{50} of 70nM. Error bars represent SEM.

Pretreatment with pargyline prevents the potentiation of [^{3}H]2-BFI by phenylethylamine, probably because occupation of the active site is required. There is a slight decrease from control in both treatment groups from the 1 nM to the 1 μM range, which is typical of phenylethylamine displacing [^{3}H]2-BFI from the *in vivo* produced binding site.

As an MAO-B substrate that is present *in vivo*, phenylethylamine could provide an explanation as to the formation of the I_2-site *in vivo*. Indeed, phenylethylamine appears to create a site that increases [^{3}H]2-BFI binding on MAO-B. To compare the similarity of the phenylethylamine-induced I_2-site to the *in vivo* and TCP-induced sites, a basic binding curve was produced to determine the K_D of [^{3}H]2-BFI to the

site. The site was induced with 100 µM phenylethylamine, with the binding occurring on ice to prevent extensive catabolism of substrate.

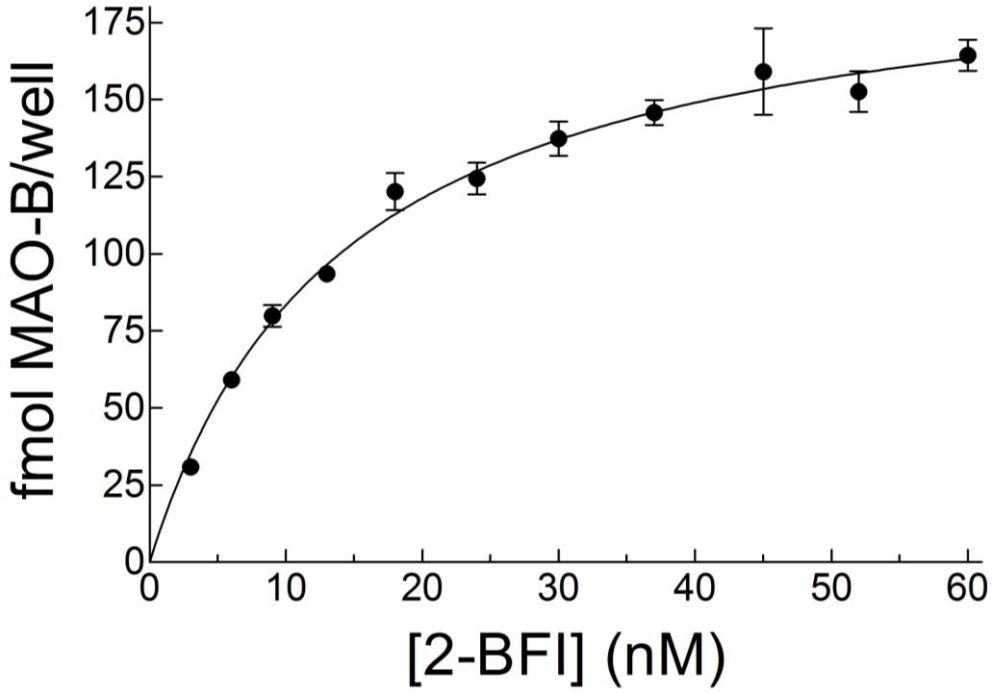

Figure 3.4.4.9 Binding of [^{3}H]2-BFI to the phenylethylamine-induced I_2-site on WT-hMAO-B
Binding of [^{3}H]2-BFI to MAO-B in the presence of 100 µM phenylethylamine. Non-linear regression determined K_D and B_{MAX} to be 33±12 nM and 540 fmol/well, respectively. Error bars represent SEM.

Although the data are not ideal, values produced are similar to the TCP-induced I_2-site, with a K_D of 33 and a B_{MAX} of 1200 pmol/µg protein. The B_{MAX} is a lot larger than the B_{MAX} found with TCP, although part of this can be explained by the variability in pipetting the membrane particle stock. The site also appears very similar to the *in vivo* created site.

The proposed idea of a substrate forming the I_2-binding site *in vivo* is complicated by the fact that the site could only exist when substrate is bound to the active site. The act of homogenising, washing and separating MAO-B from human tissue would dilute substrate to a negligible level, essentially eliminating the

presence of an I_2-binding site, yet binding assays consistently show a 10-15% fraction of MAO-B possessing an I_2-site. This can be explained by an interesting property of phenylethylamine kinetics, discussed in Section 3.4.5

3.4.5 Formation of I_2-Site by Phenylethylamine

During kinetic assays, it was observed that a continuous reading of a given concentration of phenylethylamine did not stay linear for as long as it should (i.e. before substrate has depleted enough to reduce the rate). This has been observed by other laboratories in the past[111]. Even odder was the observation that increasing the concentration of phenylethylamine increases the rate of "curving off".

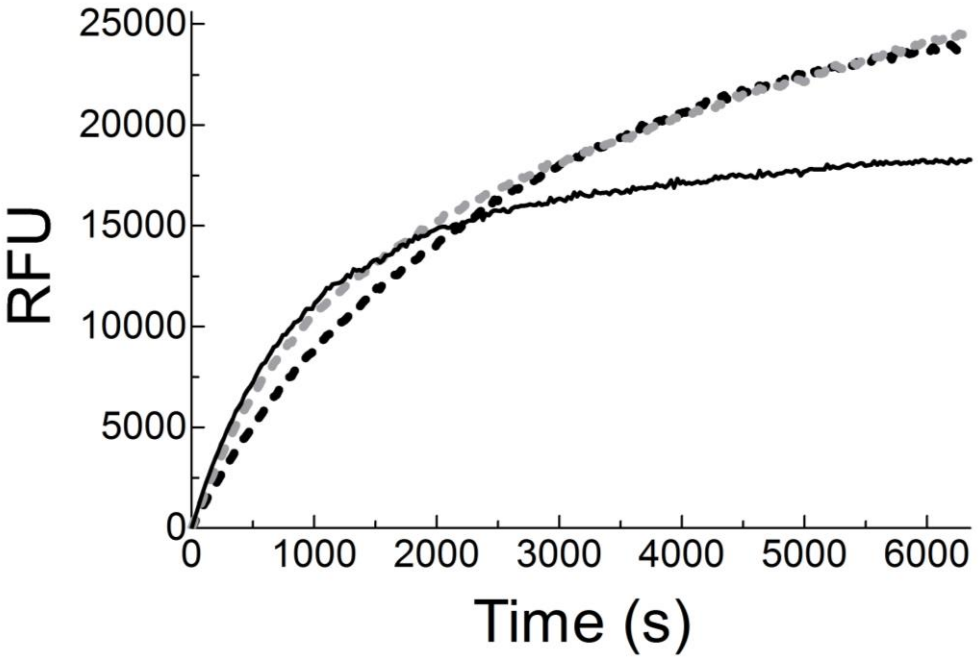

Figure 3.4.5.1 Inactivation of hMAO-B by the presence of phenylethylamine
Formation of product by MAO-B in the presence of 10(black dashed line), 100(grey dashed line) and 1000(solid line) μM phenylethylamine.

Figure 3.4.5.1 shows the concentration dependent "curving off" displayed by phenylethylamine. The black dashed line represents a 10 μM phenylethylamine. The possibility of substrate depletion or product inhibition as a reason for these results were considered. If substrate depletion was occurring, linearity should be observed for a longer period of time. That higher concentrations of phenylethylamine results in a greater rate of "curving off" is also surprising.

To investigate product inhibition and the reversibility of the curving phenomenon, enzyme was incubated with phenylethylamine or water and the reaction allowed to proceed until inhibition had occurred. The samples were spun down in a centrifuge at 5,000 rcf for 5 minutes and the supernatant poured off. Buffer was then added and the enzyme pellet was suspended. This procedure was repeated another two times to ensure phenylethylamine had been removed. The activity of the phenylethylamine-incubated enzyme across five concentrations of phenylethylamine (0, 15, 45, and 90 μM) was consistently lower than the control enzyme incubated with only water.

Based on this result, some irreversible change appears to occur when the enzyme catabolises phenylethylamine At this point it was unclear whether the change was something in the enzyme or phenylethylamine was creating an irreversible adduct. If the irreversible inhibition was a result of adduct formation, the difference may be large enough to see on mass spectrometry analysis. Two samples were sent to Dr. Randy Whittal (Department of Chemistry) for analysis: purified hMAO-B preincubated for 2 hours with either water or 20mM phenylethylamine. Both samples were then washed by centrifugation (at 5,000 rcf

for 5 minutes) and re-suspended three times prior to submission. The result obtained from MALDI-TOF mass spectrometric analysis indicated that the preincubated enzyme had a mass of 167 Da greater than the mass of control enzyme. Although this does not correspond precisely to the mass of phenylethylamine (120 Da), it does indicate that some type of adduct is formed in the catabolism of phenylethylamine.

To investigate the formation of an I_2-site by the irreversible inhibition, 2 mM phenylethylamine was incubated with MAO-B for one hour, washed via centrifugation and re-suspension, and then used in a [^{3}H]2-BFI binding assay to determine a K_D.

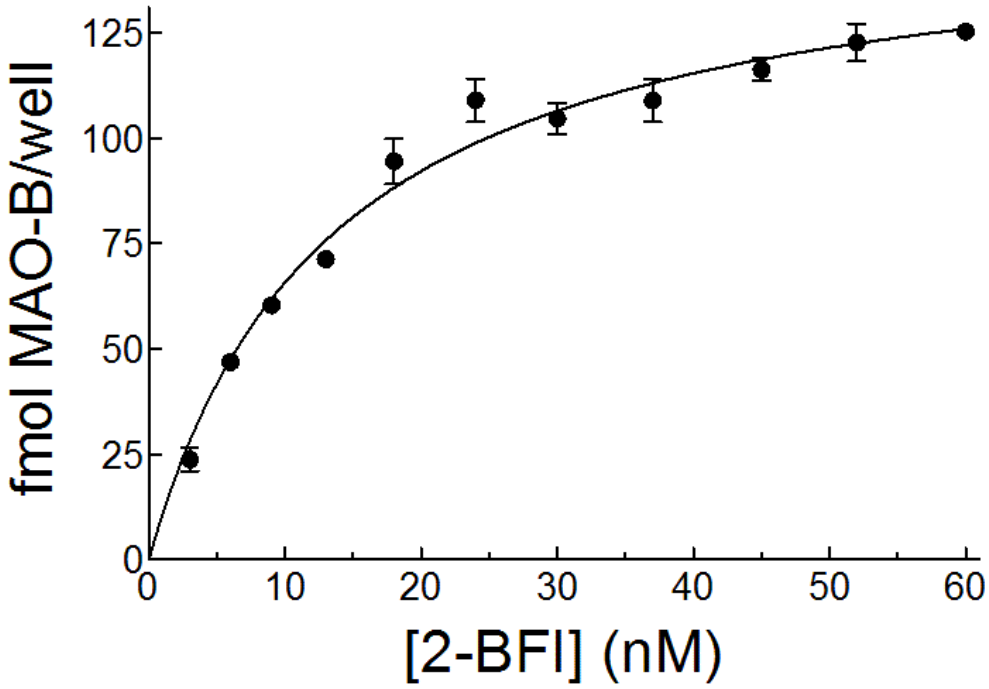

Figure 3.4.5.2 Binding of [^{3}H]2-BFI to the phenylethylamine-induced I_2-site on WT-hMAO-B
Binding of [^{3}H]2-BFI to MAO-B following a one hour preincubation with 2 mM phenylethylamine(n=3). K_D and B_{MAX} were determined to be 13±1 nM and 150±5 fmol/well, respectively, from non-linear regression. Error bars represent SEM.

The data in Figure 3.4.5.4 show a binding curve with a K_D of 13±1 nM and B_{MAX} comparable to the value seen with TCP. This confirms that substrate creates an I_2-site irreversibly. The mechanism of site formation has since been confirmed by crystal structures[64]. This also explains why kinetic assays do not show inhibition of activity at nanomolar concentrations: the 2-BFI binding site is on non-functional enzyme, presumably with an active site occupied by a ligand responsible for forming the I_2 site, which does not contribute a velocity in activity assays.

A possible explanation for why increasing phenylethylamine concentration increases the rate of curving off, and thus adduct formation, can be explored using the structural basis of MAO-B. If phenylethylamine enters the active site and interacts with the flavin, the presence of the substrate in the active site may cause a change in conformation in the entrance cavity (via closing the Ile199 gate), creating a transient I_2-site. At high concentrations of phenylethylamine (in excess of 100 μM), the probability of phenylethylamine binding to this transient site *increases* (as shown by Figure 3.4.4.8), blocking the exit of imine from the active site. This would increase the chance of the imine forming an adduct within the active site, increasing the rigidity of the enzyme in the "closed" gate conformation (see Figure 3.4.5.3).

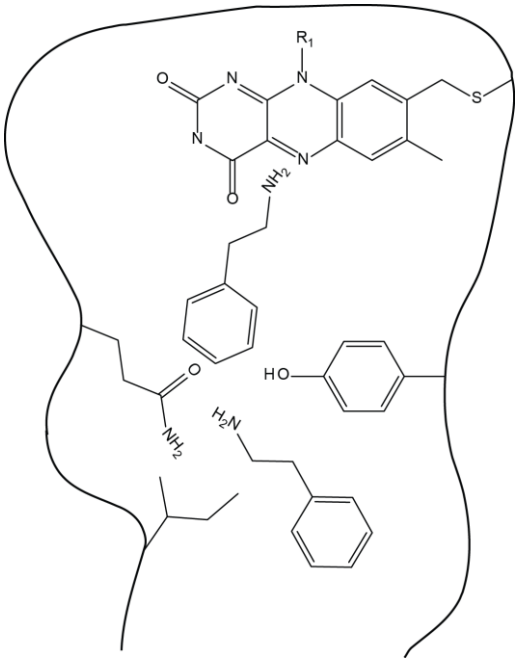

Figure 3.4.5.3 Binding of Two Phenylethylamine Molecules
At high concentrations, phenylethylamine is able to bind within the entrance cavity when during a transient conformation that has the Ile199 and Gln206 gate closed.

The proposition of a transient state being created by phenylethylamine provides a new explanation for both nanomolar binding of [^{3}H]2-BFI to MAO-B and the micromolar concentrations required to inhibit MAO-B activity. Kinetic assays rely on active enzyme to derive parameters for inhibitors, while the high affinity site appears to be expressed on only *non-functional enzyme*.

The concept of a transient binding pocket being formed by MAO-B when phenylethylamine is substrate can be applied to 2-BFI to help verify the concept. The image in Figure 3.4.5.4 shows the transient state binding site being created by phenylethylamine with 2-BFI binding within the pocket. If this transient state is similar to the high-affinity site on MAO-B seen in binding experiments, we would expect to see 2-BFI affect the rate of curving off at nanomolar concentrations. To

determine this, 20 μM phenylethylamine was followed in the spectrophotometer in the presence of a range of 2-BFI concentrations (Figure 3.4.5.5).

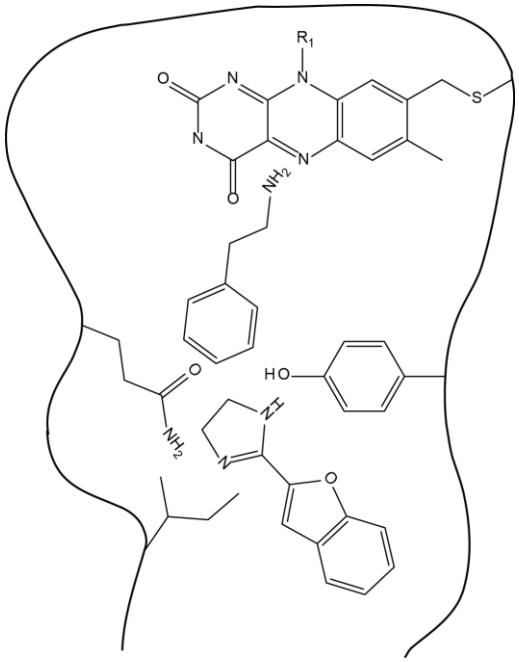

Figure 3.4.5.4 Formation of a Transient State with 2-BFI binding
Binding of phenylethylamine in the substrate-binding site may lead to transient changes in the entrance cavity that allow 2-BFI to bind with high affinity.

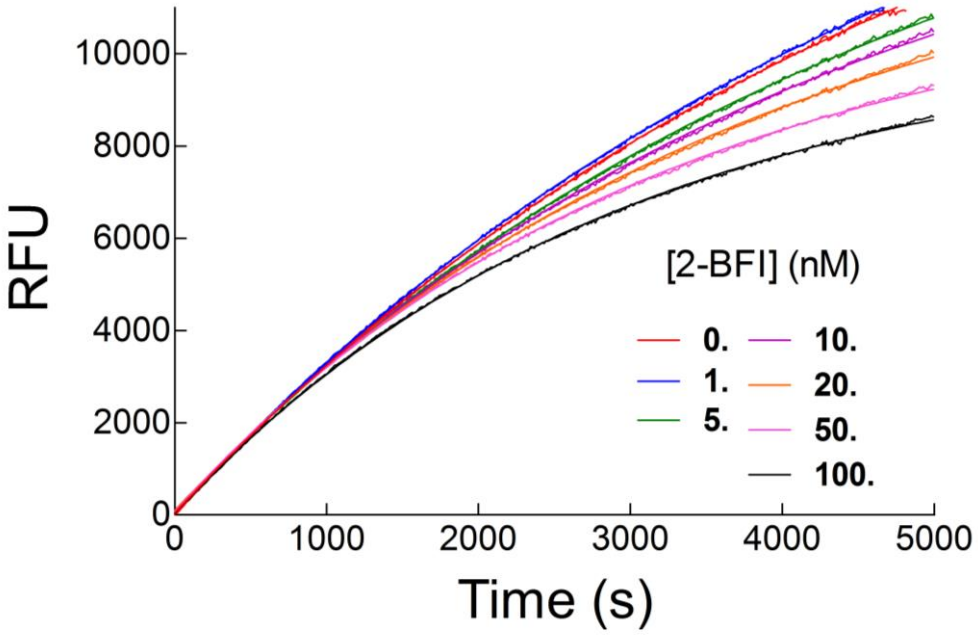

Figure 3.4.5.5 Phenylethylamine inhibition attenuated by 2-BFI
Product formation from the oxidation of 20 µM phenylethylamine versus time (0-5000 seconds) in the presence of 0, 1, 5, 10, 20, 50, and 100 nM 2-BFI (n=1).

20 µM phenylethylamine was used because it was found to be the K_{Mox} value (from kinetic experiments) and it curves off relatively slowly. The curves all start with an identical rate, with the lowest concentrations of 2-BFI present remaining the closest to linear, clearly showing an effect of 2-BFI on MAO-B function in the *nanomolar* range.

To quantify the degree of curving off caused by 2-BFI, the results in Figure 3.4.5.5 were fitted to a one-phase exponential equation, from which the half-life can be determined. Binding of 2-BFI to a transient state could increase the likelihood of irreversible inhibition occurring, thus causing 2-BFI's "effect" to be a change in half-life. Since an increase in 2-BFI effect results in a decreased half-life, the inverse of half-life (Tau) transforms the data to be a positive result relative to 2-BFI

concentrations. Plotting Tau versus concentration of 2-BFI (after correcting for baseline curving) yields the hyperbolic curve presented in Figure 3.4.5.6.

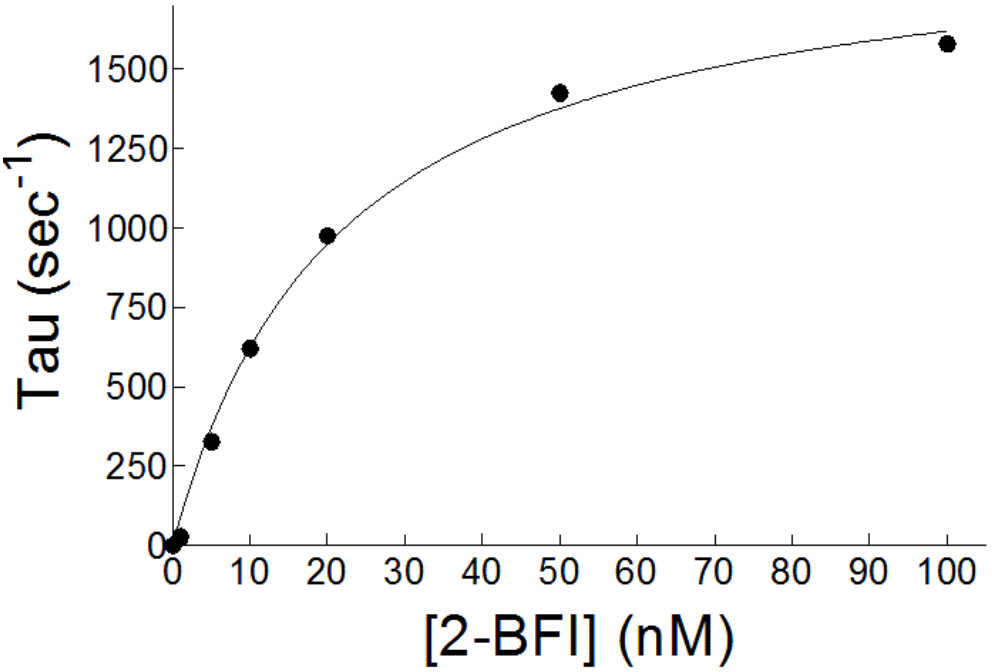

Figure 3.4.5.6 Concentration dependence of 2-BFI attenuated phenylethylamine inhibition
Transformation and re-plot of the half-life values obtained in Figure 3.4.5.5. Data are fitted to a single site hyperbola and yield a K_D value of 20±2 nM and a B_{MAX} of 2000 ±76 sec^{-1}.

Fitted to a single site hyperbola, the K_D for 2-BFI binding to and accelerating the rate of time-dependent inhibition of phenylethylamine turnover is 21±2 nM. This is extremely well aligned with the value obtained from binding studies involving permanent site formation.

To confirm that the curving off seen in the presence of 2-BFI is related to the formation of the permanent I_2-site, a binding experiment involving preincubation with substrate, 2-BFI, and substrate plus 2-BFI was conducted. The inclusion of 2-BFI with phenylethylamine should increase the number of [^{3}H]2-BFI sites forming on MAO-B at a greater rate than phenylethylamine alone.

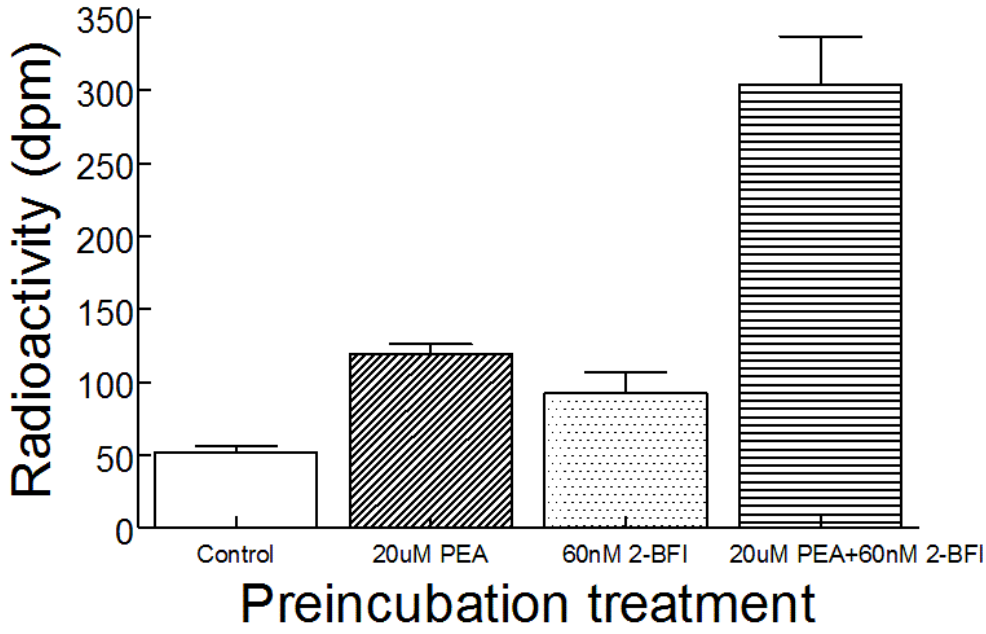

Figure 3.4.5.7 Potentiation of phenylethylamine-induced I_2-site by 2-BFI (RM1-165)

Binding of 5 nM [^{3}H]2-BFI following treatment with water (control), 20 µM phenylethylamine (PEA), 60 nM 2-BFI, and both 20 µM and 60 nM 2-BFI for one hour. Samples were then washed as described previously. Error bars represent SEM (n=7).

Preincubation of enzyme with 20 µM phenylethylamine and 60 nM 2-BFI produced more binding sites for [^{3}H]2-BFI than 20 µM phenylethylamine alone, supporting the idea that 2-BFI binds to a transient 2-BFI binding site, preventing the substrate from leaving, and increasing the likelihood of irreversible inhibition from occurring. Figure 3.4.5.7 shows that phenylethylamine is *required* for formation of the I_2-site and that 2-BFI alone does not form an I_2-site.

3.5 Implications of phenylethylamine-formed I_2-Site

Physiological function of the I_2-site is speculation at this point; however, it is possible that the I_2-site plays an important role in MAO-B regulation. It is possible that the I_2-site is a surrogate marker that substrate-based inhibition has occurred and the site itself has no physiological role. That the rate of formation of an I_2-site is related to the presence of 2-BFI at nanomolar concentrations suggests that the I_2-site does has some functional utility beyond being a marker on non-functional enzyme. The ability of phenylethylamine, an endogenous substrate, to inhibit irreversibly MAO-B in a concentration-dependent manner while simultaneously creating a non-classical I_2-site suggests that MAO-B may have the ability to be regulated based on relative concentrations of substrate in the cell. That approximately 5-20% of MAO-B from *in vivo* studies possess a high-affinity site suggests that this mechanism does play a role physiologically. Integration of multiple substrates and their concentrations is supported by data suggesting that the proportion of I_2-sites present depends on the location of the tissue sample. Binding of idazoxan to the *in vivo* site occurs at lower concentrations than in the PEA-generated site, suggesting that phenylethylamine is not the substrate involved in the formation of the site *in vivo*, and thus is unlikely to be involved in MAO-B substrate regulation (if such regulation occurs).

The idea of MAO-B as an important, highly regulated enzyme will hopefully spark new interest in MAO-B as a therapeutic target. Understanding the role and reason for suicide-inhibition with certain substrates may lead to the development of inhibitors that selectively inhibit MAO-B based on the substrates present. Such

inhibitors would allow inhibition of activity within certain tissues selectively over other tissues, allowing for very precise changes in physiology. Such selectivity is at the heart of pharmacology research and unleashes the imagination to what could be accomplished in future drug development.

4 Chapter 4: Novel inhibition of MAO-B activity

4.1 Background

The inhibition of MAO-B by competitive inhibitors was discussed previously in Section 2.7. Two published inhibitors of MAO-B, however, appear to have completely unique modes of inhibition: oleamide and 2-BFI.

Inhibition of MAO-B substrate catabolism by oleamide appears completely non-competitive in inhibitor plots. This unique presentation makes it an extremely interesting inhibitor.

2-BFI, which binds to a fraction of MAO-B in binding studies at extremely low concentrations, fails to provide inhibition of MAO-B at similar concentrations. While the reason for this has been explained in Section 3.4.5, the expected kinetic outcome has yet to be explored. It is possible that 2-BFI, at high concentrations, binds to the active site of MAO-B to yield inhibition, thus changing the apparent K_M for substrate. We also know, however, that 2-BFI binds inside the entrance cavity with high affinity when phenylethylamine is substrate, although binding to the high affinity site itself does not yield significant inhibition of initial rates. It is possible that 2-BFI binds to the entrance channel, albeit at higher concentrations than seen with the high-affinity site, thus decreasing the V_{MAX} value. Inhibition in this pattern (increase in K_M and decrease in V_{MAX}) would fit a mixed-model of inhibition.

In this section, the mechanism of inhibition by oleamide and 2-BFI are explored using the same principles described in Section 2.

4.2 Inhibition of MAO-B by Oleamide

4.2.1 Materials and Methods

For all experiments in this section, the activities of purified preparations or membrane fractions from *P. pastoris* yeast were measured continuously in 96-well plates with a SpectraMax Gemini XPS microplate reader by following the fluorescence related to the peroxidase-coupled formation of resorufin from AmplexRed[102]. Each reaction was run at 30°C in a total volume of 200 µL. Amine substrate was prepared on the day of the experiment using colourless Eppendorf™ micocentrifuge tubes for the dilutions. Inhibitor solutions were made in an identical manner. All dilutions were done in water, with the exception of oleamide dilutions which were done with less than 1% DMSO in the well during activity assays. Use of DMSO was necessary to solubilize oleamide.

The MAO-B/AmplexRed™/peroxidase solution was prepared by diluting MAO-B from a batch stock into a solution of 100 mM HEPES buffer and mixing this solution 1:1 with an AmplexRed™/peroxidase solution made up at four-times the concentration required for the experiment. The MAO-B/AmplexRed™/peroxidase solution was prepared to be used in entirety for a single experiment and was made fresh each time. During experiments involving more than one plate, enzyme was stored in the fridge until it was required in the experiment.

Plates were warmed to 30˚C prior to commencing the experiment. Assays were started by rapid addition of enzyme/AmplexRed mixture using an 8-channel pipette.

Experiments were carried out under atmospheric oxygen unless otherwise stated. When experiments were done under high and low oxygen, a positive pressure of either pure oxygen or carbon dioxide was supplied to a plastic box surrounding the SpectraMax plate reader. Pre-pipetted plates excluding enzyme were pre-incubated within this box for 20 minutes prior to addition of enzyme. The concentration of oxygen was determined through measurement with a dissolved oxygen meter.

Initial (pseudolinear) rates of product formation were determined by linear regression (SoftMax Pro v. 4.8) and were fitted to equations via the nonlinear regression function of GraphPad Prism v. 5.0c for Windows (GraphPad Software Inc., San Diego, CA).

4.2.2 Non-linear Regression to fit Models to Data

All curve fitting was carried out using the non-linear regression functionality of GraphPad Prism 5.0 (GraphPad Software Inc., San Diego, CA). For single-site hyperbola models (standard Michaelis-Menten kinetics) and sigmoidal inhibitor plots, the standard equations supplied with Prism 5 are used. These equations are:

$$Y = Vmax * X/(K_M + X)$$

For non-linear regression of single-site hyperbolas

$$Y = Bottom + (Top - Bottom)/(1 + 10^{\{LogEC_{50} - X\}})$$

For non-linear regression of sigmoidal plots

4.2.3 Determination of kinetic parameters for oleamide

Studies of the leachates from plastic led to a second discovery of a novel, potent MAO-B inhibitor: oleamide[106]. As a lipophilic substance, oleamide is somewhat difficult to work with. Specifically, the concentration of oleamide could not exceed approximately 300 μM in 1.4% DMSO, otherwise oleamide would precipitate out of solution. In all experiments using DMSO, appropriate controls were done and the amount of DMSO used was the minimum required to get the highest concentration into a solution four-fold greater than required in the well. In all cases, DMSO concentrations were kept below 1% in the reaction vessel.

Preliminary data for inhibition of substrate produced some very exciting results. Inhibitor plots were *partial* and a 30-fold increase in amine substrate concentration resulted in only a small shift in IC_{50} values. The inhibition appeared to be very potent and *non-competitive* with amine substrate.

Characterisation of oleamide as an inhibitor began with sigmoidal plots performed under 100 μM and 500 μM oxygen, shown in Figure 4.2.3.1 and Figure 4.2.3.2, respectively.

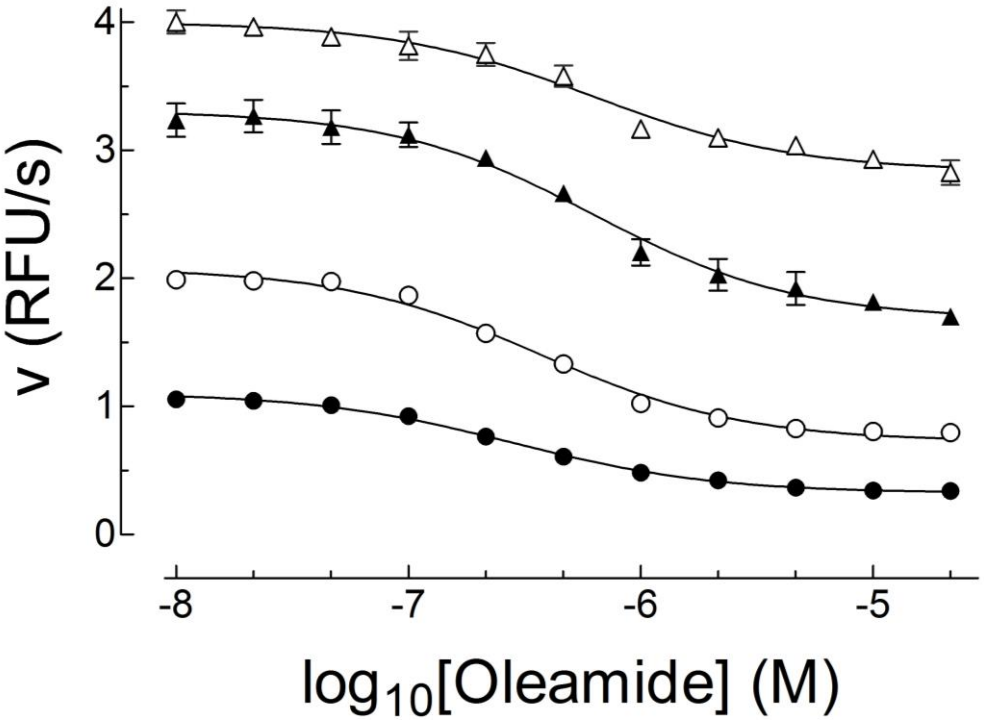

Figure 4.2.3.1 Inhibitor plots of oleamide versus phenylethylamine under low oxygen

Oxidation of 2(●), 6(○), 20(▲) and 60(△) μM phenylethylamine under 100 μM oxygen by hMAO-B (1 nM) in the presence of oleamide (n=2) fitted to a monophasic sigmoid where the Hill-slope was constrained to -1 and the bottom was allowed to fluctuate. Reported IC_{50} values for 2, 6, 20 and 60 μM phenylethylamine were 0.28, 0.37, 0.62 and 0.63 μM, respectively. Error bars represent SEM.

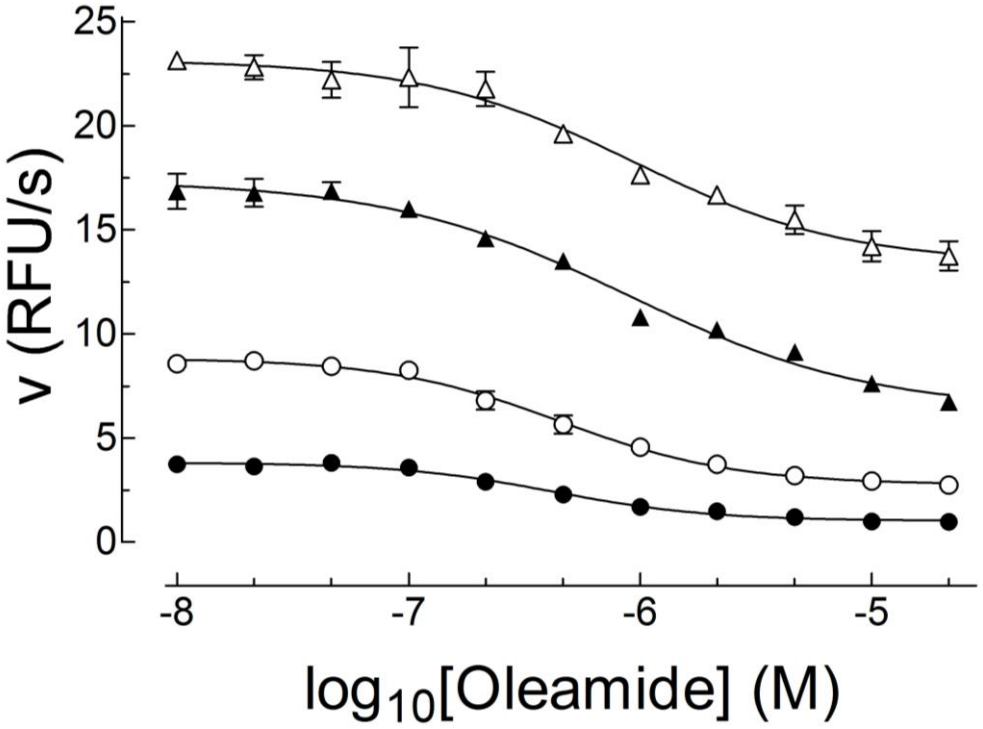

Figure 4.2.3.2 Inhibitor plots of oleamide versus phenylethylamine under high oxygen

Oxidation of 2(●), 6(○), 20(▲) and 60(△) μM phenylethylamine by hMAO-B (1 nM) under 500 μM oxygen in the presence of oleamide (n=2) fitted to a monophasic sigmoid where the Hill-slope was constrained to -1 and the bottom was allowed to fluctuate. Reported IC_{50} values for 2, 6, 20 and 60 μM phenylethylamine were 0.42, 0.45, 0.89 and 0.93 μM, respectively. Error bars represent SEM.

Two observations jump out initially: 1) The sigmoids do not appear to shift markedly to the right with the increase in phenylethylamine concentrations and 2) increasing oxygen concentration increases the ability of oleamide to inhibit phenylethylamine catabolism.

The most plausible explanation of the results, although they do appear to suggest non-competitive inhibition, is that oleamide binds to only one form of the enzyme in the range of concentrations used. The increased inhibition by oleamide in relation to the increase in oxygen suggests that $E.FAD_{ox}$ is the preferred form. This is consistent with all substrates and inhibitors investigated so far, where affinity for $E.FAD_{ox}$ is greater than the affinity for $E.FAD_{red.}$

Results from the non-linear regression obtained from Figure 4.2.3.1 and Figure 4.2.3.2 are tabulated in Table 4.2.1 for easy reference. These numbers are used to probe further into the mechanism of phenylethylamine turnover inhibition by oleamide. It should be noted that had oleamide been conducive to the use of higher concentrations, the range of concentrations tested would have been increased to attempt to see a second phase of inhibition.

Low Oxygen					
[Phenylethylamine] (μM)	IC_{50} μM	K_I μM	Top (RFU/s)	Bottom (RFU/s)	Fraction Inhibited
2	0.300	0.27	1.106	0.323	0.71
6	0.370	0.28	2.079	0.726	0.65
20	0.605	0.29	3.308	1.682	0.49
60	0.625	0.15	4.000	2.835	0.29
High Oxygen					
[Phenylethylamine] (μM)	IC_{50} μM	K_I μM	Top (RFU/s)	Bottom (RFU/s)	Fraction Inhibited
2	0.422	0.38	3.82	1.02	0.73
6	0.492	0.37	8.83	2.77	0.69
20	0.890	0.43	17.36	6.33	0.64
60	0.932	0.22	23.14	13.40	0.42

Table 4.2.1 Kinetic Parameters for Oleamide versus Phenyethylamine

Calculation of K_I values from IC_{50} values were done using the Cheng-Prusoff equation. The K_M value was set to 19 μM. The inhibition fraction describes the amount of inhibition caused by oleamide and is calculated using the equation (Top-Bottom)/Top.

Interpretation of the numbers presented in Table 4.2.1 requires some thought about the current model of phenylethylamine turnover by MAO-B. The Cheng-Prusoff equation is designed to convert IC_{50} to K_I in a one-site system, and cannot be expected to convert over directly to a two-site system. The 2 μM phenylethylamine sigmoid under low oxygen (94 μM) shows a maximum of 71% inhibition by oleamide. At this concentration, the majority of the turnover would be through V_{MAXox}. To confirm if this result makes sense with the model, the Michaelis-

Menten equation can be used to calculate the expected individual fractions of $E.FAD_{ox}$ and $E.FAD_{red}$ based on values obtained from previous experiments

To calculate the contribution of the $E.FAD_{ox}$ pathway, a V_{MAX} of 1 (relative units) and a K_{Mox} of 20 μM are used. The parameters for the K_{Mred} $E.FAD_{red}$ are 42 and V_{MAX} of 1 in relative units (based on V_{MAXred}/V_{MAXox} from Table 2.8.1).

Michaelis-Menten Equation $$v = \frac{V_{max}[S]}{K_M + [S]} \quad \text{Eq. 2.15}$$

$E.FAD_{ox}$ Contribution $$v = \frac{1[2\mu M]}{20\ \mu M + [2\mu M]} = 0.090 \quad \text{Eq. 2.16}$$

$E.FAD_{red}$ Contribution $$v = \frac{1.1[2\mu M]}{42\ \mu M + [2\mu M]} = 0.045 \quad \text{Eq. 2.17}$$

$E.FAD_{ox}$ Fraction $$F = \frac{0.090}{0.090 + 0.045} = 0.67 \quad \text{Eq. 2.18}$$

This simple calculation shows that at 2μM phenylethylamine approximately 67% of the activity comes from the $E.FAD_{ox}$ pathway, a result matching very closely with the observations listed in Table 4.2.1 for the high oxygen column. Replicate calculations for 6, 20, 60 μM phenylethylamine yields $E.FAD_{ox}$ fractions of 0.65, 0.61, and 0.56, respectively. This matches extremely well with the values for high oxygen except for the 60 μM phenylethylamine value of 0.56 (which is 0.42 in Table 4.2.1). The incongruent decrease in the observed value is likely due to the greater flux through $E.FAD_{red}$, which begins to occur *at the expense* of flux through $E.FAD_{ox}$. Such an occurrence is expected when substrate concentration approaches and exceeds K_{Mred}.

The change in flux concept is supported further by the low oxygen data wherein the rate of change in the fraction of inhibition by oleamide is greater than predicted. In a low-oxygen environment, the rate of oxidation for reduced enzyme is decreased, thus increasing the likelihood of the reduced form of the enzyme existing. As phenylethylamine concentrations are increased, a far greater percentage of the overall turnover goes through the $E.FAD_{red}$ pathway than under atmospheric or high-oxygen conditions. In other words, reducing the oxygen content in the presence of phenylethylamine reduces the likelihood of oxidised enzyme existing, in turn leading to a smaller fraction of catalysis available to be inhibited by oleamide.

This phenomenon also appears in the conversion of IC_{50} to K_I for the oleamide data. As shown in Table 4.2.1, the calculated K_I values for oleamide are approximately 0.28 and 0.40 μM for low oxygen and high oxygen, respectively. At 60 μM phenylethylamine, the calculated K_I drops to 0.15 and 0.22 μM. The major fault in calculating the K_I from IC_{50} in this case is that the Cheng-Prusoff equation is only for a one-site model. Consider that, in essence, flux through $E.FAD_{red}$ *inhibits* $E.FAD_{ox}$. The Cheng-Prusoff equation attributes this inhibition to the inhibitor, resulting in the inhibitor appearing more potent than it is.

There are consequences to phenylethylamine decreasing the apparent K_I value as the proportion of reduced enzyme increase. At a given substrate concentration under conditions of low oxygen, K_I should be underestimated to a greater degree than under conditions of high oxygen. This is because under low-oxygen, more enzyme is in the reduced form compared to a high-oxygen environment. It is also

expected that as concentrations of substrate increase, the K_I of oleamide as calculated by the Chung-Prusoff equation for inhibition at $E.FAD_{ox}$ will decrease.

Numerous iterations of analysis point to oleamide being a competitive inhibitor of substrate at $E.FAD_{ox}$ but not at $E.FAD_{red}$. This unique property provides the opportunity to investigate the more complicated kinetics of benzylamine oxidation.

Unlike phenylethylamine, the reductive half-reaction (the transfer of a proton from substrate to flavin) of amine bond breakage is the rate limiting step for benzylamine (rather than flavin oxidation)[97]. The consequence of this is that more enzyme exists in the oxidised form during steady state than with phenylethylamine. It is expected that oleamide will produce inhibition of benzylamine turnover that looks very similar to the inhibition of phenylethylamine turnover. The one expected difference between the two substrates when inhibited by oleamide is that flux through the oxidised form of the enzyme when benzylamine is substrate should be less affected by oxygen than phenylethylamine. A large reason for this is the relative increase in K_M for oxygen when phenylethylamine is substrate[97]. Therefore, the flux through $E.FAD_{red}$-S is more dependent on oxygen concentration when phenylethylamine is substrate. Benzylamine flux through $E.FAD_{red}$-S, with its relatively high K_{Mred}:K_{Mox} ratio, is more substrate-dependent.

In sigmoidal plots, this will appear as IC_{50} values that are relatively consistent until concentrations of substrate become high enough to increase flux through $E.FAD_{red}$-S. At such a point, it is expected that oleamide will cause less inhibition of amine turnover under low-oxygen than high-oxygen.

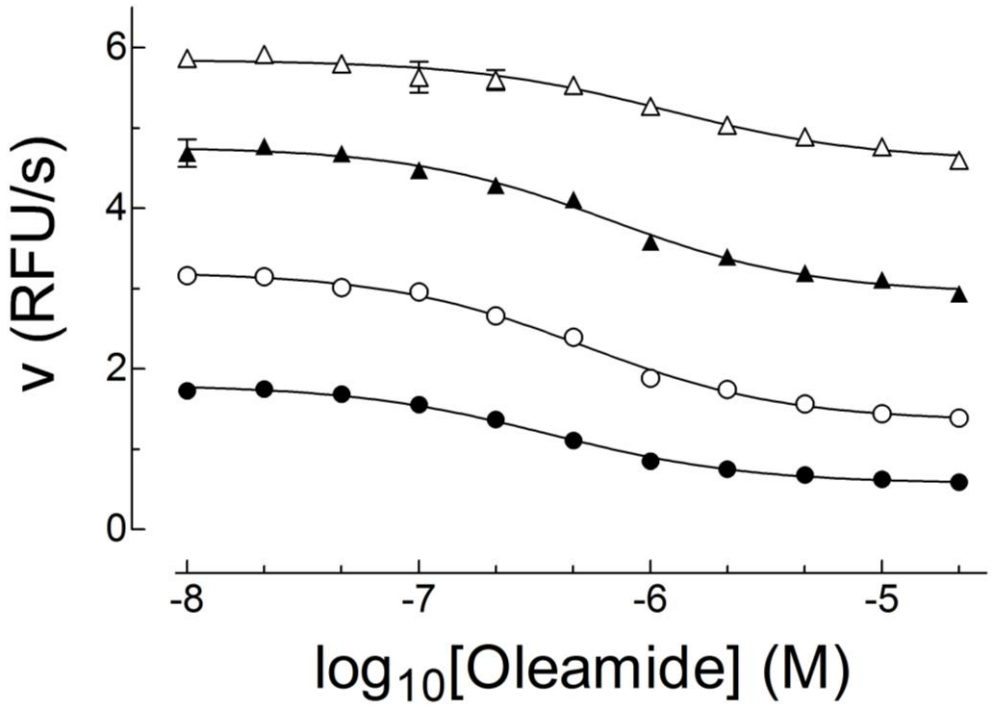

Figure 4.2.3.3 Inhibitor plots of oleamide versus benzylamine under low oxygen

Oxidation of 50(●), 150(○), 500(▲) and 1500(△) μM benzylamine by hMAO-B (1 nM) under 100 μM oxygen in the presence of oleamide (n=2) fitted to a monophasic sigmoid where the Hill-slope was constrained to -1 and the bottom was allowed to fluctuate. Reported IC_{50} values for oleamide at concentrations of 50, 150, 500 and 1500 μM benzylamine were 0.36, 0.52, 0.67 and 1.18 μM, respectively. Error bars represent SEM.

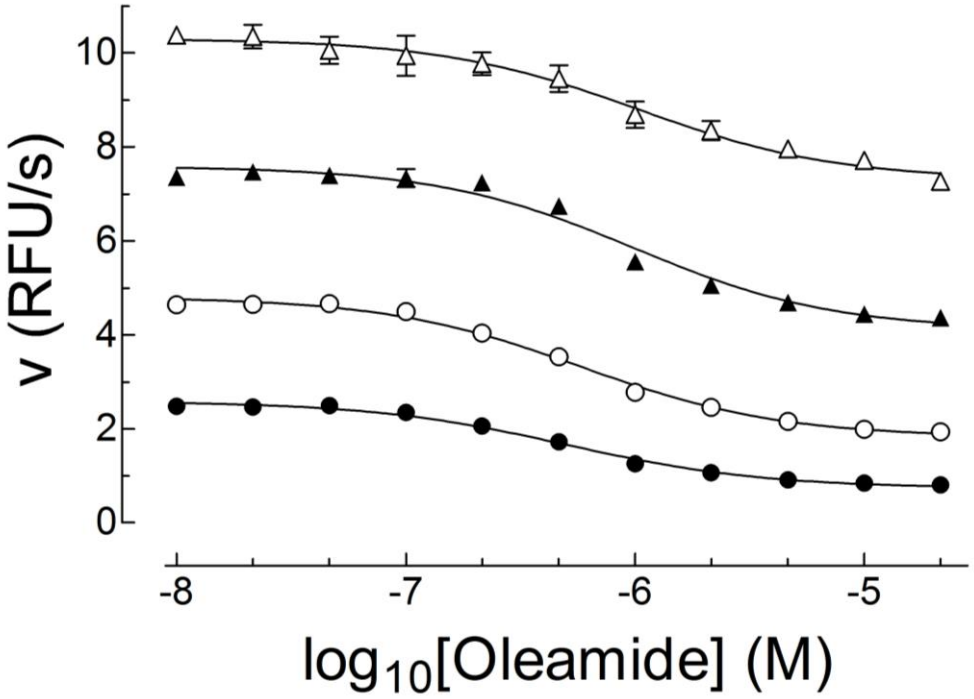

Figure 4.2.3.4 Inhibitor plots of oleamide versus benzylamine under high oxygen

Oxidation of 50(●), 150(○), 500(▲) and 1500(△) μM benzylamine by hMAO-B (1 nM) under 500 μM oxygen in the presence of oleamide (n=2) fitted to a monophasic sigmoid where the Hill-slope was constrained to -1 and the bottom was allowed to fluctuate. Reported IC_{50} values for oleamide at concentrations of 50, 150, 500 and 1500 μM benzylamine were 0.50, 0.59, 0.99 and 1.03 μM, respectively. Error bars represent SEM.

Low Oxygen					
[Benzylamine] (μM)	IC_{50} μM	K_I μM	Top (RFU/s)	Bottom (RFU/s)	Fraction Inhibited
50	0.367	0.24	1.80	0.57	0.68
150	0.523	0.20	3.21	1.35	0.58
500	0.666	0.10	4.77	2.94	0.38
1500	1.183	0.07	5.85	4.59	0.21
High Oxygen					
[Benzylamine] (μM)	IC_{50} μM	K_I μM	Top (RFU/s)	Bottom (RFU/s)	Fraction Inhibited
50	0.502	0.32	2.59	0.73	0.72
150	0.586	0.22	4.81	1.82	0.62
500	0.992	0.15	7.59	4.10	0.46
1500	1.026	0.06	10.31	7.30	0.29

Table 4.2.2 Kinetic Parameters for oleamide versus Benzylamine

Calculation of K_I values from IC_{50} values were done using the Cheng-Prusoff equation. The K_M value was set to 19 μM. The inhibition fraction describes the amount of inhibition caused by oleamide and is calculated using the equation (Top-Bottom)/Top.

Similar to the results when phenylethylamine is the substrate, benzylamine is partially inhibited by oleamide. As expected, calculated K_I values decrease as substrate concentration increase. Changes in oxygen concentration have very little effect on the fraction inhibited until substrate concentrations reach and exceed K_{Mred}. At this point, a greater fraction of the turnover of benzylamine is bound to $E.FAD_{red}$, reducing the opportunity for oleamide to bind. Increasing oxygen concentrations creates slightly more oxidised enzyme for oleamide to bind and inhibit.

As done with phenylethylamine, predicted fraction-inhibited values for 50, 150, 500, 1500 μM benzylamine were calculated and found to be 0.74, 0.66, 0.53 and 0.43, respectively. The K_{Mox} and K_{Mred} values used in the calculations were 103.5 and 670 μM, respectively. The V_{MAXred}:V_{MAXox} was set to 1.8. All values used were based upon averaging results found in Table 2.8.1.

Fraction-inhibited values, when compared to calculated values, indicate that benzylamine binding to $E.FAD_{red}$ inhibits the production of $E.FAD_{ox}$, much in the way that phenylethylamine does. Lowering the oxygen concentration also decreases benzylamine's susceptibility to inhibition by oleamide.

The results with oleamide provide great insight into how MAO-B handles substrates. The information obtained suggests that the effects of oleamide should be described by an equation for a two-site model with inhibition at $E.FAD_{ox}$. The equation used for oleamide was a competitive at both $E.FAD_{ox}$ and $E.FAD_{red}$, with the non-linear regression consistently making the K_{Ired} so large that no reduction in rate was occurring through the $E.FAD_{red}$ pathway. Further validation of this model

of inhibition was done by fitting kinetic curves for a two-site model using non-linear regression. The reason for selecting the two-site model is that if there are subtleties in the kinetic curve, the K_{Ired} may be revealed. If non-linear regression finds that K_{Ired} does not exist, it will simply make the value for K_{Ired} very large.

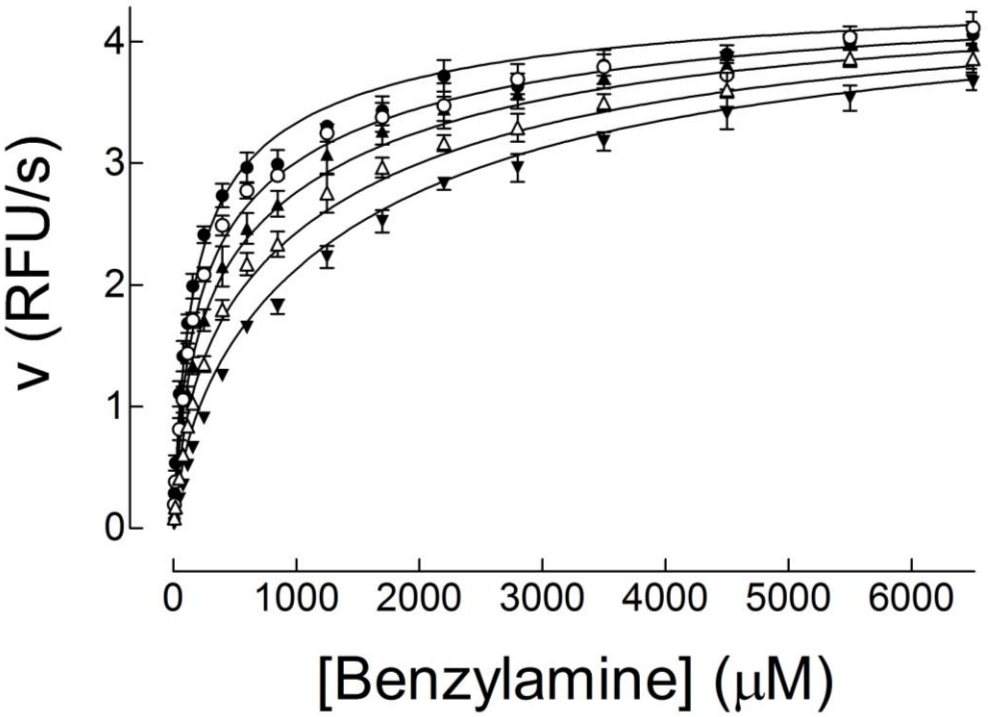

Figure 4.2.3.5 Inhibition of hMAO-B by oleamide versus benzylamine under low oxygen

Oxidation of benzylamine (10-6500μM) by hMAO-B (1 nM) under 100 μM oxygen in the presence of 0(●), 0.25(○), 0.54 (▲), 1.2(△) and 2.5(▼) μM oleamide (n=3) globally fitted to a two-site model with competitive at both $E.FAD_{ox}$ and $E.FAD_{red}$ (Eq. 2.14). Error bars represent SEM. Fits yielded a value of 170±10 and 1800±150 μM for K_{Mox} and K_{Mred}, respectively. K_{Iox} was found to be 1.0±0.1 μM. K_{Ired} was found to extremely large (1.003e+021 μM) with large errors. The global R^2 was 0.9771.

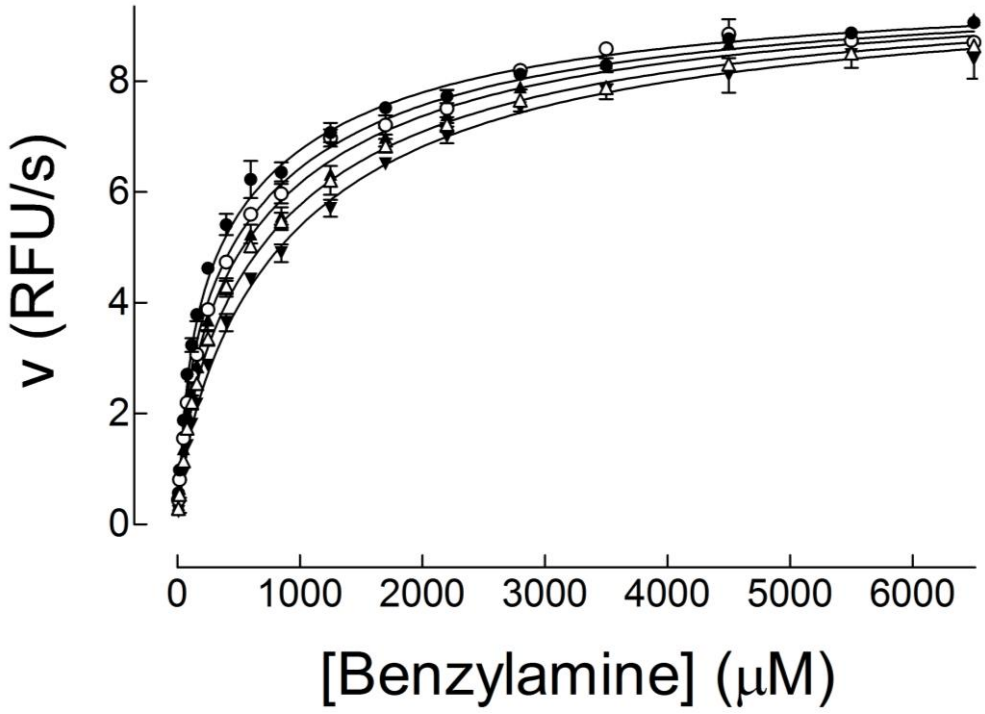

Figure 4.2.3.6 Inhibition of hMAO-B by oleamide versus benzylamine under high oxygen

Oxidation of benzylamine (10-6500μM) by hMAO-B (1 nM) under 500 μM oxygen in the presence of 0(●), 0.25(○), 0.54 (▲), 1.2(△) and 2.5(▼) μM oleamide (n=3) globally fitted to a two-site model with competitive at both $E.FAD_{ox}$ and $E.FAD_{red}$ (Eq. 2.14). Error bars represent SEM. Fits yielded a value of 93 ±8 and 1100±70 μM for K_{Mox} and K_{Mred}, respectively. K_{Iox} and found to be 1.4±0.1 μM. K_{Ired} was found to extremely large (6.750e+018 μM) with massive errors. The global R^2 was 0.9929.

Under low-oxygen concentrations, the kinetic curves visually indicate the inhibition is quickly overcome by benzylamine as V_{MAX} is quickly achieved in the presence of oleamide. High-oxygen conditions also show benzylamine achieves V_{MAX} in the presence of oleamide, albeit at much higher concentrations than under low-oxygen.

This fits well with the current model because as benzylamine concentrations increase, so does the flux through $E.FAD_{red}$-S. Under low-oxygen, enzyme is less likely to be in an oxidised form than under high oxygen. The lack of availability of oxidised enzyme prevents inhibition by oleamide. Under high-oxygen, more

oxidised enzyme is produced allowing oleamide to continue inhibiting MAO-B. Oleamide then competes with benzylamine for binding at $E.FAD_{ox}$. The competitive nature of this binding means that at high enough concentrations, benzylamine should be able to overcome the inhibition entirely. However, at such high concentrations, the majority of enzyme is in the reduced state anyway.

The K_I values obtained from the global analysis were, as expected, higher than those calculated from the IC_{50} values. High-oxygen and low-oxygen conditions yield K_I values of 1.38±0.15 and 1.09±0.11 μM, respectively. The K_I value can be used to calculate how much inhibition is expected from 2.5 μM oleamide in the presence of 6500 μM benzylamine at $E.FAD_{ox}$. This will tell us if the inhibition that is seen under high-oxygen conditions can be attributed to oleamide.

$$v = \frac{V_{max}[S]}{K_M(1 + \frac{[I]}{K_I}) + [S]} \quad \text{Eq. 2.19}$$

$$v = \frac{1[6500\mu M]}{90\mu M(1 + \frac{[2.5\mu M]}{1.09\mu M}) + [6500\mu M]} \quad \text{Eq. 2.20}$$

$$v = 0.95 \quad \text{Eq. 2.21}$$

The data points on the high-oxygen curve for the oxidation of 6500 μM benzylamine in the presence of 0 and 2.5 μM average to 9.03 and 8.392 RFU/s, respectively. This suggests that at 6500 μM benzylamine, 2.5 μM oleamide is responsible for 7% inhibition, while the calculated value indicates that the inhibition should be around 5%. Considering the potential error at a single point,

the numbers match very well. It therefore seems reasonable to conclude that oleamide most likely inhibits oxidation of benzylamine by binding to $E.FAD_{ox}$ and negligibly to $E.FAD_{red}$.

4.2.4 Non-Imidazoline Inhibitor Constants

Probing MAO-B with multiple inhibitors under different conditions has provided a wealth of information. It has allowed for the testing of a new mathematical model that describes differential binding and activity of two oxidation states of MAO-B. The mathematical model allows parameter-quantification and characterization of novel inhibitors. Kinetic constants from all the kinetic experiments with non-imidazoline inhibitors are compiled into Table 4.2.3.

Amphetamine											
		Two-Site Model, Competitive at both									
Substrate	Figure Number	K_{Mox} (μM)	K_{Mred} (μM)	V_{MAXox}	V_{MAXred}	K_{Iox} (μM)	K_{Ired} (μM)	KIred:KIox	KMred:KMox	VMAXred:VMAXox	R^2
Phenylethylamine (Atmospheric)	2.7.6.1	12 ± 1	16 ± 1	4.4 ± 1.5	4.5 ± 4.9	**262 ± 90**	**1950 ± 800**	**7.44**	**1.39**	**1.01**	0.9932
D_2-Phenylethylamine (Atmospheric)	2.7.6.2	29 ± 5	62 ± 6	3.7 ± 0.6	10.1 ± 0.6	**320 ± 90**	**1600 ± 190**	**5.00**	**2.11**	**2.75**	0.9961
Benzylamine (Atmospheric)	2.7.6.3	110 ± 12	730 ± 90	5.4 ± 0.3	7.7 ± 0.1	**730 ± 90**	**5000 ± 900**	**6.85**	**6.65**	**1.42**	0.9820
Amitriptyline											
		Two-Site Model, Competitive at both									
Substrate	Figure Number	K_{Mox} (μM)	K_{Mred} (μM)	V_{MAXox}	V_{MAXred}	K_{Iox} (μM)	K_{Ired} (μM)	KIred:KIox	KMred:KMox	VMAXred:VMAXox	R^2
Phenylethylamine (Atmospheric)	2.7.7.1	12 ± 1	71 ± 6	8.6 ± 0.3	12.5 ± 0.2	**58 ± 6**	630 ± 60	10.9	5.9	1.4	0.9917
Benzylamine (Low Oxygen)	2.7.7.3	65 ± 3	1110 ± 110	3.7 ± 0.1	5.1 ± 0.0	**170 ± 10**	∞		17.2	1.4	0.9919
Benzylamine (High Oxygen)	2.7.7.4	85 ± 0	890 ± 150	3.2 ± 0.2	4.6 ± 0.1	**100 ± 20**	∞		10.6	1.5	0.9674
Benzylamine (Atmospheric)	2.7.7.5	82 ± 13	500 ± 30	4.4 ± 0.3	12.4 ± 0.1	**34 ± 6**	1800 ± 250	53.2	6.1	2.8	0.9868
DiHEMDA											
		Two-Site Model, Competitive at both									
Substrate	Figure Number	K_{Mox} (μM)	K_{Mred} (μM)	V_{MAXox}	V_{MAXred}	K_{Iox} (μM)	K_{Ired} (μM)	KIred:KIox	KMred:KMox	VMAXred:VMAXox	R^2
Phenylethylamine (Atmospheric)	2.7.8.1	38 ± 10	54 ± 10	5.6 ± 2.4	2.3 ± 0.2	**2.8 ± 0.6**	**14 ± 4**	**5.11**	**1.44**	**0.41**	0.9683
Benzylamine (High Oxygen)	2.7.8.3	170 ± 20	1200 ± 100	4.4 ± 0.2	8.0 ± 0.1	**3.9 ± 0.4**	**30 ± 5**	**7.56**	**7.06**	**1.81**	0.9939
Benylamine (Low Oxygen)	2.7.8.4	100 ± 10	780 ± 90	2.4 ± 0.2	4.2 ± 0.0	**5.3 ± 0.8**	**32 ± 7**	**6**	**8**	**2**	0.9878
D_2-Phenylethylamine (Atmospheric)	2.7.8.6	1100 ± 300	1900 ± 400	6.6 ± 1.1	6.9 ± 0.5	**5.1 ± 0.8**	**24 ± 4**	**5**	**2**	**1**	0.9919
AVERAGE						**4.3**	**25.0**				
Oleamide											
		Two-Site Model, Competitive at both									
Substrate	Figure Number	K_{Mox} (μM)	K_{Mred} (μM)	V_{MAXox}	V_{MAXred}	K_{Iox} (μM)	K_{Ired} (μM)	KIred:KIox	KMred:KMox	VMAXred:VMAXox	R^2
Benzylamine (Low Oxygen)	4.2.3.5	170 ± 10	1800 ± 150	3.0 ± 0.1	4.4 ± 0.1	**1.0 ± 0.1**	∞		**10.6**	**1.5**	0.9771
Benzylamine (High Oxygen)	2.2.24	93 ± 8	1100 ± 70	4.4 ± 0.2	9.8 ± 0.1	**1.4 ± 0.1**	∞		**11.8**	**2.2**	0.9934

Table 4.2.3 Compilation of Kinetic Parameters for Reversible MAO-B Inhibitors
Compilation of kinetic values determined from kinetic analyses.

4.3 Imidazolines Inhibition of MAO-B

4.3.1 Materials

Purified preparations (hMAO-B) and mitochondrial membrane fractions (WT-hMAO-B and mutants Ile199Phe and Cys172Ala) of human MAO-B from *Pichia pastoris* (yeast) were graciously donated by Dr. Dale Edmondson (Emory University, Atlanta, Georgia).Amplex Red was obtained from Invitrogen (Burlington, ON, Canada). 2-BFI was purchased from Tocris-Cookson (Ellisville, MO). Deuterated substrates were provided by Dale Edmondson (Emory University, Atlanta). All other substrates, inhibitors and reaction constituents were obtained from Sigma–Aldrich (Oakville, ON, Canada).

4.3.2 Methods

For all experiments in this section, the activities of purified preparations or membrane fractions from *P. pastoris* yeast were measured continuously in 96-well plates with a SpectraMax Gemini XPS microplate reader by following the fluorescence related to the peroxidase-coupled formation of resorufin from AmplexRed[102]. Each reaction was run at 30°C in a total volume of 200 µL. Amine substrate was prepared on the day of the experiment using colourless Eppendorf™ micocentrifuge tubes for the dilutions. Inhibitor solutions were made in an identical manner. All dilutions were done in water.

The MAO-B/AmplexRed™/peroxidase solution was prepared by diluting MAO-B from a batch stock into a solution of 100 mM HEPES buffer and mixing this solution 1:1 with an AmplexRed™/peroxidase solution made up at four-times the concentration required for the experiment. The MAO-B/AmplexRed™/peroxidase solution was prepared to be used in entirety for a single experiment and was made fresh each time. During experiments involving more than one plate, enzyme was stored in the fridge until it was required in the experiment.

Plates were warmed to 30˚C prior to commencing the experiment. Assays were started by rapid addition of enzyme/AmplexRed mixture using an 8-channel pipette.

Experiments were carried out under atmospheric oxygen unless otherwise stated

Initial (pseudolinear) rates of product formation were determined by linear regression (SoftMax Pro v. 4.8) and were fitted to equations via the nonlinear regression function of GraphPad Prism v. 5.0c for Windows (GraphPad Software Inc., San Diego, CA).

4.3.3 Non-linear Regression to fit Models to Data

All curve fitting was carried out using the non-linear regression functionality of GraphPad Prism 5.0 (GraphPad Software Inc., San Diego, CA). For single-site hyperbola models (standard Michaelis-Menten kinetics) and sigmoidal inhibitor plots, the standard equations supplied with Prism 5 are used. These equations are:

$$Y = Vmax * X/(K_M + X)$$

For non-linear regression of single-site hyperbolas

$$Y = Bottom\ +\ (Top - Bottom)/(1 + 10^{\{LogEC_{50} - X\}})$$

For non-linear regression of sigmoidal plots

$$Y = Bottom\ +\ (Top - Bottom)/(1 + 10^{\{LogEC_{50} - X) * HillSlope\}})$$

For sigmoidal plots with a variable Hill-slope

$$SPAN = -Bottom + Top$$
$$Part1 = Span * Fraction1/(1 + 10^{\{X - LogEC_{50_1}\}})$$
$$Part2 =\ Span * (1 - Fraction1)/(1 + 10^{\{X - LogEC_{50_2}\}})$$
$$Y = Bottom\ +\ PART1\ + PART2$$

For two-site sigmoidal plots

4.3.4 Modelling Imidazoline Inhibition

Analyses of imidazoline-based compounds frequently provide poor fits with competitive inhibition models. Based upon information presented in Sections 3.4.5 and 4.1, a model of mixed inhibition is most appropriate. In a model of mixed inhibition, either substrate or inhibitor can bind to the enzyme first, but the binding of one affects the affinity of the other. The crystal structure of MAO-B suggests that if the I_2-site ligand binds first, the substrate will be unable to bind. Importantly, the rapid equilibrium equation to describe both scenarios is indistinguishable. In an identical process to the derivation of the two-site competitive inhibition equation (Eq. 2.14), substitutions based on the classical mixed inhibition equation (Eq. 2,22) are used to derive Eq. 2.23.

Classical Mixed Inhibition

$$v = \frac{V_{MAX}[S]}{K_M\left(1 + \frac{[I]}{K_I}\right) + [S]\left(1 + \frac{[I]}{\alpha K_I}\right)} \quad \text{Eq. 2.22}$$

$$v_{tot} = \frac{V_{MAX_{ox}}[S]}{K_{M_{ox}}\left(1 + \frac{I}{K_{I_{ox}}}\right) + [S]\left(1 + \frac{[I]}{\alpha K_{I_{ox}}}\right)}\left\{1 - \frac{[S]}{K_{M_{red}}\left(1 + \frac{[I]}{K_{i_{red}}}\right) + [S]\left(1 + \frac{[I]}{\beta K_{I_{red}}}\right)} - \frac{[I]}{K_{I_{red}}\left(1 + \frac{[S]}{K_{M_{red}}}\right) + [I]\left(1 + \frac{[S]}{\beta K_{M_{red}}}\right)}\right\} + \frac{V_{MAX_{red}}[S]}{K_{M_{red}}\left(1 + \frac{[I]}{K_{I_{red}}}\right) + [S]\left(1 + \frac{[I]}{\beta K_{I_{red}}}\right)} \quad \text{Eq. 2.23}$$

Equation 2.23 is used to analyse all kinetic assays involving 2-BFI using non-linear regression. The equation has many of the same shortcomings as other equations used throughout, although it provides good estimates of kinetic parameters and allows for validation of the model of inhibition.

4.3.5 *Inhibition of Phenylethylamine Turnover by 2-BFI*

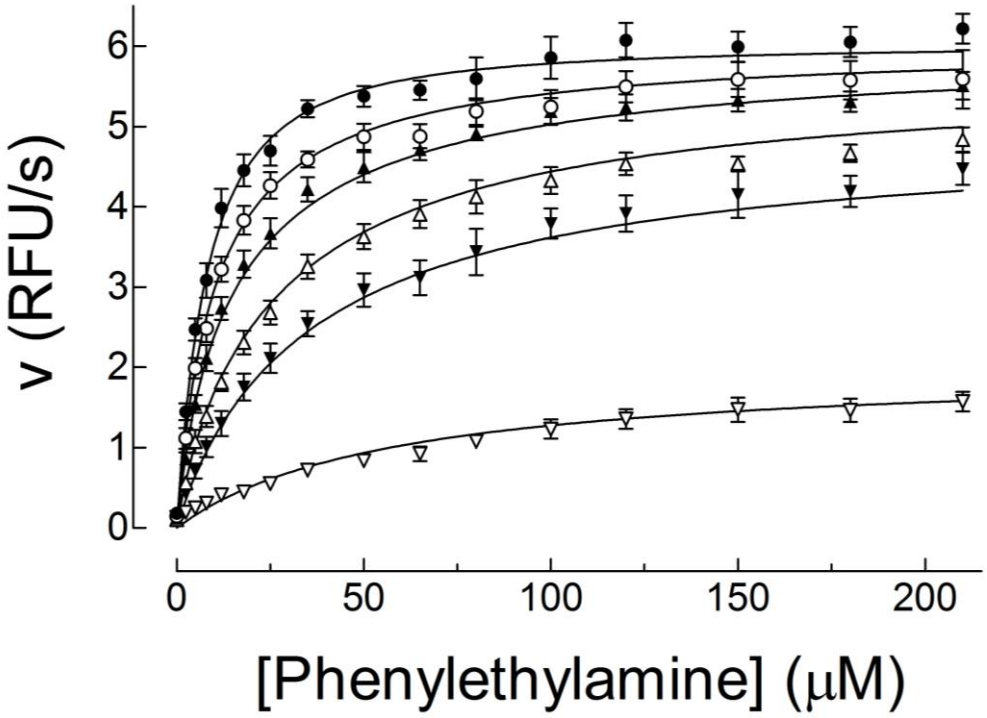

Figure 4.3.5.1 Inhibition of hMAO-B by 2-BFI versus phenylethylamine

Oxidation of phenylethylamine (2.5-210μM) by hMAO-B (2 nM) in the presence of 0(●), 2(○), 6(▲), 20(△), 60(▼) and 200(▽) μM 2-BFI (n=4) globally fitted to a two-site model with mixed inhibition (***Eq. 2.23***). Error bars represent SEM. Fits yielded a value of 10±2 and 30±4 μM for K_{Mox} and K_{Mred}, respectively. K_{Iox} and K_{Ired} were found to be 8±3 and 100±30 μM. A complete listing of parameters can be found in Table 4.3.1 Kinetic Constants for 2-BFI versus Phenylethylamine. The global R^2 was 0.9786.

2-BFI Kinetic Constants	**Phenylethylamine**		
K_{Mox} (μM)	10	±	2
K_{Mred} (μM)	30	±	4
K_{Iox} (μM)	8	±	3
K_{Ired} (μM)	100	±	30
α	0.62	±	0.38
β	2.36	±	0.86
V_{MAXred}:V_{MAXox}	1.11		
R^2	0.9786		

Table 4.3.1 Kinetic Constants for 2-BFI versus Phenylethylamine

Kinetic constants ± SEM derived from Figure 4.3.5.1.

The model provides consistent data on phenylethylamine, with very reasonable values for K_{Mox}, K_{Mred} and V_{MAXred}:V_{MAXox}. These results provide a K_{Iox} and K_{Ired} of 8 and 100 μM, respectively, which are typical of the inhibition reported in the literature. Interestingly, α is a value of less than one, implying that the binding of PEA to $E.FAD_{ox}$ decreases the K_{Iox} of 2-BFI for the enzyme. When bound to the $E.FAD_{red}$ form of the enzyme, however, PEA appears to increase K_{Ired} two-fold. An important aspect to remember when considering these data is that an α value of less than one means that the binding of phenylethylamine increases the enzyme's affinity for 2-BFI. Although this is an interesting finding, it could easily be an artefact of non-perfect data.

With such interesting results, it was hoped that sigmoidal curves would provide further insight into how, or potentially where, 2-BFI is carrying out its inhibitory action. Once again, although both 2-BFI and phenylethylamine have different affinities for MAO-B, it is most likely that sigmoidal plots will appear monophasic. Consider that binding of inhibitor to $E.FAD_{ox}$ reduces K_{Mox} to 0.62 of normal, producing an apparent K_{Mox} of 6.3 μM. Binding of inhibitor to $E.FAD_{red}$ increases K_{Mred} by a factor of 2.36, yielding an apparent K_{Mred} of 72.1 μM. This is an apparent K_{Mred}:K_{Mox} ratio of 11.5, which is very similar to the K_{Ired}:K_{Iox} ratio of 13.6. With this considered, the data presented in Figure 4.3.5.2are fitted to a biphasic curve in hopes of being able to see two phases.

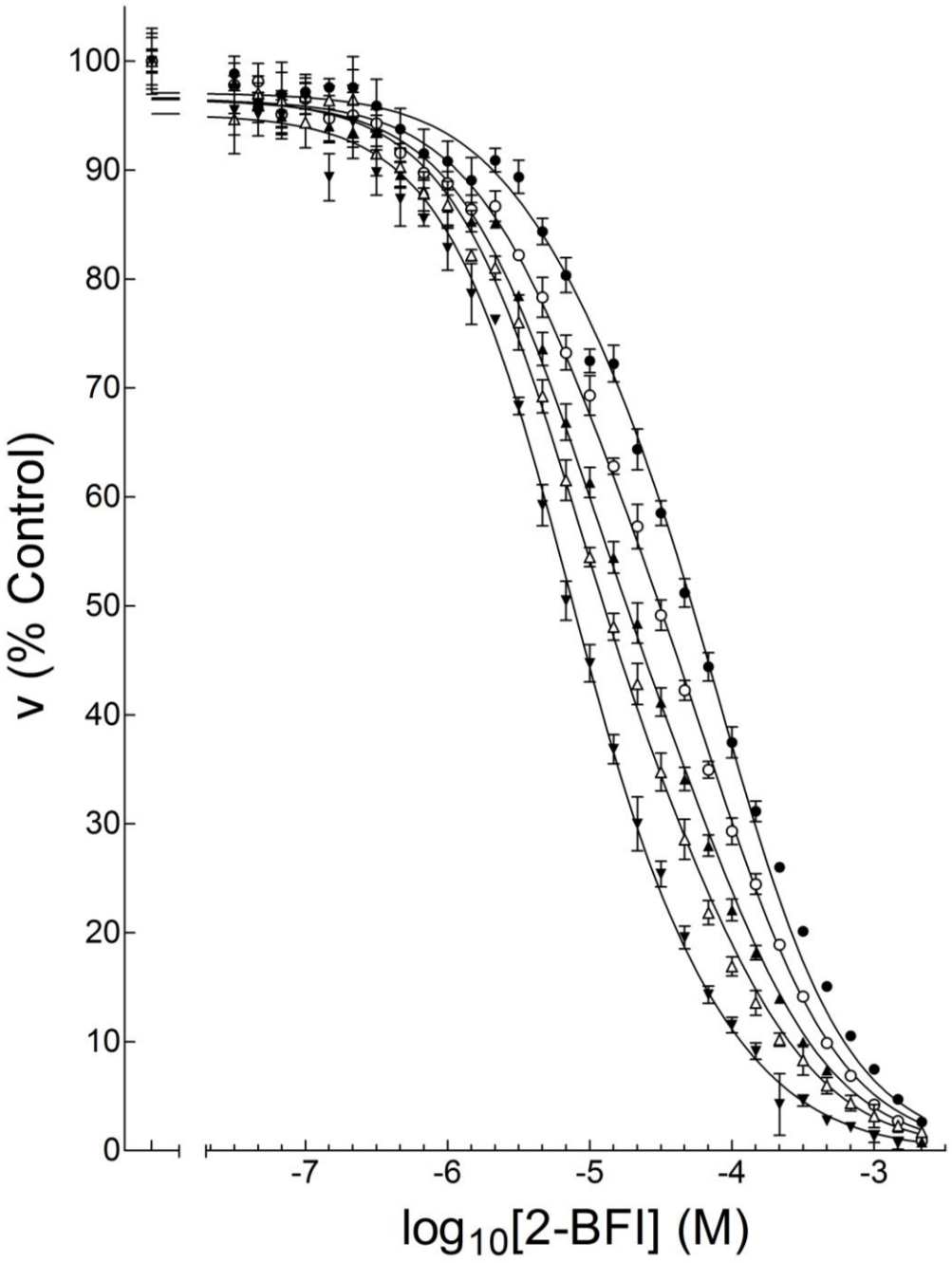

Figure 4.3.5.2 Inhibitor plots of 2-BFI versus benzylamine under low oxygen

Oxidation of 3(●), 6(○), 10(▲), 16(△), 30(▼) μM phenylethylamine by hMAO-B (3nM) in the presence of 2-BFI. Data are fitted to biphasic sigmoids with both Hill-slopes constrained to -1 and top constrained to 100. Error bars represent SEM (n=3). Results are presented in Table 4.3.2 Inhibitor Plot Derived Constants for 2-BFI versus Phenylethylamine

Phenylethylamine inhibition by 2-BFI (Results)					
	3μM PEA	6μM PEA	10μM PEA	16μM PEA	30μM PEA
Fraction	0.1084	0.1787	0.1602	0.167	0.1473
IC_{50-1} (μM)	0.11	0.58	0.41	0.58	0.95
IC_{50-2} (μM)	9.98	20.46	28.51	46.77	70.15

Table 4.3.2 Inhibitor Plot Derived Constants for 2-BFI versus Phenylethylamine
Non-linear regression results from fitting of data in **Error! Reference source not found.**Figure 4.3.5.2. to a biphasic sigmoid equation with top constrained to 100 and Hill-slopes constrained to -1.

The results provide two IC_{50} values that do not match up with the values obtained from the kinetic analysis (Figure 4.3.5.1), although the sigmoids are essentially monophasic. The IC_{50-2} value at the lowest concentration of phenylethylamine (3 μM) is reasonable value for inhibition at $E.FAD_{ox}$. Assuming most of the activity is likely going through $E.FAD_{ox}$ at this concentration of phenylethylamine, the Cheng-Prusoff equation yields a K_I value of 8.7 μM when using 20 μM as K_{Mox}. Continuing upwards in phenylethylamine concentrations, IC_{50-2} values continue to increase, albeit at a disproportionate rate. This is in support of the mathematics behind the K_{Ired}:K_{Iox} calculations. As the concentration of substrate increases, a shift towards enzyme being in a more reduced form occurs, resulting in the shift in the IC_{50} value towards representing K_{Ired}. The near identical K_{Ired}:K_{Iox}, however, masks this being shown as a change in fraction. As a whole, these results also provide some evidence that an α value of 0.62 and a β value of 2.36 are reasonable for phenylethylamine.

The data presented in Table 4.3.2 show that a very small fraction of inhibition (approximately 10-15%) occurs at sub-micromolar concentrations. The values, unfortunately, are still too large to match up to the high-affinity binding site (Section 3.4.5, page 104),

4.3.6 Inhibition of Benzylamine Turnover by 2-BFI

The exciting results found in the inhibition of phenylethylamine turnover in the presence of 2-BFI need to be confirmed using different a different substrate. Once again, benzylamine was used in both kinetic and inhibitor activity assays because of its kinetic differences from phenylethylamine.

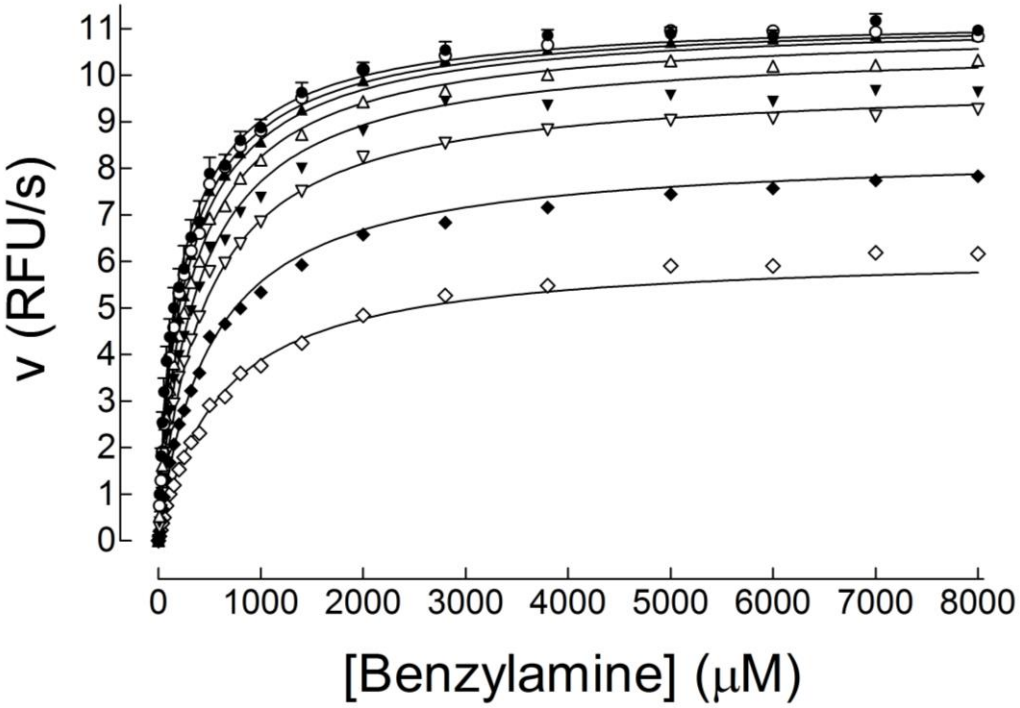

Figure 4.3.6.1 Inhibition of hMAO-B by 2-BFI versus benzylamine
Oxidation of benzylamine (0-8000μM) by hMAO-B (2 nM) in the presence of 0(●), 3(○), 7(▲), 17(△), 39(▼), 90(▽). 214(◆), and 500(◇) μM 2-BFI (n=5) globally fitted to a two-site model with mixed inhibition (Eq. 2.23). Error bars represent SEM (n=3). A complete listing of parameters can be found in Table 4.3.3. The global R^2 was 0.9974.

	2-BFI Kinetic Constants					
	Phenylethylamine			Benzylamine		
K_{Mox} (μM)	10.17	±	1.59	56.73	±	9.41
K_{Mred} (μM)	30.55	±	4.01	403.20	±	28.86
K_{Iox} (μM)	7.62	±	3.19	28.21	±	17.14
K_{Ired} (μM)	103.80	±	28.33	286.30	±	37.08
α	0.62	±	0.38	0.55	±	0.45
β	2.36	±	0.86	2.09	±	0.31
V_{MAXred}:V_{MAXox}	1.11			3.15		
R^2	0.9786			0.9974		

Table 4.3.3 Kinetic Constants for 2-BFI versus Phenylethylamine and Benzylamine
Kinetic constants derived from Figure 4.3.5.1 and Figure 4.3.6.1. Although already shown, phenylethylamine data are presented again for easy comparison.

While it was not expected, it is interesting that α and β values are so similar for phenylethylamine and benzylamine. That the α-value is below 1 again is significant. The V_{MAXred}:V_{MAXox} is also higher than seen before as well. The results for benzylamine are very consistent with previously obtained values, although the K_{Iox} and K_{Ired} values with benzylamine are slightly higher than when phenylethylamine was substrate, an indication that the model is not perfect. Of interest is that the βK_{Mred}:αK_{Mox} value of 27, unlike phenylethylamine, is not very similar to the K_{Ired}: K_{Iox} value of 10.1, suggesting that sigmoidal plots should be biphasic for benzylamine.

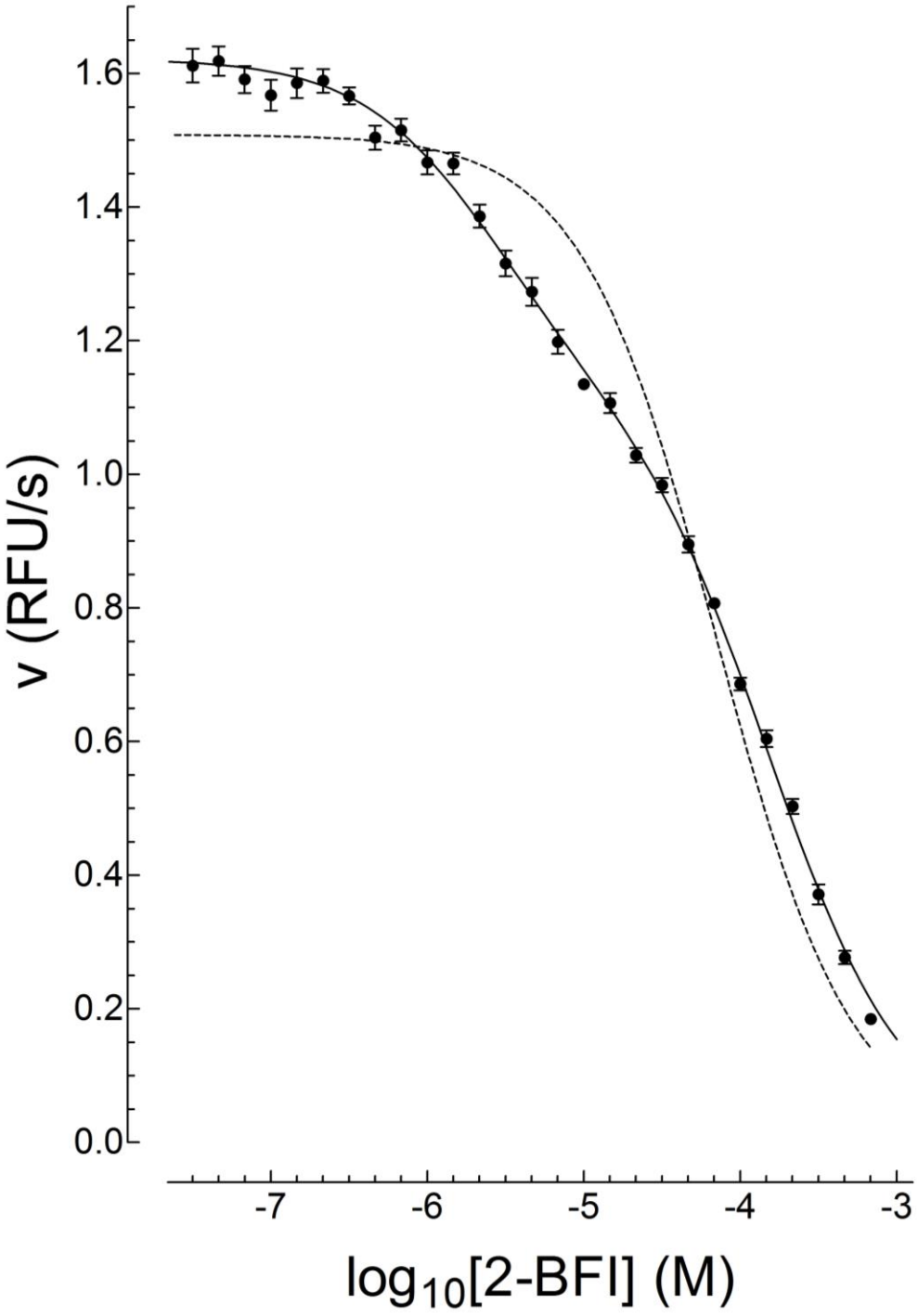

Figure 4.3.6.2 Inhibition of 30 µM benzylamine turnover by 2-BFI

Oxidation of 30(●) µM benzylamine by hMAO-B (3nM) in the presence of 2-BFI. Data are fitted to a biphasic sigmoid with both Hill-slopes constrained to -1(solid line) and a monophasic sigmoid with a variable Hill slope (dashed line). $IC_{50\text{-}1}$ and $IC_{50\text{-}2}$ were found to be 5.95 and 219.8 µM, respectively. The fraction was found to be 0.48. Error bars represent SEM (n=9).

Inhibition of benzylamine turnover by 2-BFI yields a very clear two-site fit. The dashed line is a monophasic sigmoid with a variable Hill-slope. The first IC_{50} (5.95 μM) corresponds well to the K_{Iox} value for 2-BFI derived from kinetic data. The IC_{50-2} (219.8 μM) corresponds well to K_{Ired}. The fraction (0.48) is significantly lower than expected at 30 μM benzylamine, which should be above 0.7 based on the oleamide data (see Section 4.2.3 for explanation). That more enzyme is in the reduced form is also suggested by the higher than normal V_{MAXred}:V_{MAXox} obtained from kinetic analyses, although the reason for this is not clear.

Interestingly, there does not appear to be any sub-micromolar inhibition occurring. Raw rates show no indication of curving off, unlike phenylethylamine.

The clear, biphasic nature of 2-BFI makes it a great tool to probe the activity of MAO-B, much in the same way that oleamide and amitriptyline provided invaluable information. 2-BFI inhibitor plots, with concentrations spaced at one-sixth log units, in the presence of benzylamine were prepared under both atmospheric and low oxygen.

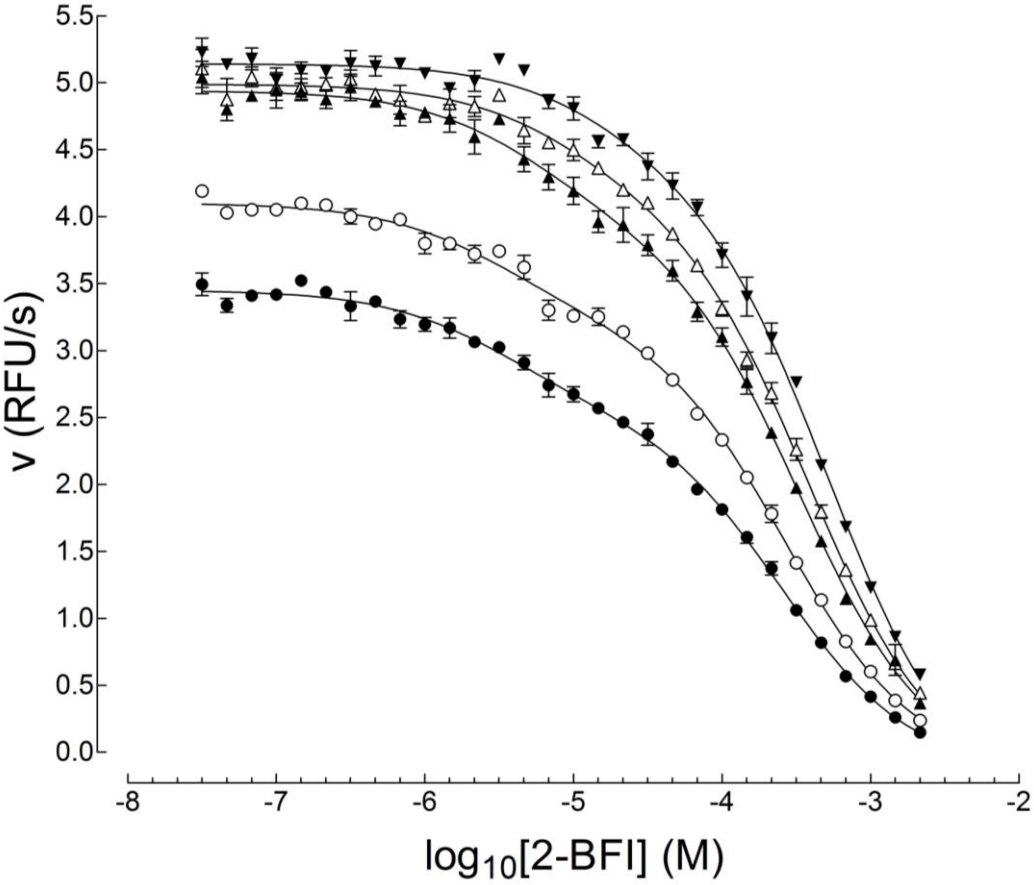

Figure 4.3.6.3 Inhibitor plots of 2-BFI versus benzylamine under atmospheric oxygen

Oxidation of 60(●), 100(○), 160(▲), 220(△) and 300(▼) µM benzylamine by hMAO-B (3nM) in the presence of 2-BFI under atmospheric oxygen. Data are fitted to a biphasic sigmoid with both Hill-slopes constrained to -1. Results are tabulated in Table 4.3.4. Error bars represent SEM (n=3).

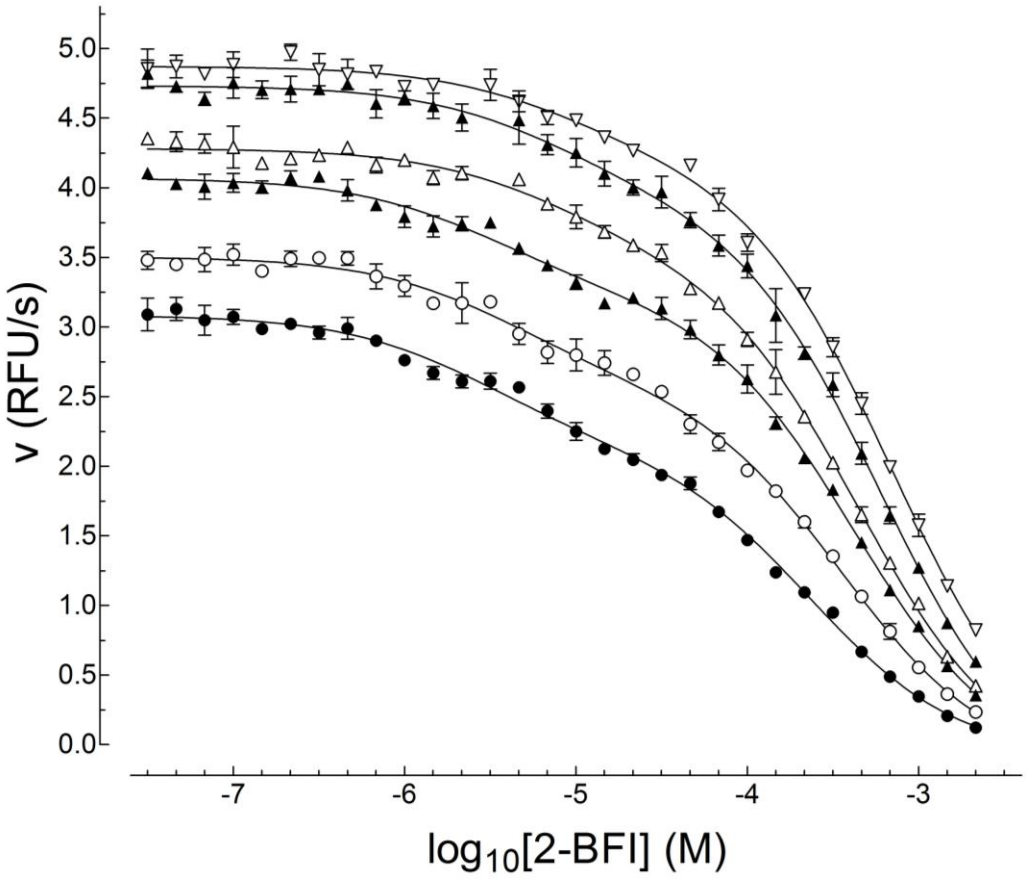

Figure 4.3.6.4 Inhibitor plots of 2-BFI versus benzylamine under low oxygen

Oxidation of 30(●), 60(○), 100(▲), 200(△), 300(▼) and 400(▽) μM benzylamine by hMAO-B (3nM) in the presence of 2-BFI under 100μM oxygen. Data are fitted to a biphasic sigmoid with both Hill-slopes constrained to -1. Results are tabulated in Table 4.3.4. Error bars represent SEM (n=3).

Atmospheric Oxygen

	[Benzylamine] (µM)				
	60	100	160	220	300
Fraction	0.24	0.20	0.18	0.12	0.09
IC_{50-1} (µM)	2.86	2.81	4.92	6.50	10.81
IC_{50-2} (µM)	208.45	233.88	289.73	309.03	387.26

Low (100 µM) Oxygen

	[Benzylamine] (µM)					
	30	60	100	200	300	400
Fraction	0.37	0.30	0.25	0.16	0.15	0.12
IC_{50-1} (µM)	2.84	2.95	4.19	7.60	7.78	8.91
IC_{50-2} (µM)	212.81	239.88	363.08	452.90	602.56	695.02

Table 4.3.4 Parameters for 2-BFI versus benzylamine under atmospheric and low oxygen
Tabulation of values obtained from experiments presented in Figure 4.3.6.3and Figure 4.3.6.4.

As seen in results with amitriptyline and oleamide, substrate concentration primarily dictates the fraction of benzylamine catabolism that goes via the $E.FAD_{red}$ pathway. The fraction, once again, is far lower than expected based upon previous results that suggest more than 50% of enzyme is in the oxidised form at 60 µM benzylamine. In the presence of 2-BFI, benzylamine appears to mimic the metabolism of phenylethylamine in as much as a significant portion of the enzyme is in the reduced form. There also appears to be an interaction between 2-BFI and oxygen, characterised by an increase in the value of IC_{50-2} when oxygen concentration is low. This effect appears to be amplified as the concentration of substrate increases. While this may be an artefact of the experiment, it must also be considered as a potentially valid result.

More research into the relationship between oxygen and 2-BFI needs to be done in order to understand how 2-BFI forces more of the enzyme into the reduced form in the presence of benzylamine. One potential explanation is that by decreasing K_{Mox} for benzylamine, more enzyme exists in the reduced form if the rate of reoxidation is not increased. Even this would only be a fraction of the story, however, and it is purely speculation based upon the values obtained from a small number of experiments.

4.3.7 2-BFI Inhibition of Benzylamine oxidation in Mutants

Although not discussed in detail during the kinetics section, kinetic data collected with imidazoline ligands provide a support role in determining the location and properties of the imidazoline site. As part of localising the I_2-site, two mutants were screened versus 2-BFI and 100 μM benzylamine. One mutant has a phenylalanine replacing Ile199, while the other mutant has an alanine at the 172nd position rather than a cysteine (C172A). As mentioned in previous chapters, Ile199 works as a gate between the active site and the entrance channel.

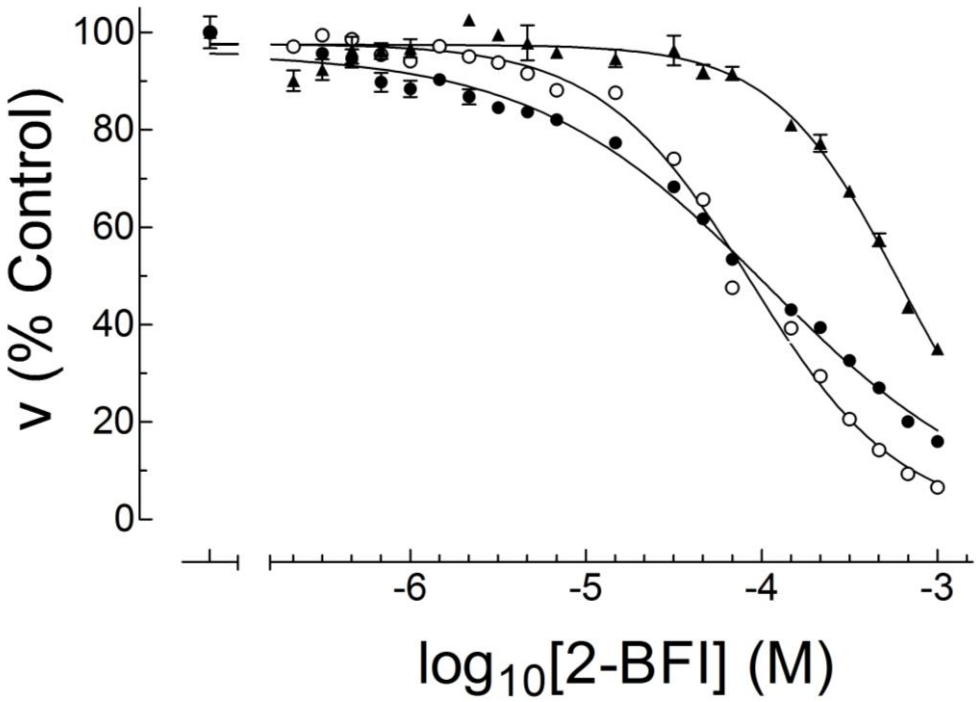

Figure 4.3.7.1 Inhibitor plots of 2-BFI versus benzylamine for wild-type and mutant MAO-B

Oxidation of 30 µM benzylamine by WT-MAO-B (●), Ile199Phe MAO-B(○), and Cys172Aala MAO-B (▲) in the presence of 2-BFI. WT-MAO-B is fitted to a biphasic sigmoid with both Hill-slopes constrained to -1, yielding fraction of 0.1861 and $IC_{50\text{-}1,2}$ of 0.746 and 117.2 µM, respectively. I199F and C172A are fitted to a monophasic sigmoid with the Hill-slope constrained to one, yielding IC_{50} values of 86 and 605 µM, respectively. Error bars represent SEM.

Without full kinetic curves available for analysis, the information produced in Figure 4.3.7.1 is very preliminary. Of interest is the shift towards an apparent monophasic curve. As discussed previously, this can be explained if the mutations cause a change in the kinetic parameters such that K_{Mox}:K_{Mred} approximates K_{Iox}:K_{Ired}. Another possible explanation is that both Ile199Phe and Cys172Ala play a role in transducing the oxidation state of the enzyme to the entrance cavity where substrate handling may be regulated. Such an idea is briefly discussed in Section 3.4.5; however further kinetic and binding experiments are required to determine precisely the consequences and roles of Ile199 and Cys172 in MAO-B-mediated catabolism of amines.

In general, studying the kinetics of MAO-B in the presence of 2-BFI continues to be problematic. Even in carefully done experiments with many data points, the high-affinity reported from radioligand binding could not be seen. This is likely because the high-affinity site is only found in significant amounts on non-functioning enzymes. There is some evidence to suggest the existence of a transient high-affinity site existing on a small number of enzyme-substrate complexes; however, it appears that such a site contributes to the creation of non-functioning enzyme, thus not affecting the initial rates used in rapid-equilibrium analyses. Furthermore, obtaining many steady-state kinetic parameters through non-linear regression requires near perfect data to determine all values with any confidence. While kinetic data are of high quality, more variables need to be added to describe adequately the complete interaction between 2-BFI and MAO-B. The kinetics presented have provided some insight into 2-BFI inhibition of MAO-B, but they do not tell the entire story.

5 Chapter 5: Concluding Remarks

5.1.1 Summary

Throughout this work, the goal was to understand the nature of the I_2 site on MAO-B and to explain the discrepancies in the literature between the nanomolar affinity results seen in radioligand binding assays and the micromolar affinities seen in kinetic experiments. The work began with first understanding fully the way in which MAO-B handles substrates in order to be able to determine through mathematics the mechanism of inhibitors. Once a model was developed that adequately explained the results seen with competitive inhibitors, it was modified to account for 2-BFI kinetics. The presence of a high-affinity I_2 binding site on human MAO-B was verified through binding experiments, and a connection between substrates and the binding sites was made. A schematic showing the structural changes that occur in MAO-B when substrate is irreversibly bound to the substrate is shown in Figure 5.1.1.1. When we discovered that phenylethylamine is capable of producing the I_2 site, it quickly became clear that the high affinity site may exist only on inactivated enzyme.

The combination of kinetic and binding assays laid out sufficient evidence to conduct crystallographic studies involving MAO-B and 2-BFI, in collaboration with Andrea Mattevi (University of Pavia, Italy) and Dale Edmondson (Emory University, Atlanta). The work has since been published and clearly shows that 2-BFI binds in the entrance cavity near the Ile199 gate[64]. The works described herein, including kinetics and binding, were successfully published in September of 2010 [63]. While

enzyme kinetics and binding experiments may have fallen out of favour with many scientists, the methods have once again provided valuable insight into the basic chemistry that is vital for life.

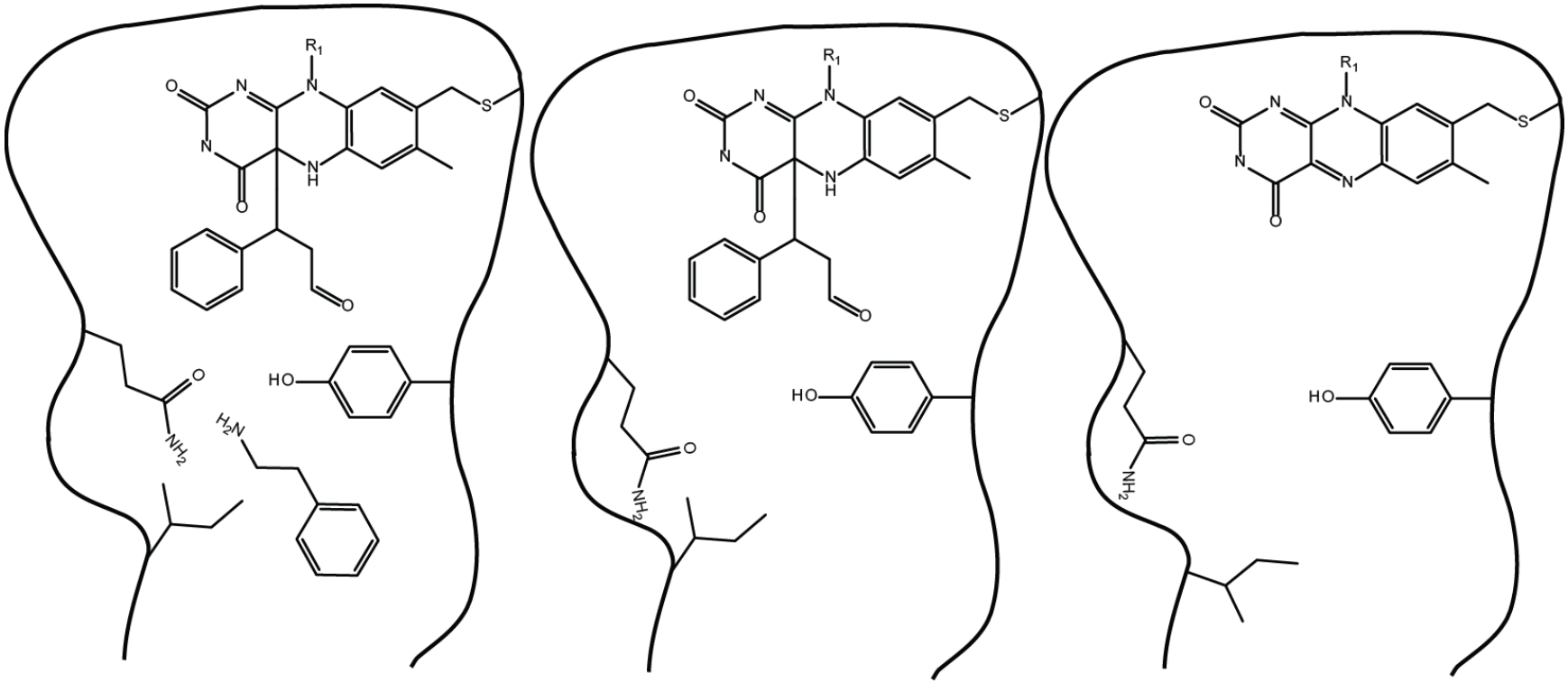

Figure 5.1.1.1 Structural changes and the I2 binding site on MAO-B

The I_2-site on hMAO-B appears to be formed when an irreversible reaction occurs in the substrate-binding cavity, leading to a conformational change in Ile199 and Gln 206 (left). This conformation change produces a pocket that yields a high affinity site for 2-BFI. The Ile199 gate may be involved in substrate specificity of MAO-B as it regulates between creating a bipartite cavity (centre) and a single cavity when in the open conformation (right). The physiological role of the I_2-site formed in the entrance cavity of MAO-B is unknown. Based on kinetic experiments, the site may provide a novel way of regulating the activity of MAO-B by modulating the rate of irreversible inhibition by endogenous substrates.

5.1.2 Future Directions of Research

Many questions remain regarding the role of the binding site within the substrate entrance cavity of MAO-B. The current research has focused on amine substrates and the effect imidazolines have on amine catabolism. Further kinetics studies investigating the effect the inhibitors have on oxygen as a substrate could provide important information regarding the role of the entrance cavity and any role it might play in regulating amine turnover. Ideally, MAO-B kinetics with oxygen as a substrate would provide great insight and much needed kinetic constants.

The most interesting and pressing information outstanding is the causative agent for the *in vivo* I_2-site formation. The current research has not yielded a site with identical characteristics as those described in the literature from either human platelets or rat brain. The causative agent could be an amine substrate or a tight-binding inhibitor used by cells to specifically regulate MAO-B activity. Determining the causative agent will certainly have physiological implications which could be significant in understanding the role of MAO-B.

The increase in our understanding about the formation of the I_2-site makes it now possible to characterise an array of imidazoline ligands versus *in vivo* and *in vitro* created sites. The unique role the I_2-site appears to play with regulation of enzyme activity could lead to novel drugs and new approaches to specifically treat numerous human diseases.

5.1.3 Implications of Findings

The knowledge that 2-BFI can modify the rate of inhibition caused by substrate at nanomolar concentrations presents a potential opportunity for the creation of more specific modulation of brain activity and suggests that MAO-B may play a more important role in human physiology than it is currently attributed. At nanomolar concentrations, 2-BFI does not directly inhibit MAO-B activity. In the presence of substrates like phenylethylamine, however, 2-BFI at nanomolar concentrations potentiates the ability of the substrate to become an irreversible inhibitor. This allows for highly selective inhibition of MAO-B which is dependent on the concentration of the *substrates in the environment* of the enzymes. For example, if a biogenic amine present in trace levels such as octopamine was able to reduce the K_D for 2-BFI 100-fold compared to a more common substrate like dopamine, the presence of 2-BFI and octopamine could create non-functioning enzyme at a higher rate than in areas of the brain where octopamine is not present.

Given that PEA is an endogenous substrate for MAO-B and creates a high-affinity site on non-functioning MAO-B that is similar (but not identical) to the *in vivo* formed site, it seems likely that more than one endogenous ligand can contribute to the formation of the of the high affinity site. This is supported by evidence from the literature showing that some I_2-ligands showed multiple affinities (biphasic displacement curves) for the endogenously created site[83,86-88]. This has important implications in the utility of targeting MAO-B in disease states. Not all regions of the brain have identical cellular constituents.

The concentrations and role of neurotransmitters in physiology can vary greatly depending of the neural network they are a part of, which has proven to be a challenge for clinicians in treating mental illness and neurological disorders. For example, current treatment for depression includes the use of selective serotonin reuptake inhibitors (SSRIs) such as fluoxetine and paroxetine. These drugs are highly specific to serotonin reuptake on neurons, but they are not specific to any particular area of the brain. These medications will bind indiscriminately to serotonin transporters (SERTs), leading to the patient experiencing side effects such as nausea, weight gain, sexual dysfunction and worsening depression in some patients. If there was a way to specifically target SERTs in specific parts of the brain, there is a chance that side-effects could be decreased and the disorders could be treated more effectively.

The implications of our research suggest that it may be possible to target MAO-B activity specifically in areas where certain substrates are present. Given that different regions of the brain are constituted of different neurotransmitters, it may be possible to target regions of the brain that consist of specific combinations of neurotransmitters. Indeed, significant progress needs to be made in the understanding of disease states and the function of MAO-B before any therapeutic implications can be further speculated upon. Even if not a useful target in human physiology, the information provided by this research of MAO-B suggests that enzymes can be targeted regionally based upon the environment of the enzyme.

6 Bibliography

1. Schiedeberg, O. Uber das verhaltniss des ammoniaks und der primaren monoaminbasen zur harstoffbildung im thirerkorper. Archives of Experimental Pathology and Pharmacology 1877;8:1.

2. Blaschko H. Amine oxidase and amine metabolism. Pharmacological Reviews 1952;4:415-58.

3. Dale HH, Dixon WE. The action of pressor amines produced by putrefaction. The Journal of Physiology 1909;39:25-44.

4. Ewins AJ, Laidlaw PP. The fate of parahydroxyphenylethylamine in the organism. The Journal of Physiology 1910;41:78-87.

5. Hare M. Tyramine Oxidase. A new enzyme system in the liver. Biochemistry Journal 1928;22:968.

6. Ewins,A.J., Laidlaw,P.P. The fate of indolethylamine in the Organism. Biochemistry Journal 1913;7:18.

7. Thompson RHS, Tickner A. The occurrence and distribution of mono-amine oxidase in blood vessels. The Journal of Physiology 1951;115:34-40.

8. Bhagvat K, Blaschko H, Richter D. Amine oxidase. Biochemistry Journal 1939;33:1338.

9. Langemann H. Enzymes and their substrates in the adrenal gland of the ox. British Journal of Pharmacology and Chemotherapy 1951;6:318.

10. Zeller E. Uber den enzymatischen Abbau von Histamin and Diaminen. Helv Chim Acta 1938;21:880.

11. Blaschko H, Richter D, Schlossmann H. The oxidation of adrenaline and other amines. Biochemistry Journal 1937;31:2187.

12. Pugh C, Quastel J. Oxidation of aliphatic amines by brain and other tissues. Biochemistry Journal 1937;31:286.

13. Kohn H. Tyramine oxidase. Biochemistry Journal 1937;31:1693.

14. Best C. The disappearance of histamine from autolysing lung tissue. Journal of Physiology 1929;67:256.

15. Erwin VG, Hellerman L. Mitochondrial Monoamine Oxidase. Journal of Biological Chemistry 1967;242:4230-8.

16. Oreland L. Purification and properties of pig liver mitochondrial monoamine oxidase. Archives of Biochemistry and Biophysics 1971;46:410.

17. Walker W, Kearney E, Seng R, Singer T. Sequence and structure of a cysteinyl flavin peptide from monoamine oxidase. Biochemical and Biophysical Research Communications 1971;44:287.

18. Ghisla S, Hemmerich P. Synthesis of the flavocoenzyme of monoamine oxidase. FEBS Letters 1971;16:229.

19. Schnaitman C, Erwin VG, Greenawalt J. The submitochondrial localization of monoamine oxidase. An enzymatic marker for the outer membrane of rat liver mitochondria. Journal of Cell Biology 1967;32:719.

20. Tong J, Meyer JH, Furukawa Y, *et al*. Distribution of monoamine oxidase proteins in human brain: implications for brain imaging studies. J Cereb Blood Flow Metab 2013;.

21. Billett EE. Monoamine Oxidase (MAO) in human peripheral tissues. Neurotoxicology 2004;25:139-48.

22. Johnston J. Some observations upon a new inhibitor of monoamine oxidase in brain tissue. Biochemistry and Pharmacology 1968;17:1285.

23. Knoll J. The pharmacology of (-)deprenyl. Journal of Neural Transmission Suppliment 1986;22:75.

24. Houslay M, Tipton K. The nature of electrophoretically separable multiple forms of rat liver monoamine oxidase. Biochemistry Journal 1973;135:173.

25. Collins G, Youdim M, Sandler M. Multiple forms of monoamine oxidase. Comparison of *in vitro* and *in vivo* inhibition patterns. Biochem.Pharmacol. 1972;21:1995.

26. Bach A, Lan N, Johnson D, *et al*. cDNA cloning of human liver monoamine oxidase A and B: molecular basis of differences in enzymatic properties. Proceedings of the National Academy of Sciences 1988;85:4934.

27. Hall T, Uruena G. Distribution of monoamine oxidase activity in tissues of the urodeles *Ambystoma tigrinum* (tiger salamander) and *Necturus maculosus* (mudpuppy). Comparative Biochemistry and Physiology 1983;74:35.

28. Kinemuchi H, Sunami Y, Ueda T, Morikawa F, Kamijo K. Inhibition of carp liver mitochondrial monoamine oxidase by some commonly-used detergents. Japanese Journal of Pharmacology 1983;33:1007.

29. Yoshino M, Obata T, Sho S, Kinemuchi H. Enzymatic and molecular characteristics of a new form of monoamine oxidase, distinct from form-A and form-B. Japan Journal of Pharmacology 1984;35:105.

30. Hall T, Uruena G. Monoamine oxidase activity in several tissues of the goldfish. Comparative Biochemistry and Physiology 1982;72:145.

31. Hall T, Yurgens P, Figueroa H, *et al*. Monoamine oxidase types A and B in the vetebrate brain. Comparative Biochemistry and Physiology 1982;71:107.

32. Hall T, Lea R, Vowles D, Harvey S. Biochemistry and physiology of monoamine oxidase activity in the ring dove. Comparative Biochemistry and Physiology 1985;82:417.

33. Baker P. Monoamine oxidase in the eye,brain, and whole embryo of developing Xenopus laevis. Developmental Biology 1966;14.

34. Wang CC, Borchert A, Ugun-Klusek A, *et al*. Monoamine Oxidase A expression is vital for embryonic brain development by modulating developmental apoptosis. Journal of Biological Chemistry 2011;286:28322-30.

35. Brunner H, Nelen M, van Zandovoort P, *et al*. X-linked borderline mental retadation with prominent behaioral distrubance: phenotype, genetic localisation, and evidence for disturbed monoamine metabolism. American Journal of Human Genetics 1993;52:1032.

36. Whibley A, Urquhart J, Dore J, *et al*. Deletion of MAOA and MAOB in a male patient causes severe developmental delay, intermittent hypotonia and stereotypical hand movements. Eur J Hum Genet 2010;18:1095-9.

37. Saito M, Yamagata T, Matsumoto A, *et al*. MAOA/B deletion syndrome in male siblings with severe developmental delay and sudden loss of muscle tonus. Brain and Development 2014;36:64.

38. Boadle M, Blaschko H. Cockroach amine oxidase: classification and substrate specificity. Comparative Biochemistry and Physiology 1968;25.

39. Okabe H, Noma A. Studies on the starfish. Activities and distribution of enzymes in the starfish Asterina pectinifera. Comparative Biochemistry and Physiology 1974;49:599.

40. Weyler W, Salach J. Purification and propertoes of mitochondrial monoamine oxidase type A from human placenta. Journal of Biological Chemistry 1985;260:13199.

41. Bond PA, Cundall RL. Properties of monoamine oxidase (MAO) in human blood platelets, plasma, lymphocytes and granulocytes. Clinica Chimica Acta 1977;80:317-26.

42. Donnelly CH, Murphy DL. Substrate- and inhibitor-related characteristics of human platelet monoamine oxidase. Biochemical Pharmacology 1977;26:853-8.

43. Denney R, Patel N, Fritz R, Abell C. A monoclonal antibody elicited to human platelet monoamine oxidase. Isolation and specificity for human monoamine oxidase B but not A. Molecular Pharmacology 1982;22:500.

44. Erwin VG, Hellerman L. Mitochondrial monoamine oxidase. Purification and characterization of the bovine kidney enzyme. Journal of Biological.Chemistry. 1967;242:4230.

45. Salach J, Weyler W. Iron content and spectral properties of highly purified bovine liver monoamine oxidase. Archives of Biochemistry and Biophysics 1981;212:147.

46. Billett E. Monoamine oxidase in human peripheral tissues. Neurotoxicology 2004;25:139.

47. Bortolato M, Shih JC. Behavioral outcomes of monoamine oxidase deficiency: preclinical and clinical evidence. In: Anonymous International Review of Neurobiology. Academic Press:13-42.

48. Arai R, Karasawa N, Kurokawa K, Kanai H, Horiike K, Ito A. Differential subcellular location of mitochondria in rat serotonergic neurons depends on the presence and the absence of monoamine oxidase type B. Neuroscience 2002;114:825-3.

49. Bortolato M, Shih JC. Behavioral outcomes of monoamine oxidase deficiency: preclinical and clinical evidence. In: Anonymous International Review of Neurobiology. Academic Press, 2011:13-42.

50. Luque J, Kwan S, Abell C, Da Prada M, Richards G. Cellular expression of mRNAs encoding monoamine oxidase A and B in the rat central nevous system. The Journal of Comparative Neurology 2004;363:665.

51. Jahng J, Houpt T, Wessel T, Chen K, Shih J, Joh T. Localization of monoamine oxidase A and B mRNA in the rat brain by*in situ* hybridization. Synapse 1997;25:30.

52. Fowler J, Logan J, Volkow N, Wang G. Translational neuroimagin: Positron Emission Tomography studies of Monoamine Oxidase. Molecular Imaging and Biology 2005;7:377.

53. Nakamura S, Kawamata T, Akiguchi I, Kameyama M, Nakamura N, Kimura H. Expression of monoamine oxidase B activity in astrocytes of senile plaques. Acta Neuropathologica 1990;80:419-25.

54. Fornai F, Chen K, Giorgi S, Geis M, Alessandri M, Shih J. Striatal dopamine metabolism in monoamine oxidase-b deficient mice: a brain dialysis study. Journal of Neurochemistry 1999;73:2434.

55. Garrick N, Murphy D. Species differences in the deamination of dopamine and other substrates for monoamine oxidase in brain. Psychopharmacology (Berl) 1980;72:27-33.

56. Bortolato M, Chen K, Shih J. Monoamine oxidase inactivation: from pathophysiology to therapeutics. Adv Drug Deliv Rev 2008;60:1527.

57. Binda C, Mattevi A, Edmondson DE. Structure properties of human monoamine oxidases A and B. International Review of Neurobiology 2011;100:1.

58. Binda C, Newton-Vinson P, Hubalek F, Edmondson DE, Mattevi A. Structure of human monoamine oxidase B, a drug target for the treatment of neurological disorders. Nature Structural and Molecular Biology 2002;9:22-6.

59. Li M, Binda C, Mattevi A, Edmondson DE. Functional role of the aromatic cage in human monoamine oxidase B: Structures and catalytic properties of Tyr435 mutant proteins. Biochemistry (N Y) 2006;45:4775-84.

60. Son S, Ma J, Kondou Y, Yoshimura M, Yamashita E, Tsukihara T. Structure of human monoamine oxidase A at 2.2-Å resolution: The control of opening the entry for substrates/inhibitors. Proceedings of the National Academy of Sciences 2008;105:5739-44.

61. Binda C, Li M, Hubalek F, Restelli N, Edmondson DE, Mattevi A. Insights into the mode of inhibition of human mitochondrial monoamine oxidase B from high-resolution crystal structures. Proceedings of the National Academy of Sciences 2003;100:9750-5.

62. Binda C, Hubálek F, Li M, Edmondson DE, Mattevi A. Crystal structure of human monoamine oxidase B, a drug target enzyme monotopically inserted into the mitochondrial outer membrane. FEBS Lett 2004;564:225-8.

63. McDonald G, Olivieri A, Ramsay R, Holt A. On the formation and nature of the imidazoline I_2 binding site on human monoamine oxidase-B. Pharmacological Research 2010;62:475.

64. Bonivento D, Milczek EM, McDonald GR, *et al*. Potentiation of ligand binding through cooperative effects in monoamine oxidase B. Journal of Biological Chemistry 2010;285:36849-56.

65. Milczek E, Binda C, Rovida S, Mattevi A, Edmondson D. The 'gating' residues Ile199 and Tyr326 in human monoamine oxidase B function in substrate and inhibitor recognition. The FEBS Journal 2011;278:4860.

66. O'Connor J, Howlett K, Wagner R. Side effects accompanying use of iproniazid. American Review of Tuberculosis 1953;68:270.

67. Zeller E, Bardsky J. *In vivo*inhibition of liver and brain monoamine oxidase by 1-isonicotinyl-2-isopropyl hydrazine. Proceedings of the Society for Experimental Biology and Medicine 1952;81:459-461.

68. Schlidkraut J. The catecholamine hypothesis of affective disorders: a review of supporting evidence. American Journal of Psychiatry 1965;122:509.

69. Anderson M, Hasan F, McCrodden J, Tipton K. Monoamine oxidase inhibitors and the cheese effect. Neurochemical Research 1993;18:1145.

70. Lee M, Jensen B, Regier L. Depression treatment chart. In: Pharmacotherapy: A pathophysiologic approach. 8th Edition ed.

71. Berlin I, Hunneyball I, Greiling D, Jones S, Fuder H, Stahl H. A selective reversible monoamine oxidase B inhibitor in smoking cessation: effects on its own and in association with transdermal nicotine patch. Psychopharmacology (Berl) 2012;223:89-98.

72. Holt A. Imidazoline binding sites on receptors and enzymes: Emerging targets for novel antidepressant drugs? Journal of Psychiatry and Neuroscience 2003;28:409.

73. Bousquet P, Feldman J, Schwartz J. Central cardiovascular effects of α-adrenergic drugs: differences between catecholamines and imidazolines. The Journal of Pharmacology and Experimental Therapeutics 1984;200:232.

74. Ernsberger P, Meeley MP, Mann JJ, Reis DJ. Clonidine binds to imidazole binding sites as well as α2-adrenoceptors in the ventrolateral medulla. European Journal of Pharmacology 1987;134:1-13.

75. Coupry I, Podevin RA, Dausse J, Parini A. Evidence for imidazoline binding sites in basolateral membranes from rabbit kidney. Biochemical and Biophysical Research Communications 1987;147:1055-60.

76. Langin D, Lafontan M. [^{3}H]Idazoxan binding at non-α2-adrenoceptors in rabbit adipocyte membranes. European Journal of Pharmacology 1989;159:199-203.

77. Parini A, Coupry I, Graham RM, Uzielli I, Atlas D, Lanier SM. Characterization of an imidazoline/guanidinium receptive site distinct from the α-2 adrenergic receptor. Journal of Biological Chemistry 1989;264:11874.

78. Bousqeut P, Greney H, Bennai F, *et al*. Imidazoline Receptors and Cardiovascular Regulations. Annals of the New York Academy of Science 1995;763:526-30.

79. Bousquet P. Recent advances in imidazoline receptor research. Expert Opinion in Investigational Drugs 1995;4:431.

80. Morgan N, Chan S, Brown C, Tsoli E. Characterization of the imidazoline binding site involved in regulation of insulin secretion. Annals of the New York Academy of Science 1995;763:361-73.

81. Tesson F, Prip-Buus C, Lemoine A, Pegorier JP, Parini A. Subcellular distribution of imidazoline-guanidinium-receptive sites in human and rabbit liver. Major localization to the mitochondrial outer membrane. Journal of Biological Chemistry 1991;266:155-60.

82. Tesson F, Limon-Boulez I, Urban P, *et al*. Localization of I_2-imidazoline binding sites on monoamine oxidases. Journal of Biological Chemistry 1995;270:9856-61.

83. Wiest SA, Steinberg MI. Binding of [^{3}H]2-(2-benzofuranyl)-2-imidazoline (BFI) to human brain: Potentiation by tranylcypromine. Life Sciences 1997;60:605-1.

84. Parini A, Moudanos CG, Pizzinat N, Lanier SM. The elusive family of imidazoline binding sites. Trends in Pharmacological Science 1996;17:13-6.

85. Lione LA, Nutt DJ, Hudson AL. [^{3}H]2-(2-Benzofuranyl)-2-imidazoline: a new selective high affinity radioligand for the study of rabbit brain imidazoline I2 receptors. European Journal of Pharmacology 1996;304:221-9.

86. Wiest SA, Steinberg MI. ^{3}H[2-(2-benzofuranyl)-2-imidazoline] (BFI) binding in human platelets: modulation by tranylcypromine. Naunyn Schmiedebergs Archives of Pharmacology 1999;360:209,216; 216.

87. Steinberg M, Wiest S, Pickard R, Chenn K, Shih J. Binding of the imidazoline ligand ^{3}H-2-Benzofuranyl-2-Imidazoline (BFI) to human brain and platelets: Potentiation by tranylcypromine and role of MAO isoforms. Annals of the New York Academy of Science 1999;881:193-8.

88. Olmos G, Alemany R, Boronat M, Garca-Sevilla J. Pharmacologic and Molecular Discrimination of I2-Imidazoline Receptor Subtypesa. Annals of the New York Academy of Science 1999;881:144-60.

89. Bromberg-Martin ES, Matsumoto M, Hikosaka O. Dopamine in Motivational Control: Rewarding, Aversive, and Alerting. Neuron 2010;68:815-34.

90. Brown A. Influence of oxygen and concentration on alcoholic fermentation. Journal of the Chemical Society 1892;61:369.

91. Henri V. Theorie generale d l'action de quelques diastases. Comptes Rendus of the Academy of Science, Paris 1902;135:916.

92. Michaelis L, Menten M. Die Kinetik der Invertinwirkung. Biochemische Zeitschrift 1913;49.

93. Duggleby RG. Analysis of enzyme progress curves by nonlinear regression. In: Methods in enzymology. Academic Press, 1995:61-90.

94. Milczek EM, Bonivento D, Binda C, Mattevi A, McDonald IA, Edmondson DE. Structural and mechanistic studies of mofegiline inhibition of recombinant human monoamine oxidase B. Journal of Medicinal Chemistry 2008;51:8019-26.

95. Botting NP. Isotope effects in the elucidation of enzyme mechanisms. Natural Products Report 1994;11:337-53.

96. Houslay M, Tipton K. The reaction pathway of membrane-bound rat liver mitochondrial monoamine oxidase. Biochemistry Journal 1973;135:735.

97. Husain M, Edmondson DE, Singer TP. Kinetic studies on the catalytic mechanism of liver monoamine oxidase. Biochemistry (N Y) 1982;21:595-600.

98. Edmondson DE, Binda C, Wang J, Upadhyay AK, Mattevi A. Molecular and mechanistic properties of the membrane-bound mitochondrial monoamine oxidases. Biochemistry (N Y) 2009;48:4220-3.

99. Tan AK, Ramsay RR. Substrate-specific enhancement of the oxidative half-reaction of monoamine oxidase. Biochemistry (N Y) 1993;32:2137-43.

100. Ramsay R. Substrate regulation of monoamine oxidases. Journal of Neural Transmission Supplement 1998;52:139.

101. Ramsay RR, Koerber SC, Singer TP. Stopped-flow studies on the mechanism of oxidation of N-methyl-4-phenyltetrahydropyridine by bovine liver monoamine oxidase B. Biochemistry (N Y) 1987;26:3045-50.

102. Holt A, Palcic M. A peroxidase-coupled continuous absorbance plate-reader assay for flavin monoamine oxidases, copper-containing amine oxidases and related enzymes. Nature Protocols 2006;1:2498-2505.

103. Green A. Inhibition of rat and mouse brain monamine oxidases by (+)-amphetamine. Biochemistry Journal 1971;121:37.

104. Pearce LB, Roth JA. Human brain monoamine oxidase type B: mechanism of deamination as probed by steady-state methods. Biochemistry (N Y) 1985;24:1821-6.

105. Roth JA. Evidence for a single catalytic binding site on human brain type B monoamine oxidase. Journal of Neurochemistry 1976;27:1107.

106. McDonald GR, Hudson AL, Dunn SMJ, *et al*. Bioactive contaminants leach from disposable laboratory plasticware. Science 2008;322:917.

107. Ramsay R, Olivieri A, Holt A. An improved approach to steady-state analysis of monoamine oxidases. Journal of Neural Transmission 2011;118:1003-19.

108. Raddatz R, Parini A, Lanier SM. Imidazoline/guanidinium binding domains on monoamine oxidases. Journal of Biological Chemistry 1995;270:27961-8.

109. Raddatz R, Parini A, Lanier SM. Localization of the imidazoline binding domain on monoamine oxidase B. Molecular Pharmacology 1997;52:549-53.

110. Newton-Vinson P, Hubalek F, Edmondson DE. High-level expression of human liver monoamine oxidase B in *Pichia pastoris*. Protein Expression and Purification 2000;20:334-45.

111. Hiroyasu K, Yuichiro A, Lars O, Keith F. T, Christopher J. F. Time-dependent inhibition of monoamine oxidase by β-phenethylamine. Biochemistry and Pharmacology 1982;31:959-64.

112. Eglen R, Hudson AK, Kendall DA, Nutt DJ, Morgan NG, Wilson VG, Dillon MP. Seeing through a glass darkly: casting light on imidazoline I sites. Trends in Pharmacological Sciences1998;19:381-90.

113. Lione LA, Nutt DJ, Hudson AL. [^{3}H]-2-(2-benzofuranyl)-2-imidazoline: a new selective high affinity radioligand for the study of rabbit brain imidazoline I_2 receptors. European Journal of Pharmacology 1996;304:221-9

114. Lalies MD, Hibell A, Hudson AL, Nutt DJ. Inhibition of central monoamine oxidase by imidazoline-2 site-selective ligands. Annals of the New York Academy of Science 1999;881:114-7